TRG

AD 608954

[redacted]

PROCESSING COPY

COPY 1 OF 1 hard

HARD COPY $.5.00

MICROFICHE $.1.00

ARCHIVE COPY 176p

DDC

RECEIVED

DEC 18 1964

DDC-IRA A

[redacted]

DISCLAIMER NOTICE

THIS DOCUMENT IS THE BEST QUALITY AVAILABLE.

COPY FURNISHED CONTAINED A SIGNIFICANT NUMBER OF PAGES WHICH DO NOT REPRODUCE LEGIBLY.

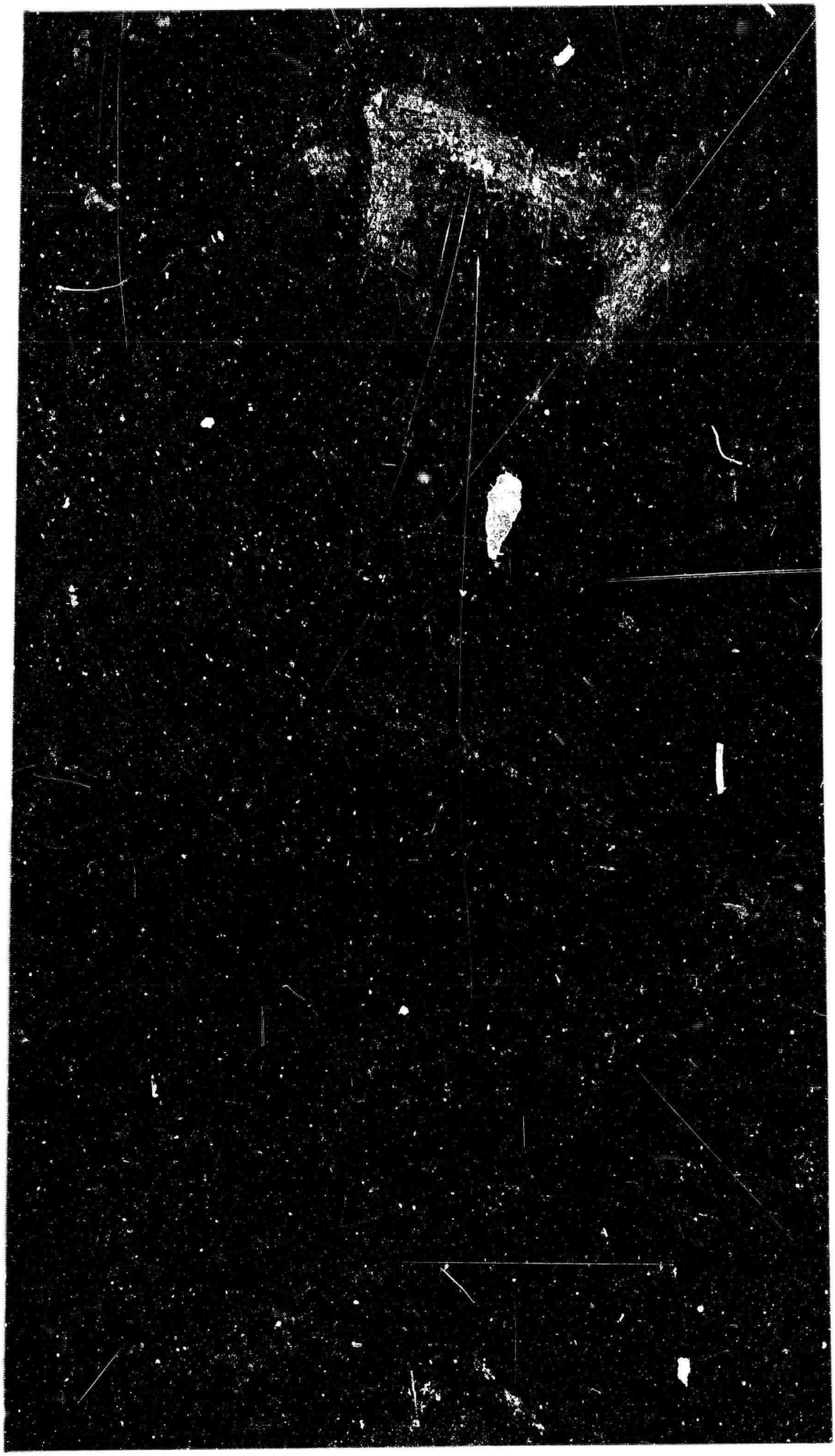

RESEARCH ON PROPERTIES OF LASER DEVICES (U)

TRG, Incorporated
Syosset, New York

AFOSR
ASTIA Document No.

TRG-134-TR-6

Contract No. AF49(638)-673
AFOSR Task No. 12
ARPA Order No. 6-58

RESEARCH ON PROPERTIES OF LASER DEVICES (U)

TRG, Incorporated
Syosset, New York

January 19, 1962

Prepared for
OFFICE OF SCIENTIFIC RESEARCH
AIR RESEARCH AND DEVELOPMENT COMMAND
UNITED STATES AIR FORCE
Washington, D. C.

Maurice C. Newstein, Editor

Richard T. Daly
Department Head

TECHNICAL RESEARCH GROUP

ABSTRACT

LASER amplification corresponding to a gain of 6% per meter was measured at 3μ in cesium vapor optically pumped with light from a helium discharge lamp. Amplification and oscillation at 1μ were measured in a helium-neon system based on collisions of the second kind. The amplification parameters, when optimized resulted in a gain of 9% per meter. Krypton-xenon and zinc vapor are other media utilizing collisions of the second kind which were investigated. Crystals of calcium tungstate containing either Dy^{3+} or Nd^{3+} were grown. LASER oscillation was observed from two crystals of $CaWO_4$:Nd. Direct amplification of the output of a ruby oscillator in a second ruby rod was demonstrated. Three methods of achieving single pulse output from ruby oscillators are described. A pulse of 2×10^6 watts peak power was achieved by one method. A broadband emission was discovered in normally pink ruby (.04% Cr by weight). It accounts for 30% of the total emission, making the quantum efficiency unity. A theoretical analysis of the properties of cube corner interferometers has been experimentally verified.

G.

P.

List of Authors

Sections of this report were written by R. Daly, G. Gould, G. Grosof, B. Hammond, S. Jacobs, R. Martin, M. Newstein, P. Rabinowitz, T. Shultz, J. Sjoblom and R. Targ.

TABLE OF CONTENTS

TABLE OF CONTENTS (continued)

TABLE OF CONTENTS (continued)

TABLE OF CONTENTS (continued)

TABLE OF CONTENTS (continued)

I. Introduction and Summary of Results

The immediate objective of this research is to produce working models of LASER devices, together with the experimental and theoretical information necessary to describe and predict their performance.

In this section we summarize the results that have been obtained to date.

1.0 Optical Pumping of Cesium Vapor by Helium Lamp

During the present period we have completed construction of a 1 cm diameter Cs/He LASER tube with an optically pumped length of 90 cm. With this apparatus we have measured directly light amplification at $\lambda = 3.2$ microns. The measured amplification coefficient corresponded to a gain of approximately 6%.

More recently the light source and reflector have been improved, increasing the effective optical pumping, and hence the gain, by a factor of 2.5.

The construction of an oscillator designed for a 7.18 micron output is now under way.

2.0 Direct Discharge Excitation of LASER Media

Three methods of direct discharge excitation utilizing collisions of the second kind were studied during the present period. They were:

a) excitation of Ne by He,

b) excitation of Xe by Kr and

c) excitation of Zn by Zn

2.1 Helium-Neon

A quartz helium-neon discharge tube was constructed, one meter long and 1.5 cm in diameter. When filled with 1.0 mm of helium and 100 microns of neon and excited with rf power at 20 Mc, it exhibited 2% amplification per meter integrated across the total linewidth at $\lambda = 1.1523$ microns. Further optimization of gain parameters was accomplished in the optical resonator cavity.

A type of oscillator cavity was constructed in which one reflector was flat, the other spherical. The optical system was deliberately made non-confocal in order to relax requirements on alignment. Strong oscillations were observed at $\lambda = 1.1523$ microns. Amplification parameters when optimized resulted in a gain of 9% per meter in a tube 7 mm in diameter, filled with 1.5 mm of helium, and

170 microns of neon. Initial observations of the intensity distribution in the LASER beam with an image amplifier tube, indicated between four and ten modes simultaneously in oscillation.

2.2 Krypton-Xenon

A series of experiments was performed in order to study the feasibility of building a gas discharge LASER containing xenon pumped by collisions of the second kind with krypton metastable atoms. The experiments performed were to ascertain whether indeed, there could be a directed transfer of energy from the krypton system to the xenon system. The first series looked for enhanced emission of light from levels that would be selectively excited by the krypton; the second series looked for selective depopulation of the krypton metastable states as a function of the xenon partial pressure. Because of the increase in lifetime in the discharge of the lower level of the proposed LASER due to resonance light trapping, a series of experiments were performed to ascertain this lifetime. The results of the three series of experiments indicate that krypton is interacting with xenon, a result not in the previous literature.

2.3 Zinc-Zinc

Under particular experimental conditions, excitation of the 6^3S level of zinc in a discharge has been observed to be almost

entirely due to self collisions of the second kind between metastables.

Under these conditions, the maximum lifetime of the trapped resonance level of Zn (4^3P_1) is $\tau = 1 \times 10^{-3}$ sec at a pressure, $P_{Zn} = 0.6$ mm Hg. With helium admixed at $P_{He} = 1.0$ mm Hg, the electron thermalization time is 10^{-5} sec.

3.0 Optical Pumping of Ruby-Amplifier

Direct amplification of the output of a ruby oscillator in a second ruby rod was demonstrated. The measured single pass gain was 2 at room temperature in a ruby cylinder 5.56 cm long. The inferred single pass gain of 12.5 in a ruby eight inches long was obtained by exciting it to oscillation at room temperature with no coating at either end.

4.0 Optical Pumping of Ruby-Oscillator

Two long ruby crystals were excited to oscillation to obtain high output energy. The measured output at room temperature was 2 joules from a rod .362" in diameter and 7.56" long and ~ 12 joules from a rod .625" in diameter and 5.5" long.

Single pulse output was obtained from ruby by two methods. In the first a Kerr cell was used to modulate the Q of the oscillation cavity (consisting of a ruby rod with an external mirror). Single pulses of 0.2μsec duration were obtained with a peak power of about

2×10^6 w. The second method employed the optical thyratron action of an unexcited ruby absorber within the oscillation cavity. Single pulses were achieved but are not yet always reproducible.

A prior attempt to achieve intense single pulses is reported. This technique consisted of exciting the ruby with a second intense flash of short duration superimposed on a normal excitation flash. A series of strong relaxation oscillations of about 15 μsec duration was achieved.

A broad band emission was discovered in normally pink ruby (.04% Cr by weight). It accounts for 30% of the total emission from the ruby rod, making the quantum efficiency unity.

The output energy from a ruby LASER as a function of the end coating (reflectivity and transmission) of the ruby crystal was measured. The results confirm the existence of an optimum reflectivity of a relatively low value for maximum output energy.

5.0 Optical Pumping of Rare Earth Crystals

The study of the optical pumping of rare earth ions during this period has mainly centered on the investigation of calcium tungstate crystals containing either Dy^{3+} or Nd^{3+}. Two crystals of $CaWO_4$:Nd have been polished to optical tolerances. LASER oscillation has been observed in both at 1.065μ. No oscillation has yet been observed (at 5740A) in the several crystals of $CaWO_4$:Dy tried.

6.0 Growth of Rare Earth Doped Crystals

The foremost type of single crystals grown in this period was the tungstate (scheelite) type. The great majority of specimens consisted of calcium tungstate ($CaWO_4$) doped with various concentrations of $Na_{0.5}Dy_{0.5}WO_4$ in one series and of $Na_{0.5}Nd_{0.5}WO_4$ in another series. Six Dy-doped crystals were grown (all at predetermined orientation by seeding), and five of these were annealed. Six Nd-doped crystals were similarly grown, three of which were annealed. One crystal was grown from a melt of $Na_{0.5}La_{0.5}WO_4$ which proved to be inhomogeneous by observation and by chemical analysis of the crystal. In place of the induction furnace used for the above crystal growths, a resistance furnace was designed and built for the lower-melting host material: lead molybdate ($PbMoO_4$).

The earlier study of anhydrous lanthanum chloride as a host crystal was supplemented in this period by a study of anhydrous strontium chloride ($SrCl_2$). The resistance furnace used for lead molybdate was modified by maintaining an inert gas-hydrogen chloride atmosphere about the crucible of molten $SrCl_2$ to prevent its hydrolysis and oxidation. Pulling a crystal from this melt (to be doped with divalent samarium chloride) will be attempted.

A new material for incorporating rare earth ions was prepared: yttrium vanadate (YVO_4). It melts at about 1800°C and seems to promote line fluorescence of rare earths.

7.0 Optical Devices

Experimental and analytical work has shown that efficient coupling in optical pumping can be achieved using a reflective circular cylinder. Efficiencies are higher than diffuse cavities or reflective ellipses under conditions where the lamp and sample diameters are not negligible compared to the cavity diameter.

A theoretical analysis of the properties of cube corner interferometers has been experimentally verified. An attempt was made to build an oscillator using such an interferometer as a resonant cavity.

II. Optical Pumping of Cesium Vapor by Helium Lamp

1.0 Summary of Work Performed

During the present period we have completed construction of a 1 cm diameter Cs/He LASER tube with an optically pumped length of 90 cm. With this apparatus we have measured directly light amplification at $\lambda = 3.2$ microns. The measured amplification coefficient corresponded to a gain of approximately 6%. The construction of an oscillator designed for a 7.18 micron output is under way.

2.0 Analysis of Work Performed

2.1 Amplification Experiment

The following article, giving the details of the gain measurement, has been published in Physical Review Letters (Dec. 1, 1961 page 415).

COHERENT LIGHT AMPLIFICATION IN OPTICALLY PUMPED Cs VAPOR*

Submitted to:

Physical Review Letters

S. Jacobs, G. Gould
and
P. Rabinowitz
TRG, Incorporated
Syosset, New York

An excess population density in the upper of two states connected by an optical transition makes possible Light Amplification by Stimulated Emission of Radiation (LASER). This has recently been demonstrated in a gaseous system employing collisions of the second kind[1]. We have measured spatially coherent amplification in cesium vapor excited by selective optical pumping[2].

An optical pump suitable for obtaining a population inversion in cesium is the intense He 3888Å line which overlaps the 3rd cesium resonance line (see Figure 1). In 1930 Boeckner reported fluorescence in cesium excited by the He 3888Å line[3]. We have extended Boeckner's optical pumping experiment by measuring the absolute intensities of Cs fluorescent lines[4] and from these measurements have computed the populations of the associated states using transition probabilities calculated by the Bates-Damgaard method[5].

---

(1) A. Javan, W. R. Bennett, Jr. and D. R. Herriott, Phys. Rev. Letters 106, Feb. 1, 1961

(2) A. L. Schawlow and C. H. Townes, Phys. Rev. 112, 1940 (1958) and by G. Gould in an unpublished proposal to ARPA December, 1958.

(3) C. Boeckner, Bur. Standards J. Research 5, 13, July 1930.

(4) S. Jacobs, P. Rabinowitz and G. Gould submitted to J. Opt. Soc. Amer.

(5) D. R. Bates and A. Damgaard, Phil. Trans. No 842, 101, 1949.

* This work was supported by Advanced Research Projects Agency through the Air Force Office of Scientific Research.

Table I shows the populations of certain energy levels obtained under optimized conditions.

TABLE I

Cs Energy Levels	Population Density (10^6 atoms/cm^3)
$8P_{1/2}$	100
$8P_{3/2}$	30
$8S_{1/2}$	10
$6D_{3/2}$	3
$5D_{3/2}$	200

The population of the $8P_{1/2}$ energy level was substantially greater than that of the lower levels, $8S_{1/2}$ and $6D_{3/2}$. LASER action was therefore possible at the corresponding wavelengths, $\lambda = 7.2\mu$ and 3.2μ.

The amplification coefficient is related to the populations by the equation

$$k(\nu) = \frac{h\nu}{c} (B_{21}N_2 - B_{12}N_1) S(\nu) \qquad (1)$$

where $S(\nu)$ is the normalized lineshape function ($\int S(\nu)d\nu = 1$).

B is the coefficient of induced emission (Einstein B)

N_1, N_2 are the population densities.

Assuming a Doppler profile, the amplification coefficient at line center reduces to

$$k(\nu_o) = \frac{1}{I}\frac{\partial I}{\partial z} = \left(\frac{\ell n 2}{16 c^2 \pi^3}\right)^{1/2} A_{21} \frac{\lambda_o^4}{\Delta\lambda_d} \left(N_2 - \frac{g_2}{g_1} N_1\right) \qquad (2)$$

where A is the spontaneous emission coefficient (Einstein A), g_1, g_2 are statistical weights and $\Delta\lambda_d$ is the Doppler width.

The experimental apparatus for the amplification measurement consisted of an optically pumped Cs fluorescent source, an optically pumped amplification cell, a narrow band interference filter and a radiation detector (see Figure 2). The measurement was carried out at 3.2μ, rather than at 7.2μ, because of the superior detectivity of a PbS liquid nitrogen cooled detector compared with the best 7μ detectors.

The source and amplifier were heated Cs cells, 9 cm and 90 cm long respectively, positioned within reflective cavities and illuminated by helium discharge lamps. The source lamp, P_2, was

operated at 30 Mcs and modulated at 105 cps in order to avoid chopping the thermal radiation emitted by the heated Cs cell. The amplifier lamp, P_1, was operated at 400 cps, since rf power, which provides more efficient excitation, was not available to run a tube of its dimensions. The temperature of the Cs was adjusted for maximum fluorescence. The absorption coefficient at the center of the 3rd Cs resonance line was then $k_o \propto \frac{1}{r}$, where r is the cell radius. The Cs source and amplifier diameters were 4 and 10 mm respectively, corresponding to an optimum Cs temperature of 175°C in the source and 165°C in the amplifier. In order to reduce the effects of impurity gases upon the population inversion a continuously pumped vacuum system was used in the amplifier cell. The conductance was designed to establish a vacuum system gradient of no more than 3% along the amplifier tube in order to insure uniform absorption of pumping light. It was found that fluorescence lines originating from levels ordinarily populated by collisions were reduced greatly in intensity when the vacuum system was utilized.

Phase sensitive detection was used with a time constant, $\tau \approx 1/3$ sec., which made possible detection of 2×10^{-13} watts. The power reaching the 1/4 x 1/4 mm detector from the source was about 10^{-9} watts, and provided a signal-to-noise ratio of 100:1. The

discrepancy between system detectivity and observed signal-to-noise was due to mechanical vibration of the very small image with respect to the minute detector.

The direct amplification measurement was made by turning on and off the 400 cps helium lamp illuminating the amplifier cell. The detection system, locked in on 105 cps, showed an increase of $4 \pm 1\%$ each time the amplifier helium lamp was turned on. The following checks were made, each time repeating the above procedure:

1. Cs vapor pressure was reduced; gain disappeared.
2. Source power was turned off; signal went to zero and remained there.
3. Source power was on, but source light was blocked. Signal remained at zero.
4. Wavelength filter was changed to $\lambda = 3.01\mu$ ($6P_{1/2} - 5D_{3/2}$ transition); absorption was observed.
5. Linearity of the detection system was checked by introducing 3.2μ radiation after, instead of through, the amplifier cell. This was done by means of a beam splitter. The source and amplifier intensities were adjusted so that the power levels reaching the detector were comparable to their original respective values. The detection system was again locked to the source; no enhancement effect was observed.

We feel that the above checks rule out the possibility of artifact. The measured amplification is in reasonable agreement

with the value computed from Equation 2 using populations given in Table I.

$$k(\nu_c) = .002 \text{ cm}^{-1} \text{ for } \lambda = 3.2\mu$$

This coefficient may be reduced by a factor as large as 2 due to incipient hyperfine splitting in $8P_{1/2}$. Assuming a Doppler shape for boch source and amplifier, the measured amplification coefficient averaged over the lineshape, is smaller by a factor of $\sqrt{2}$ than the value at line center. From these considerations one predicts a measured gain of approximately 6% for a 90 cm cell.

Butaeva and Fabrikant recently investigated the possibility of obtaining a population inversion in Cs by a combination of optical pumping and collisions of the second kind[6]. They measured variations in the relative intensities of the 7D-6P fluorescence transitions which they suggest may be due to stimulated emission of radiation. The interpretation of Butaeva and Fabrikant rests on the assumption that the lifetimes of $6P_{1/2,3/2}$ are not appreciably lengthened by radiation trapping. According to the theory of light imprisonment due to T. Holstein[7], the lifetime of these states should be increased from the natural lifetime of 3×10^{-8} sec.[8] to

---

(6) F. A. Butaeva and V. A. Fabrikant - Research in Experimental and Theoretical Physics - In memoriam of G. S. Landsberg U.S.S.R. Acad. Sci Press 1959

(7) T. Holstein - Phys. Rev 83 1159, 1951

(8) R. Minkowski and W. Muhlenbruch - Z. Physik. 63, 198 1930.

about 10^{-4} sec., under the conditions of their experiment. Since the trapped lifetime is longer than that of any other excited Cs level, we do not believe the populations of $6P_{1/2,3/2}$ could be less than that of any other Cs level, except the ground level. This conclusion we substantiated by measurement of strong absorption in the $6P_{1/2}$ - $5D_{3/2}$ transition.

An improved apparatus is being built which we believe will increase the amplification coefficient by a factor of 5. An oscillator incorporating Cs vapor is also under construction.

We wish to thank J. Sjoblom for performing the Bates-Damgaard calculations, B. Freeman and J. Poulos for assistance in constructing the apparatus.

LIST OF FIGURES

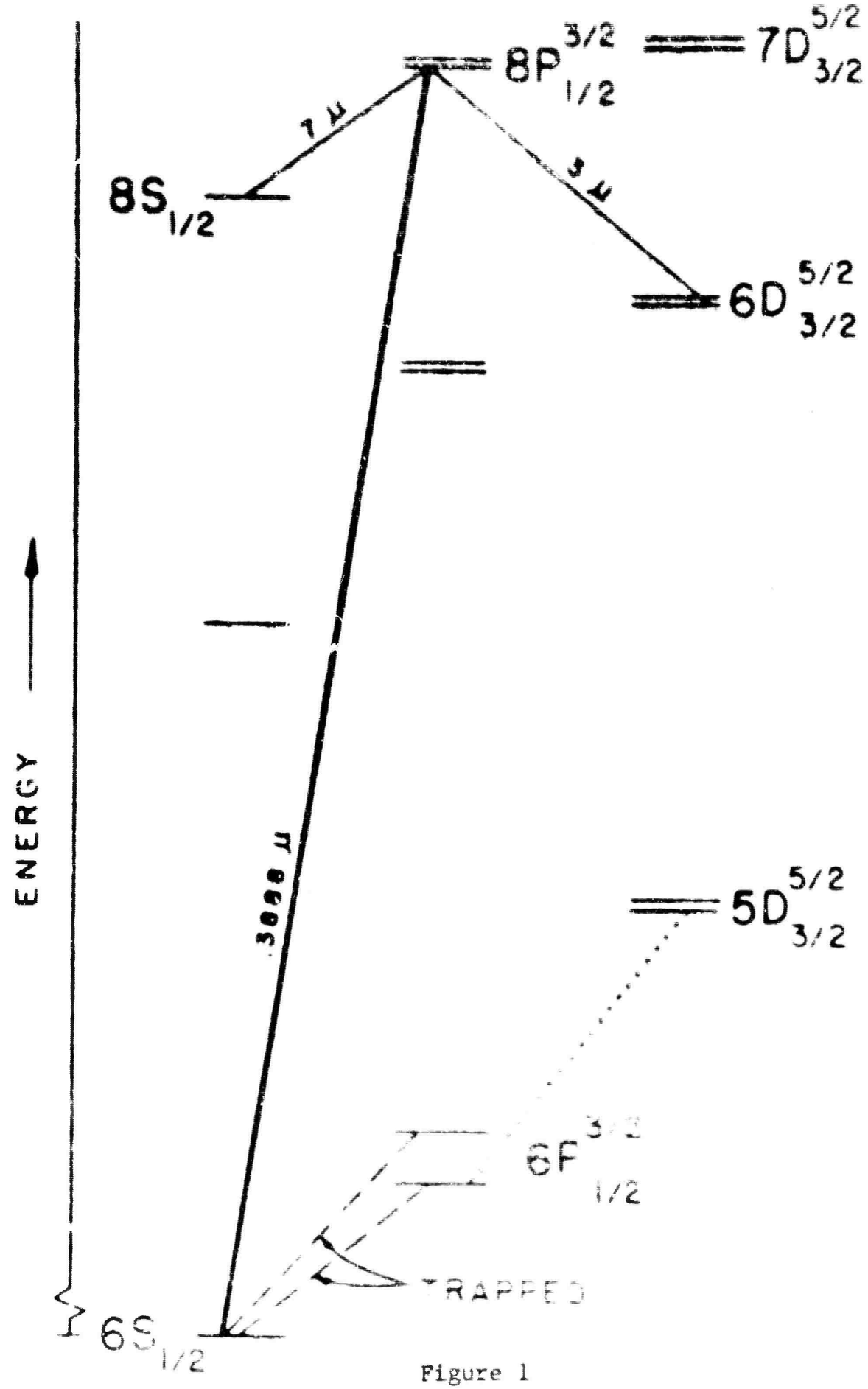
$8P^{3/2}_{1/2}$
$7D^{5/2}_{3/2}$
$8S_{1/2}$
7 μ
3 μ
$6D^{5/2}_{3/2}$
ENERGY
3000 μ
$5D^{5/2}_{3/2}$
$6F^{5/2}_{1/2}$
TRAPPED
$6S_{1/2}$

Figure 1

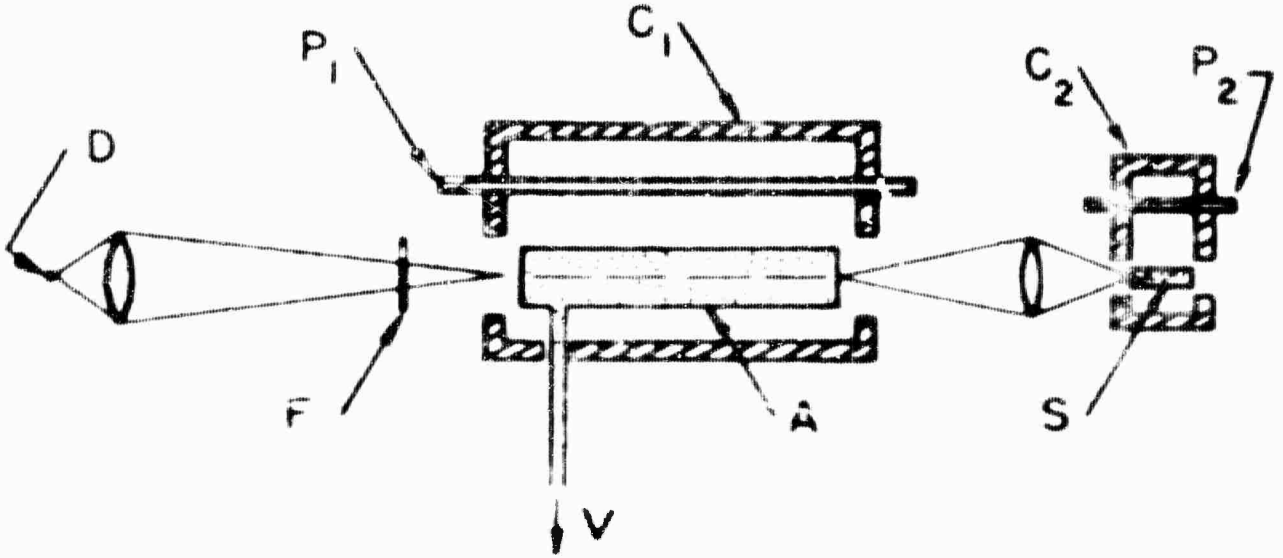

Figure 2

Summarizing the result of this gain measurement, a gain of $4 \pm 1\%$ was measured. This measured value is necessarily averaged over the whole lineshape and implies that the gain at line center was close to 6%, in good agreement with our expectations based on Cs fluorescence. More recently the light source and reflector have been improved, increasing the effective optical pumping, and hence the gain, by a factor of 2.5.

2.2 Construction of Oscillator

At the time of this writing, construction of an oscillator is more than half completed. This oscillator is designed for a 7.18μ output, where the gain coefficient is 6-1/2 times that at 3.20μ. This increase in the gain coefficient corresponds to well over 100% gain.

Although the high anticipated gain makes it possible to tolerate very great losses, there are two aspects of oscillator design which require extreme caution:

2.2.1 Windows

Since we were unable to find adequate reflectors which are resistant to attack by cesium vapor, we plan to contain the cesium in a windowed tube with the reflectors outside in an evacuated region. In addition to protecting the reflectors, this construction maintains

the interferometer elements at near-ambient temperatures, and isolates the turbulent hot air from the optical beam.

We have found no really pleasing solution to the problem of sealing vacuum-tight, 7μ transparent, interferometric quality windows onto the cesium tube in a way that does not involve either great losses or risk. The solution we have chosen is to press flat barium fluoride windows against the flattened glass tube ends and then baffle, trap and pump away the small amount of cesium that leaks through the imperfect seal. (see Figure 7.1) The windows will be oriented with their surface normals at Brewsters angle with respect to the beam, so that use may be made of this anti-reflection technique.

2.2.2 Diffraction Losses

The solution to the window problem described above involves an increase in the resonator length to 1.7 meters. This great length, combined with the long wavelength, makes the diffraction losses of the 7μ oscillator non-negligible. These losses are still quite manageable, provided the diameter is kept large. The following expression, due to Barone (9), shows approximately the way diffraction losses depend on wavelength, resonator length and diameter.

$$\text{Diffraction Loss} \propto \left(\frac{\lambda L}{D^2}\right)^{3/2}$$

(9) Stephen Barone - Research on Properties of LASER Devices Technical Report 5, page 86, July 10, 1961

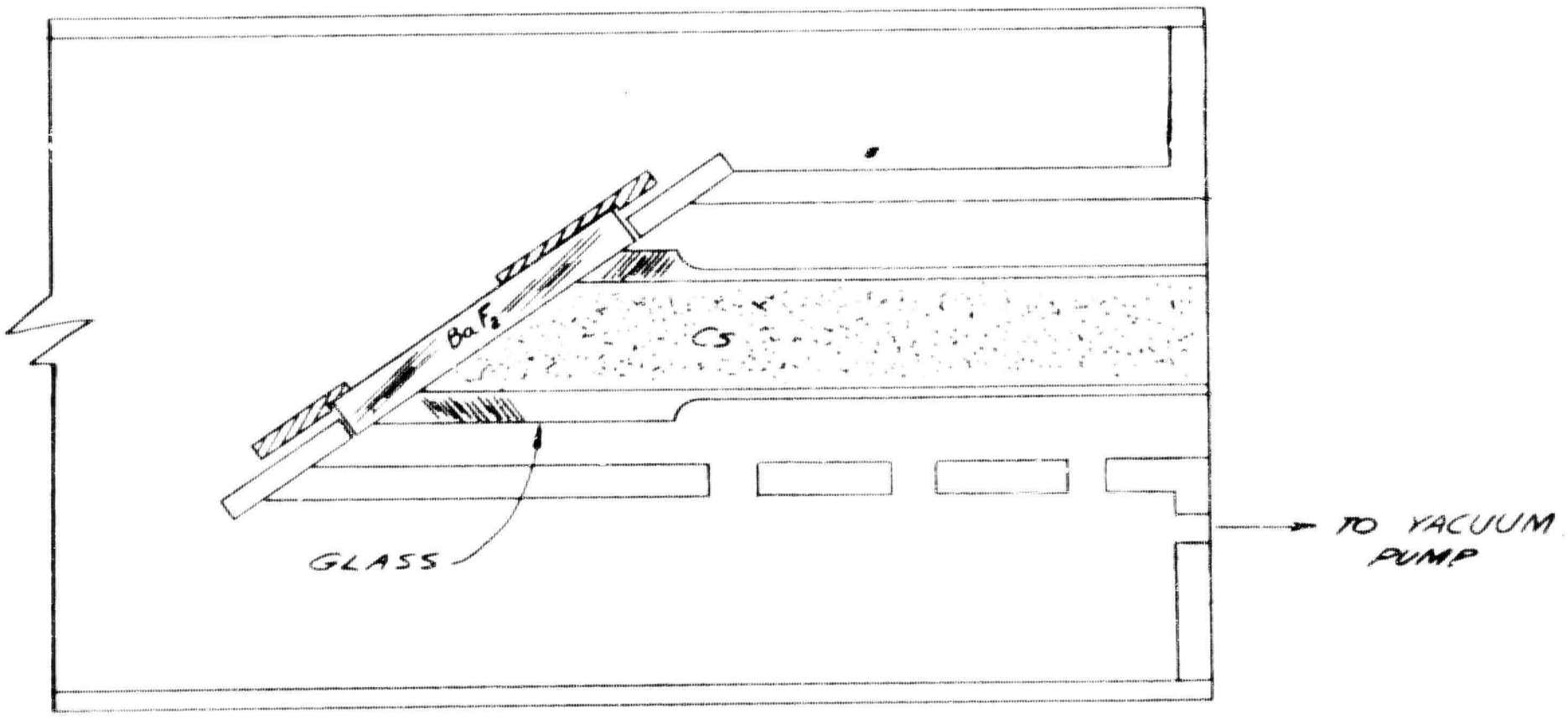

METHOD USED FOR CESIUM CONTAINMENT

Figure 2.1

(The analysis due to Fox and Li[10] is more accurate for the present case, but the preceding analytic expression shows approximately the way in which parameters enter).

The need to maintain a large diameter has led us to defer temporarily construction of a crossed roof resonator, in favor of a confocal, or near-confocal type of cavity. The beam in a crossed roof resonator has only half the diameter of that of a plane Fabry-Perot resonator, and hence, approximately 8 times the diffraction losses, while the confocal resonator[11] has been demonstrated[12] to have diffraction losses which are less than those of the plane Fabry-Perot.

3.0 Work Planned for Next Period

During the next period it is planned that the 7.18μ oscillator will be successfully operated and its various characteristics measured.

As soon as the experimental threshold for oscillation is known we will begin work on

a. constructing a 7.18μ oscillator of much smaller dimensions and

b. operating at $\lambda = 3.20\mu$

---

(10) A. G. Fox and Tingye Li, Bell System Tech. Journal 40 453 (1961)
(11) G. D. Boyd & J. P. Gordon, Bell System Tech. Journal 40 489 (1961)
(12) D. R. Herriott, private communication

III. Direct Discharge Excitation of LASER Media

1.0 Summary of Work Performed

Three methods of direct discharge excitation utilizing collisions of the second kind were studied during the present period. They were: Excitation of Ne by He, excitation of Xe by Kr, and excitation of Zn by Zn.

1.1 Helium-Neon

A quartz helium-neon discharge tube was constructed, one meter long and 1.5 cm in diameter. When filled with 1.0 mm of helium and 100 microns of neon and excited with rf power at 20 Mc, it exhibited amplification of 2%/meter integrated across the total linewidth at $\lambda = 1.1523$ microns. Further optimization of gain parameters was accomplished in the optical resonator cavity.

A type of oscillator cavity was constructed in which one reflector was flat, the other spherical. The optical system was deliberately made non-confocal in order to relax requirements on alignment. Strong oscillations were observed at $\lambda = 1.1523$ microns. Amplification parameters when optimized resulted in a gain of 9% per meter in a tube 7 mm in diameter, filled with 1.5 mm of helium, and 170 microns of neon.

1.2 Krypton-Xenon

A series of experiments was performed in order to study the feasibility of building a gas discharge LASER containing xenon pumped by collisions of the second kind with krypton metstable atoms. The experiments performed were to ascertain whether indeed, there could be a directed transfer of energy from the krypton system to the xenon system. The first series looked for enhanced emission of light from levels that would be selectively excited by the krypton; the second series looked for selective depopulation of the krypton metastable states as a function of the xenon partial pressure. Because of the increase in lifetime in the discharge of the lower level of the proposed LASER due to resonance light trapping, a series of experiments was performed to ascertain this lifetime. The results of the three series of experiments are listed below; - they indicate that krypton is interacting with xenon, a result not in the previous literature.

1. Enhancement of Xe Emission

For the transitions $2p_6 - 1s_4$

$2p_7 - 1s_4$

$2p_9 - 1s_4$

an average of five times the expected amount of emission of xenon

light was measured, over the average of three control emissions

$$3p_7 - 1s_2$$

$$2p_3 - 1s_2$$

$$4d_3 - 2p_{10}$$

in a mixture of 100μ of Kr and 8μ of Xe.

2. Depopulation of Kr $1s_5$

For three transitions out of the Kr $1s_5$ state, the increase of Xe partial pressure from 1μ to 10μ caused an average 11% decrease in absorption coefficient. The slight lowering of electron temperature by the increase of Xe pressure did not change the emission of various Kr lines examined in emission.

3. Light-trapping in Xe

Guided by Holstein's model, the absorptions out of the Xe $1s_4$ and $1s_5$ states were compared. At 1 micron of Xe, the average absorption out of the $1s_4$ to 2p states for 4 transitions was 2.1%, the average for 3 transitions from the $1s_5$ state to the 2p states was 42.9%. At higher pressures the absorption coefficients were so large from both the $1s_4$ and $1s_5$ states that meaningful measurements could not be made. This dramatic evidence tells us we are in the region where an inversion may be possible.

1.3 Zinc-Zinc

Under particular experimental conditions, excitation of the 6^3S level of zinc in a discharge has been observed to be almost entirely due to self collisions of the second kind between metastables.

Under these conditions, the maximum lifetime of the trapped resonance level of Zn (4^3P_1) is $\tau = 1 \times 10^{-3}$ sec at a pressure, $P_{Zn} = 0.6$ mm Hg. With helium admixed at $P_{He} = 1.0$ mm Hg, the electron thermalization time is 10^{-5} sec.

re

2.0 Analysis of Work Performed

2.1 Helium-Neon System

2.1.1 Amplification Experiment

An experiment to observe amplification at one or more LASER frequencies in the helium-neon system was performed. An energy level diagram of this system is given in Figure 3.1. A gain of 20% per meter was observed at $\lambda = 1.1523$ microns. This gain measurement was an average across the total linewidth, and did not give the peak spectral gain.

2.1.1.1 Design of Double Modulation Apparatus

In using the double-beam spectrophotometer described in the Xe-Kr section of this report we found that it was subject to a

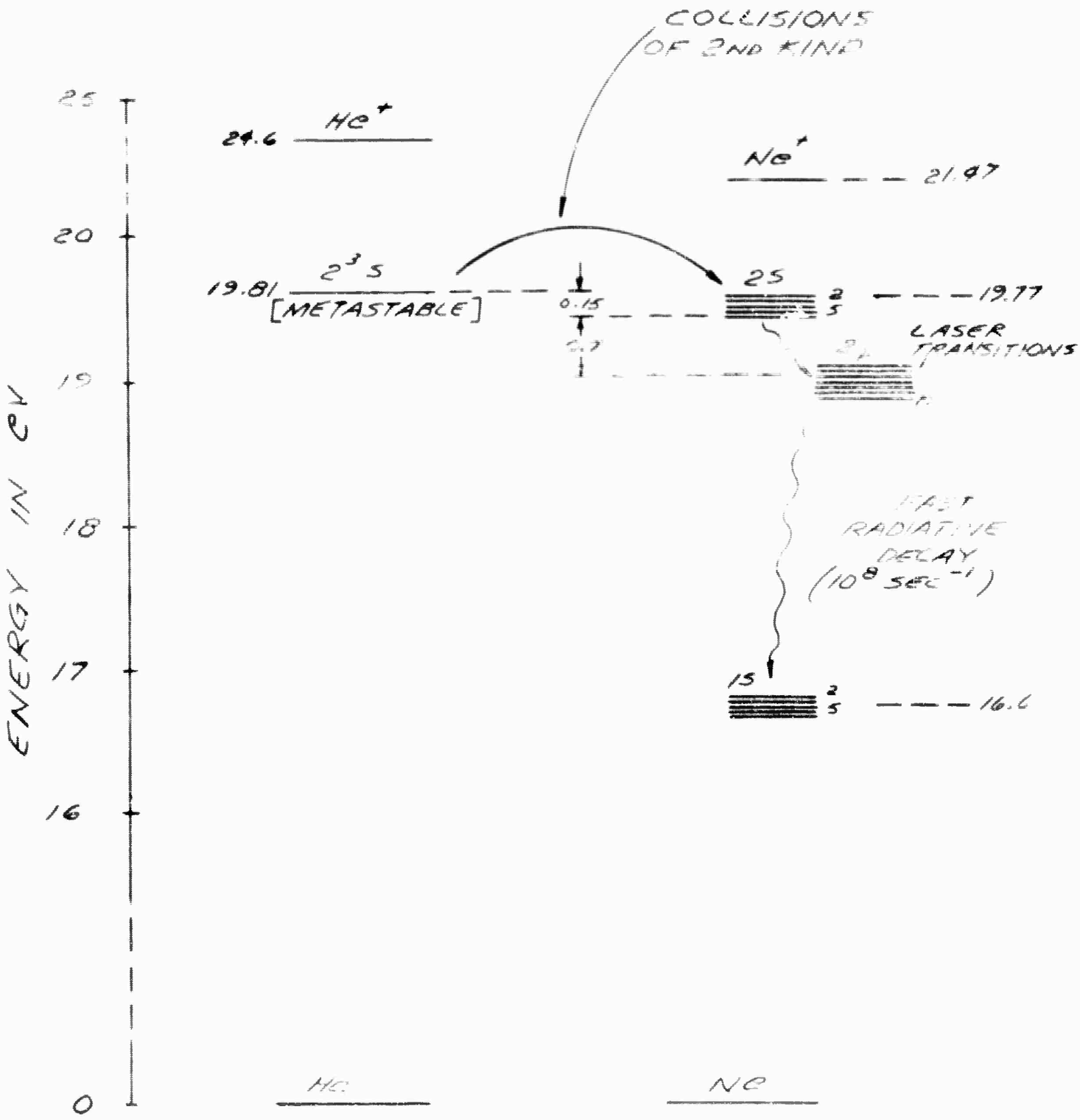

EXCITATION OF LASER TRANSITION IN NEON BY DISCHARGE IN He-Ne MIXTURE

Figure 3.1

subtle form of rf pick-up.

Though the double-beam apparatus has equal optical path lengths through the two beams, the two paths suffer different amounts of vignetting. That is, a change in the spatial distribution of the discharge in the source lamp, caused by pick-up from the rf power exciting the amplifier tube, can cause a change in the relative amount of light in the two paths. This change in angular distribution of source light manifests itself as an unbalancing of the optical bridge which was balanced in the absence of rf excitation to the amplifier tube.

Since it was found that extremely small amounts of rf pick-up could cause an apparent gain equal to the gain we were trying to measure we abandoned the double-beam system for the double modulation system which is relatively resistant to rf pick-up.

In the double modulation scheme, the source lamp is modulated at one frequency and the discharge in the amplifier tube is modulated at a different frequency. If there is either absorption or amplification there will be a mixing of the two modulation frequencies, producing the sum and difference frequencies in the absorbed or amplified wavelengths. The strength of the output signal at the difference frequency for example, will be proportional to the source intensity I_o and the amount of amplification or absorption taking place.

In the experiment performed here the source light was modulated at 1320 cps and the amplifier cell was modulated at 1 kc. This generated a difference frequency of 320 cps which was detected by a phase sensitive detector locked to an externally mixed portion of the two modulating signals (see block diagram of double-modulation apparatus, Figure 32).

We measure the difference between the source lamp signal I_o and the light leaving the 80 cm amplifier tube, $I_o e^{\alpha L}$.

Thus

$$\text{Signal} = I_o e^{\alpha L} - I_o \approx I_o \ \alpha L.$$

In our apparatus the minimum noise, N, is 6×10^{-12} watts/cycle. The minimum detectable signal occurs when signal equals noise, or when $I_o \alpha L = N$. Thus the minimum detectable amplification coefficient, α, is given by:

$$\alpha = N/I_o L = \frac{6 \times 10^{-12} \text{ watts/cycle}}{I_o \times 80 \text{ cm}} .$$

Our minimum detectable value of α for $\lambda = 1.1523\mu$ is determined by the relation $\alpha L = 1/4\%$, or $\alpha = 3 \times 10^{-5} \text{ cm}^{-1}$.

With $I_o = 2.4 \times 10^{-9}$ watts, that is 400 x N.

The sensitivity to rf pick-up described here is not inherent in double-beam systems. If one were to take sufficient pains to construct truly equivalent optical paths for both beams, then no change in source

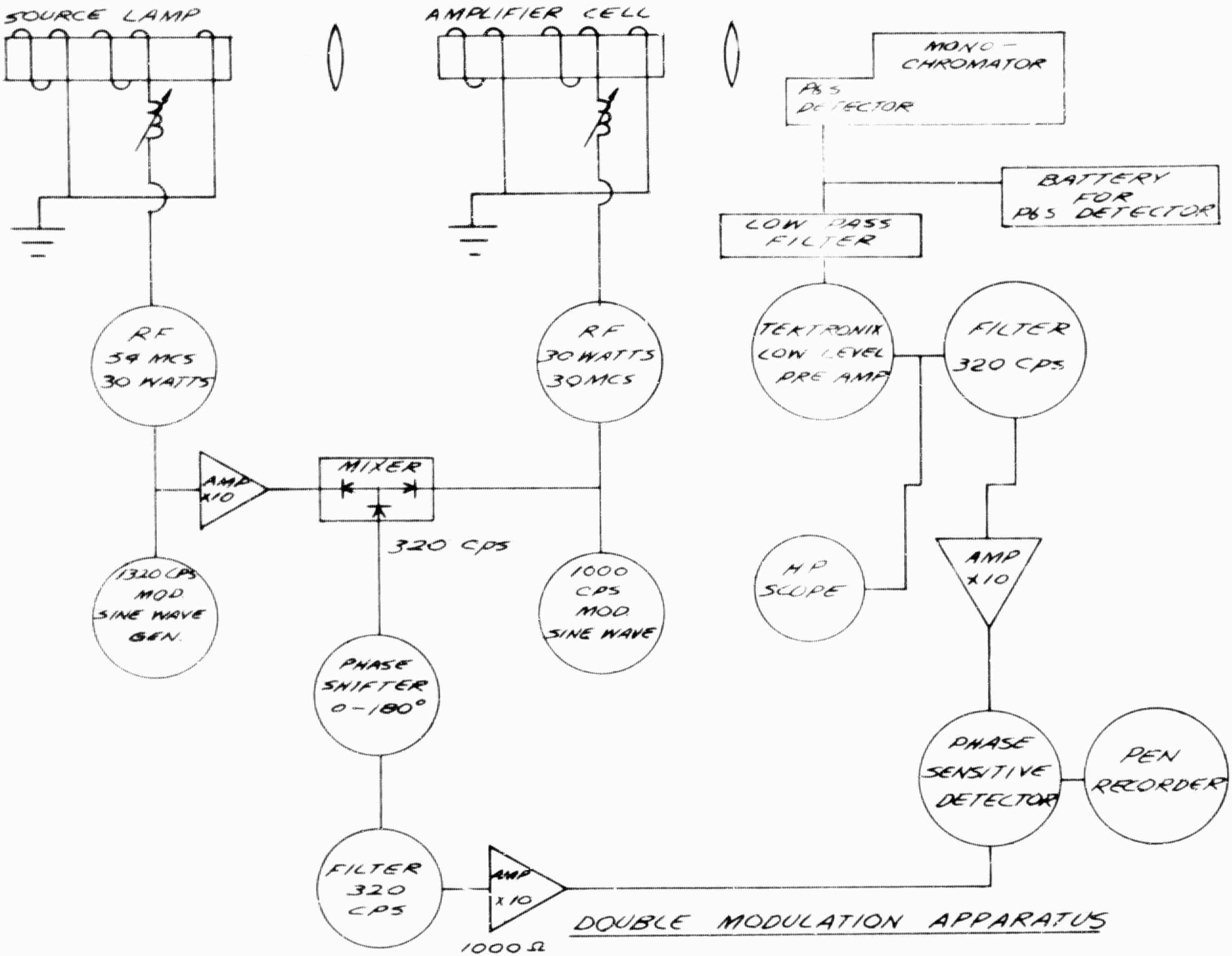
SOURCE LAMP
AMPLIFIER CELL
MONO-
CHROMATOR
PbS
DETECTOR
BATTERY
FOR
PbS DETECTOR
LOW PASS
FILTER
RF
54 MCS
30 WATTS
RF
30 WATTS
30 MCS
TEKTRONIX
LOW LEVEL
PRE AMP
FILTER
320 CPS
AMP
X10
MIXER
320 CPS
1320 CPS
MOD
SINE WAVE
GEN.
1000
CPS
MOD
SINE WAVE
HP
SCOPE
AMP
X10
PHASE
SHIFTER
0-180°
PHASE
SENSITIVE
DETECTOR
PEN
RECORDER
FILTER
320
CPS
AMP
X10
1000 Ω
DOUBLE MODULATION APPARATUS

Figure 3.2

lamp brightness would unbalance the optical bridge once balanced. In such a system one would not be permitted to use an iris to balance the bridge since the iris would necessarily be an aperture stop for one path which would introduce vignetting which would not have its counterpart in the other path.

Rather than attempting to further shield the source lamp or provide a variable attenuator of constant aperture we elected to construct the double-modulation system.

In the double beam system one loses half the available signal at the half silvered mirror where the two beams are recombined, since half of each beam is thrown away.

In a double modulation and single modulation beam system the source intensity, I_o, is given by:

$$I_o = \frac{A}{2}(1+\sin\theta_1).$$

The modulated absorption coefficient in the double modulation system is $\frac{B}{2}(1+\sin\theta_2)$. The unmodulated absorption coefficient is simply B. In the latter case the result of absorption is $I = B \times \frac{A}{2}(1+\sin\theta_1)$. The detected ac signal is

$$I_{detected} = \frac{AB}{2}\sin\theta_1.$$

In the double modulated system the result of absorption is $\frac{A}{2}(1+\sin\theta_1) \times \frac{B}{2}(1+\sin\theta_2)$. The detected ac signal is

$$I_{detected} = \frac{AB}{8} \cos(\theta_1-\theta_2).$$

Thus compared with the unmodulated system the detected double modulation signal loses half its light from the loss of one sideband i.e. $\cos(\theta_1+\theta_2)$ and it loses half of what is left simply beaause the absorber is off half the time. In our experiment we find a ratio of 4.3 rather than 4.0. This is undoubtedly due to the fact that neither modulation was truly sinusoidal. With the double modulation system we observed 1.5% gain in a mixture of 100μ Ne and 1 mm He in an 80 cm long 1.5 cm diameter discharge region, with 30 to 50 watts excitation. The source tube was 15 cm long and 1.5 cm diameter.

Gain disappeared when the rf power exceeded 50 watts, and of course no signal was seen with source or amplifier discharge alone. Absorption was seen when the He partial pressure was reduced, keeping the same total pressure.

After assuring ourselves that a sealed off tube would continue to show gain after a few days of idleness we went on to construct a He-Ne oscillator.

2.1.2 Oscillation Experiment

After measurement of gain in the He-Ne amplifier experiment, work was started on oscillators which will make use of the crossed roof and cube-corner interferometer principle. The great stability, and ruggedness of these devices is described in the Optical Devices section of this report.

Before putting any of the retroreflecting optics in it was decided to build a LASER to use as a standard against which to compare the retroreflector cavities. For this first LASER we are using a modification of the confocal cavity described by Boyd and Gordon[13]. The modified cavity has vastly reduced diffraction losses compared with the plane Fabry-Perot cavity, and the line-up of the elements is also much less critical. The results of Boyd and Gordon can be interpreted as showing that a cavity with one of the spherical mirrors replaced by a flat located such that the distance between the flat and spherical mirror is less than the focal length of the sphere will have the desired properties. In our system the separation is 120 cm and the focal length of the sphere is 195 cm.

Oscillation was observed at $\lambda = 1.1528\mu$ with approximately fifty microwatts in the LASER beam. Threshold for oscillation was

(13) G. D. Boyd and J. P. Gordon, Bell System Tech. Journal 40 489 (1961)

two watts of rf power into a twenty centimeter length discharge. One can estimate from this a gain of 9% in a meter.

2.1.2.1 Design of Oscillator Apparatus

The He-Ne LASER was constructed with internal reflectors. The reflectors are a 1.95 meter focal length spherical silvered mirror and an optical flat with multi-layer coating. See Figure 3.3 and 3.4

There is 120 cm between reflectors and 90 cm of 7mm i.d. quartz discharge tube. The spherical mirror and flat each sit in a holder connected to the discharge tube by a stainless steel b[illegible]s. The sphere is adjustable to one minute of angle with the system evacuated.

Spacing between mirrors is determined by two aluminum I-beams secured to a granite surface plate.

Light is collected from the device through the 0.8% transmitting multi-layer and the 1/20-wave flat vacuum window. Both ends of the device are demountable with knife edge seals biting into copper gaskets.

The LASER is filled from an all metal gas handling system using a cryogenic fore pump and a five liter per second ion pump. The shorter diffusion path (for a 7 mm diameter tube, rather than a 1.5 mm tube) for the neon $^1s_5$ metastables to be de-excited by collisions with

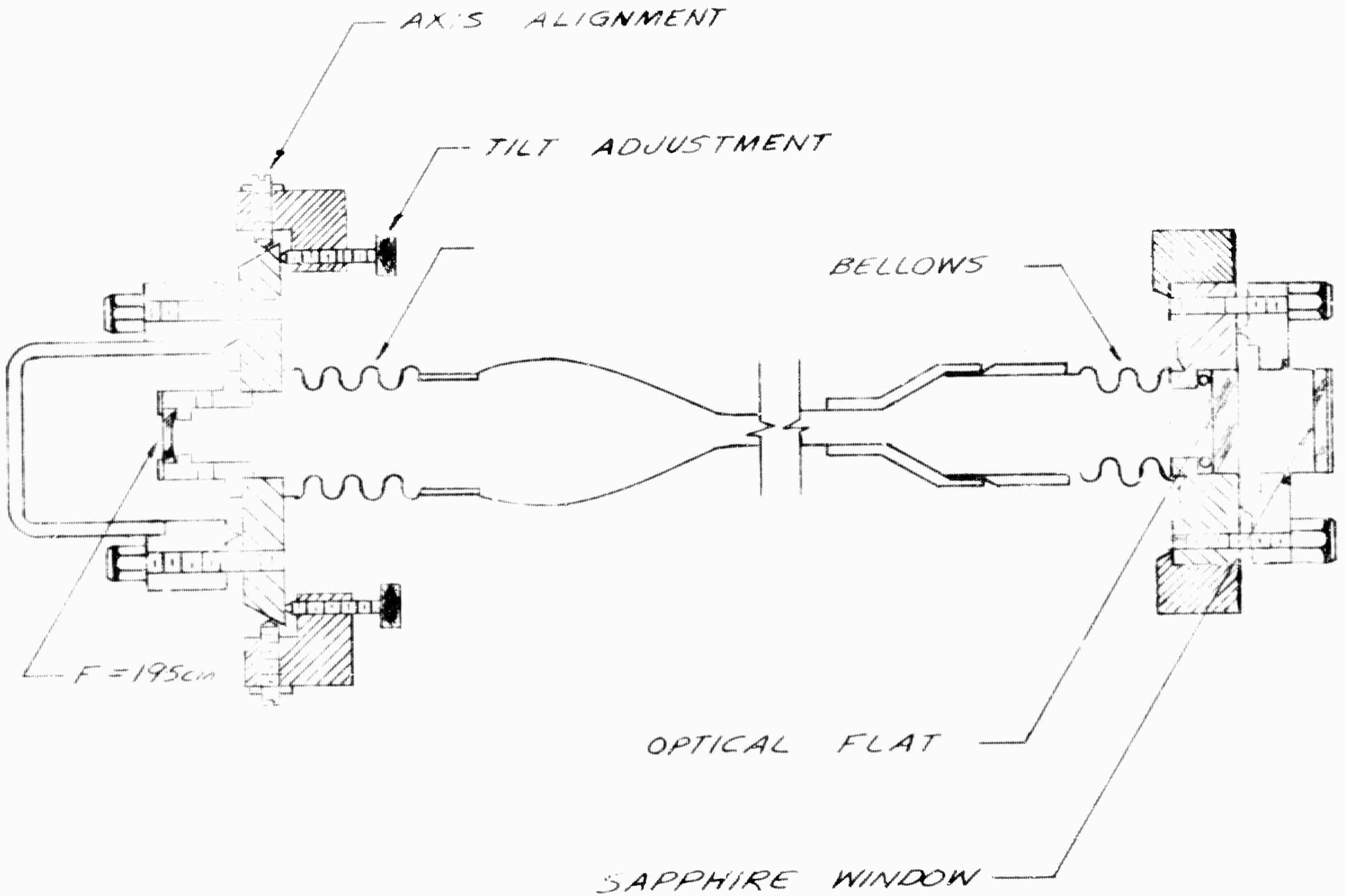

Figure 3.3

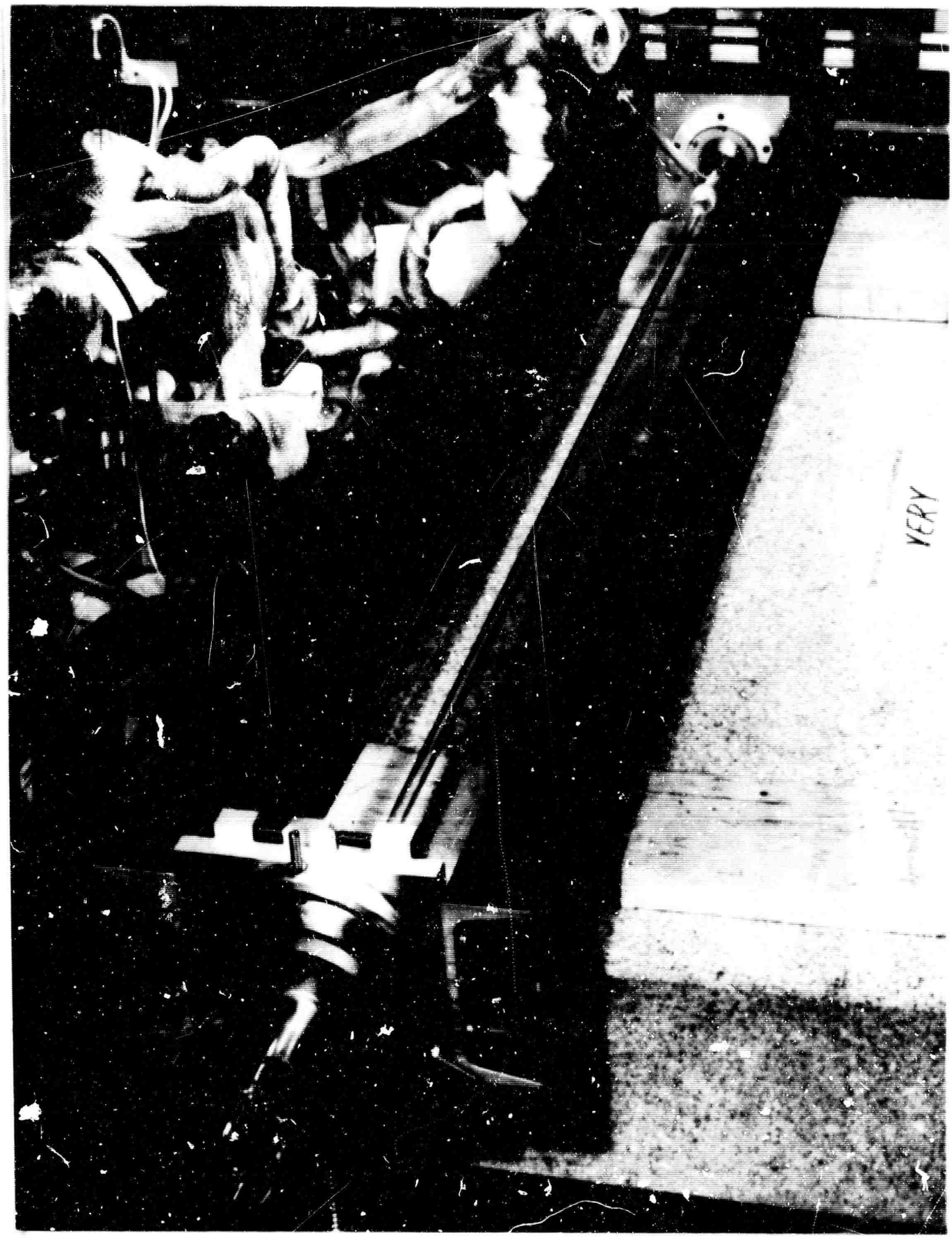

Helium-Neon Oscillator
Figure 3.4
TECHNICAL RESEARCH GROUP

the walls permitted higher transfer rates to be employed in the pumping process. Thus the neon partial pressure was raised to 170 microns, the helium partial pressure to 1.5 mm. Pressures of He and Ne are measured with a Magnevac gauge calibrated with a McLeod gauge on another vacuum system. These precautions assure that there will be no contaimination of the discharge by Hg or organic materials from oil seale fore pumps or diffusion pumps.

It has been found that an oil sealed fore pump may preceed the cryogenic fore pump to increase the pumping speed of the system for helium. This combination can bring the entire system to 1×10^{-5} mm Hg with no other pump operating. With the ion pump operating the ultimate pressure for the filling system is 2×10^{-8} mm Hg.

2.1.3 On the Question of Adding Argon to the He-Ne LASER Discharge

The suggestion has been made by A. Javan[14] that the addition of argon to the He-Ne LASER discharge would most probably give increased gain. This is predicated on the claim by W. Bennett[15] and A. Javan[14] that the major process for populating the lower levels of the LASER transitions, (the 2P configuration) is electron excitation of the Ne $1s_5$ metastable atoms upwards to the 2P states.

The following is merely a comparison of the various transfer rates to show that the suggestion is plausible.

The basic transfer rate for pumping of the upper LASER levels, (the 2s configuration) is given by W. Bennett[15,16].

$n_{Ne}\ \bar{\sigma}_{He\text{-}Ne}\ \bar{v} = 16{,}000\ sec^{-1}$ for neon pressure of 100 microns

where n_{Ne} is population of neon atoms in atoms/cm^3

$\bar{\sigma}_{He\text{-}Ne}$ is average cross-section for collisions of the second kind exciting the Ne 2s configuration in cm^2.

$\bar{v}$ is the mean relative velocity of He with respect to Ne in cm/sec.

---

14) A. Javan, talk at Gaseous Electronics Conference, 10-13-61.
15) W. Bennett, talk at TRG, Inc. 2-15-61.
16) Recalculated approximately by G. Grosof from data by A. Phelps

The transfer rates for ionization of argon by He and Ne metastable atoms are respectively,[17]

$$n_A \bar{\sigma}_{He-A} \bar{v} = n_A (9.7 \times 10^{-17} \text{ cm}^2) (13.2 \times 10^4 \text{ cm/sec})$$

$$= n_A \, 12.8 \times 10^{-12}$$

$$n_A \bar{\sigma}_{Ne-A} \bar{v} = n_A (26 \times 10^{-17} \text{ cm}^2) (6.7 \times 10^4 \text{ cm/sec})$$

$$= n_A \, 17.4 \times 10^{-12}$$

We shall ignore the direct de-excitation of the upper LASER levels, (the 2s configuration) by the argon atoms.

As an upper limit to the amount of argon that may be added in a constructive fashion, we require that

$$\text{Transfer Rate He} \rightarrow \text{A} \leq \text{Transfer Rate He} \rightarrow \text{Ne}$$

As a lower limit to the amount of argon that may be added in a constructive fashion, we require that

$$\text{Transfer Rate Ne} \rightarrow \text{A} \geq \frac{1}{T_D}$$

where T_D is the diffusion time of the Ne $1s_5$ metastable atoms to the walls. Phelps[18], et al have made a clear case that in the pressure range of the LASER discharge, and for the power density

17) Cross-sections from M. A. Biondi, Phys. Rev. 85, 653 (1951)
18) A. V. Phelps, Westinghouse Research Laboratories, Scientific Paper 6-94439-6P3

of the discharge, the major relaxation method for the $1s_5$ metastables is by diffusion - limited collisions with the walls.

$$T_D = \frac{\Lambda^2}{D_m} = 235 \times 10^{-6} \text{ seconds}$$

where $\Lambda^2 = \frac{R^2}{(2.4)^2}$ is the characteristic diffusion length squared for a long cylinder of radius R = 0.75 cm in our case.

D_m is obtained from Phelp's[19] general expression.

$D_m = 413 \text{ cm}^2/\text{sec}$. It may be noted that the diffusion coefficients for excited atoms differ from those for unexcited atoms.

The inequalities require

I. $n_A \, 12.8 \times 10^{-12} \text{ sec}^{-1} \leq 16{,}000 \text{ sec}^{-1}$

$$n_A \leq 12.5 \times 10^{14} \text{ atoms/cm}^3$$

II. $n_A \, 17.4 \times 10^{-12} \text{ sec}^{-1} \geq \frac{1}{235 \times 10^{-6} \text{ sec}}$

$$n_A \geq 24.5 \times 10^{13} \text{ atoms/cm}^3$$

$\therefore \quad 2.45 \times 10^{14} \text{ atoms/cm}^3 \leq n_A \leq 1.25 \times 10^{15} \text{ atoms/cm}^3$

converting to partial pressure of argon P_A, we obtain

$$7.56\mu \leq P_A \leq$$

---

(19) A. V. Phelps, Phys. Rev. 114, 1011 (1959)

It is prudent to add as little argon as possible, because of the argon-induced perturbation to the high-energy tail of the electron distribution. The LASER is dependent on the supply of electrons of energy greater than the 20 electro volt threshold for excitation of the "pumping" He 2^3s_1 metastable atoms.

One may calculate the electron temperature from the empirical ionization by electrons in the discharge and from various other parameters, following the method of von Engel[20]. For pure gases a solution of a universal nature is given by

$$\frac{c^x}{\sqrt{x}} = 1.2 \times 10^7 \ (epR)^2 \qquad (3.1)$$

where $x = \frac{e \sqrt{\ }}{\ c}$

$$c = \sqrt{\frac{a \sqrt{V_i}}{K^+ \rho}}$$

e = electron charge

V_i = ionization potential

k = Boltzman's constant

T_e = electron temperature defined by $1/2\ mv^2 = 3/2\ k\ T_e$

a = ionization efficiency

K^+ = ionic mobility

p = pressure

R = tube radius

---

(20) A. von Engel "Ionized Gases", Oxford p.215 (1955)

for R = 0.75 cm, and a graphical solution to equation (3.1), we obtain

GAS	Rcp	T_e
pure He	3×10^{-3}	21,000°K
pure Ne	4.5×10^{-3}	17,000°K
pure A	3.0×10^{-2}	10,500°K

We estimate the He-Ne LASER electron temperature as $T_e \approx 20{,}000°K$ or $T_e \approx 1.7$ electron volts, and that of the He-Ne-A semi-Penning mixture as $T_e \approx 15{,}000°K(?)$ $T_e \approx 1.3$ ev. The relevant quantity is f, the fraction of electrons of energy greater than 20 electron volts. This requires the integration of the Maxwellian energy distribution:

$$f_{He\text{-}Ne} = \int_{\left(\frac{20}{1.7}\right)}^{\infty} \frac{2\,Ne}{\sqrt{\pi}} \left[\left(\frac{E}{1.7}\right)^{1/2} e^{-\frac{E}{1.7}} \right] d\left(\frac{E}{1.7}\right) \approx 10^{-4}$$

$$f_{He\text{-}Ne\text{-}A} = \int_{\left(\frac{20}{1.3}\right)}^{\infty} \frac{2\,Ne}{\sqrt{\pi}} \left[\left(\frac{E}{1.3}\right)^{1/2} e^{-\frac{E}{1.3}} \right] d\left(\frac{E}{1.3}\right) \approx 10^{-6}$$

where E = electron energy in electron volts

Ne = total number of electrons/cm^3

It is thus possible that if the estimate of the drop in electron temperature is as severe as chosen, the production rate for new He metastables would be severely decreased.

2.2 Xenon-Krypton System

Because of the paucity of knowledge of the relevant parameters, the Xe Kr system has been studied in a very empirical fashion in the laboratory. The Kr $1s_5$ metastable state is known from atomic beam results to have a free state lifetime greater than 1 millisecond.

The states for which energy level coincidences exist with resonance energy defect E less than ambient kT = 209 cm^{-1} are listed below.

Kr	Xe	$E = E_{Kr} - E_{Xe}$	Possible LASER Transition	
$1s_5$	$2p_5$	- 147 cm^{-1}	2p - 1s	0.9 microns
$1s_5$	$3d_5$	+ 15 cm^{-1}	3d - 2p	4.0 microns
$1s_4$	$3d_4$	- 53 cm^{-1}	3d - 2p	4.0 microns
$1s_3$	$2s_5$	- 3 cm^{-1}	2s - 2p	1.5 microns

The most favored transition for possible LASER action is in the 4.0 micron region. Because of the added difficulty to an already complex experimental set up, no attempt was made to study the 4.0 micron transitions. A careful search for enhancement of Xe emission yielded only positive results for the 2p - $1s_4$ transitions. No correlation between the amount of enhancement and the resonance energy defect could be made for the transitions

$2p_6 - 1s_4$

$2p_7 - 1s_4$

$2p_9 - 1s_4$.

An average of five times the expected amount of emitted light was measured, over the average of three control transitions

$3p_7 - 1s_2$

$2p_3 - 1s_2$

$4d_3 - 2p_{10}$

in a mixture of 8 microns of xenon and 100 microns of krypton.

A series of experiments was performed of absorptions out of the krypton $1s_5$ metastable state as a function of xenon partial pressure to determine if indeed, energy was being transferred to the xenon system.

For three transitions out of the krypton $1s_5$ state, the increase of xenon partial pressure from 1 micron to 10 microns caused an average 11% decrease in absorption percentage. The slight lowering of electron temperature by the increase of xenon pressure did not change the emission of various krypton lines examined in emission, so that one may conclude that the depopulation was caused by collisions of the second kind with xenon atoms.

The basic transfer rate for exciting the xenon atoms by the krypton $1s_5$ metastable is

$$n_{Xe} \; \bar{\sigma}_{Kr \rightarrow Xe} \; \bar{v} = R_1 \qquad (3.2)$$

where

n_{Xe} =number of Xe atoms (cm^{-3})

$\bar{\sigma}_{Kr-Xe}$=average cross-section in cm^2

$\bar{v}$ =average relative velocity of Xe-Kr(cm/sec).

Although we do not know the cross-section for collisions of the second kind, we may make an estimate following aruguments of the type used by Massey & Burhop[21], and Rautian and Sobelman[22]. Additionally the experimental data collected by Zemansky supports the argument.

One may make a guess as to the upper limit on the cross-section for exact resonance between identical atoms undergoing optically allowed transitions as

$$\sigma_{max} \sim \frac{2\pi^3 \mu^2}{vh} ,$$

where μ is the dipole moment $\sim 10^{-18}$ e.s.u.

v is the relative velocity of atom-atom system

h is Planck's constant .

---

(21) Massey & Burhop "Electronic and Ionic Impact Phenomena"p.444 (Oxford 1952)

(22) S. Rautian and J. Sobel'man, J. Exptl. Theoret. Phys.(USSR) 39, 217 (1960)

Thus:

$$\sigma_{max} \sim 2.3 \times 10^{-13} \text{ cm}^2.$$

From a correspondence principle argument, when an energy defect exists, one requires that

$$\frac{a\Delta E}{hv} \sim 1,$$

where a = range of atom-atom interaction $\sim 10^{-8}$ cm

ΔE = energy defect = .018 ev,

in order to have a cross-section for transfer of excitation somewhere in the neighborhood of gas kinetic. Using these values of the parameters and $v \sim 4 \times 10^4$ cm/sec, one finds that the condition is satisfied.

Thus the cross-section is possibly 10^{-15} cm^2 for Kr $1s_5 \rightarrow Xe^2 p_5$. A similar argument for Kr $1s_5 \longrightarrow$ Xe $3d_5$ suggests 10^{-14} cm^2 as a possible cross-section. A rigorous analysis following the work of Buckingham and Dalgarno[23], or Stueckelberg[24] cannot be done because of the lack of knowledge of the interaction potentials of the metastable atom - ground state atom systems.

---

(23) R. Buckingham & A. Dalgarno, Proc. Roy. Soc. A213, 327 and 506, (1952)
(24) E. Stueckelberg, Helv. Acta Physica 5, 369 (1932)

It is thus the case that the Kr $1s_5$ preferentially excites the 3d configuration, at least by a factor of ten. However by cascade from the 3d to 2p configuration, a contribution to enhancement is certainly obtained.

As a limit on useable transfer rates, one should examine the predictable rate of de-exciting the Kr $1s_5$ by diffusion-limited collision with the wall. The diffusion constant for the metastable Kr atom has not been measured (to our knowledge) but one may extrapolate from the known diffusion cross sections for the other rare gas atoms in their metastable states. In general, one may use the rigid sphere model to calculate the diffusion of one rare gas metastable atom in itself or in another rare gas, if one increases the diameter of the metastable atom by 2.2 times the unexcited diameter. Then:

$$D_{12} = \frac{0.88\sqrt{v_1^2 + v_2^2}}{3\pi\,(n_1+n_2)\,(1/2(S_1 + S_2))^2} \quad \text{in cm}^2/\text{sec}$$

The coefficient for self-diffusion is obtained by letting all quantities with subscript 2 equal those with subscript 1.

where D_{12} = diffusion coefficient

v_i = average velocity in cm/sec

n_i = number of atoms of type 1

S_1 = atomic diameter cm

After one has calculated the diffusion coefficient of the Kr $1s_5$ atom in pure krypton and in pure xenon, then one may extend Blanc's law[25][26] to obtain the coefficient of diffusion in a mixture:

$$\frac{1}{D_{Kr\text{-}Xe}} = \frac{f}{D_{Kr}} + \frac{1-f}{D_{Xe}}$$

$$f = \frac{\text{number of Kr atoms}}{\text{total number of atoms in mixture}}$$

D_{Kr} = diffusion coefficient of Kr $1s_5$ in pure Kr

D_{Xe} = diffusion coefficient of Kr $1s_5$ in pure Xe

Summarizing for the conditions relevant to the experiment

	D
Kr $1s_5$ in 100μ of Kr plus 10μ of Xe	240 cm^2/sec
Kr $1s_5$ in 100μ of Kr plus 1μ of Xe	250 cm^2/sec
Xe $1s_5$ in 100μ of Kr plus 10μ of Xe	160 cm^2/sec
Xe $1s_5$ in 100μ of Kr plus 1μ of Xe	170 cm^2/sec

One wishes to examine the reciprocal of the diffusion time for the pumping Kr metastable. For the cylindrical geometry employed

$$T_D = \frac{\Lambda^2}{D_m}$$

T_D = diffusion time in sec

$\Lambda = \frac{R}{2.4}$ in cm

(25) A. V. Phelps, Phys. Rev. 114, 1011 (1959)
(26) T. Holstein, Phys. Rev. 100, 1230A (1955)

$$T_D = \frac{.044 \text{ cm}^2}{250 \text{ cm}^2/\text{sec}}$$

$$T_D = 176\mu \text{ sec}$$

One can put a lower bound on useful $\sigma_{Kr\text{-}Xe}$ from the requirement that $R_1 \geq \frac{1}{T_D}$. From equation (3.2)

$$\sigma_{Kr\text{-}Xe} \geq \frac{1}{n_{Xe}\, \bar{v}\, T_D}$$

$$\sigma_{Kr\text{-}Xe} \geq \frac{1}{3.2 \times 10^{13} \text{ cm}^{-3}\ 4 \times 10^{4}\ \frac{\text{cm}}{\text{sec}}\ 176 \times 10^{-6} \text{ sec}}$$

$$\sigma_{Kr\text{-}Xe} \geq 4.4 \times 10^{-15} \text{ cm}^2$$

This shows that we are pretty much at the limit as regards reducing the tube diameter with the partial pressures employed. One may roughly estimate the number of excited $2p_5$ xenon atoms from extrapolating "typical" metastable populations in "typical" discharges[27].

$$n^*_{Kr}\, R_1 = \frac{n^*_{Xe}}{T}$$

where n^*_{Kr} is number of Kr $1s_5$ atom cm^{-3}

n^*_{Xe} is number of excited $2p_5$ Xe

T = Xe $2p_5$ lifetime, guessed as 10^{-7} sec

(27) V. Hughes, G. Tucker, E. Rhoderick and G. Weinreich, Phys. Rev. 91, 828 (1953)

$n^*_{Kr} \approx 10^{-4}\ n_{Kr}$ where n_{Kr} is population of normal krypton atoms

$n^*_{Kr} \approx 10^{-4}\ \ 3.22 \times 10^{15}\ cm^{-3}$

$n^*_{Kr} \approx 3.22 \times 10^{11}\ cm^{-3}$

$\therefore\ n^*_{Xe} \approx (3.22 \times 10^{11}\ cm^{-3})\ (5600\ sec^{-1})\ (10^{-7}\ sec)$

$n^*_{Xe} \approx 1.8 \times 10^{8}\ cm^{-3}$

Because the lower level of the possible LASER transitions $2p\text{-}1s_4$ is both light-trapped above certain pressures, and is populated by collisions from the populous Xe $1s_5$ metastable, a small diameter tube is required, so as to allow resonance photons $1s_0$ - $1s_4$ to escape to the walls and also to quench Xe $1s_5$ metastables.

The trapping lifetime is defined from Holstein, as

$$T_{trapping} \approx \frac{T_{natural}}{g}$$

where g is the escape factor, the number of absorptions and emissions the average resonance photon makes prior to its collision with the walls. For cylindrical symmetry,

$$g = \frac{1.60}{k_o R\ \sqrt{\pi}\ \sqrt{\log k_o R}}$$

where k_o = absorption coefficient at the center of a Doppler broadened line.

R = radius of cylinder.

A plot of theoretical lifetimes-for-trapping versus pressure is given for two choices of natural lifetime. An examination of the graph* tells us that only at xenon partial pressures less than several microns will one find a chance of inverting the 2p - $1s_4$ populations.

A series of experiments was performed of absorptions out of the Xe $1s_4$ and $1s_5$ states to the 2p configuration, in an effort to obtain knowledge of the trapping lifetimes, and as a corollary, the natural lifetimes. It was found that at 1 micron of xenon in 100 microns of krypton, the average absorption out of the $1s_4$ to 2p states for four transitions was 2.1%, the average for three transitions from the $1s_5$ state to 2p states was 42.9%. At higher pressures the absorption coefficient was so large from both the $1s_4$ and $1s_5$ states that meaningful[28] measurements could not be made. This clearcut evidence tells us that we are in the region where an inversion may be possible.

---

(28) J. Dixon & F. Grant, Phys. Rev. 107, 118 (1957)

* See Figure 3.5

Figure 3.5

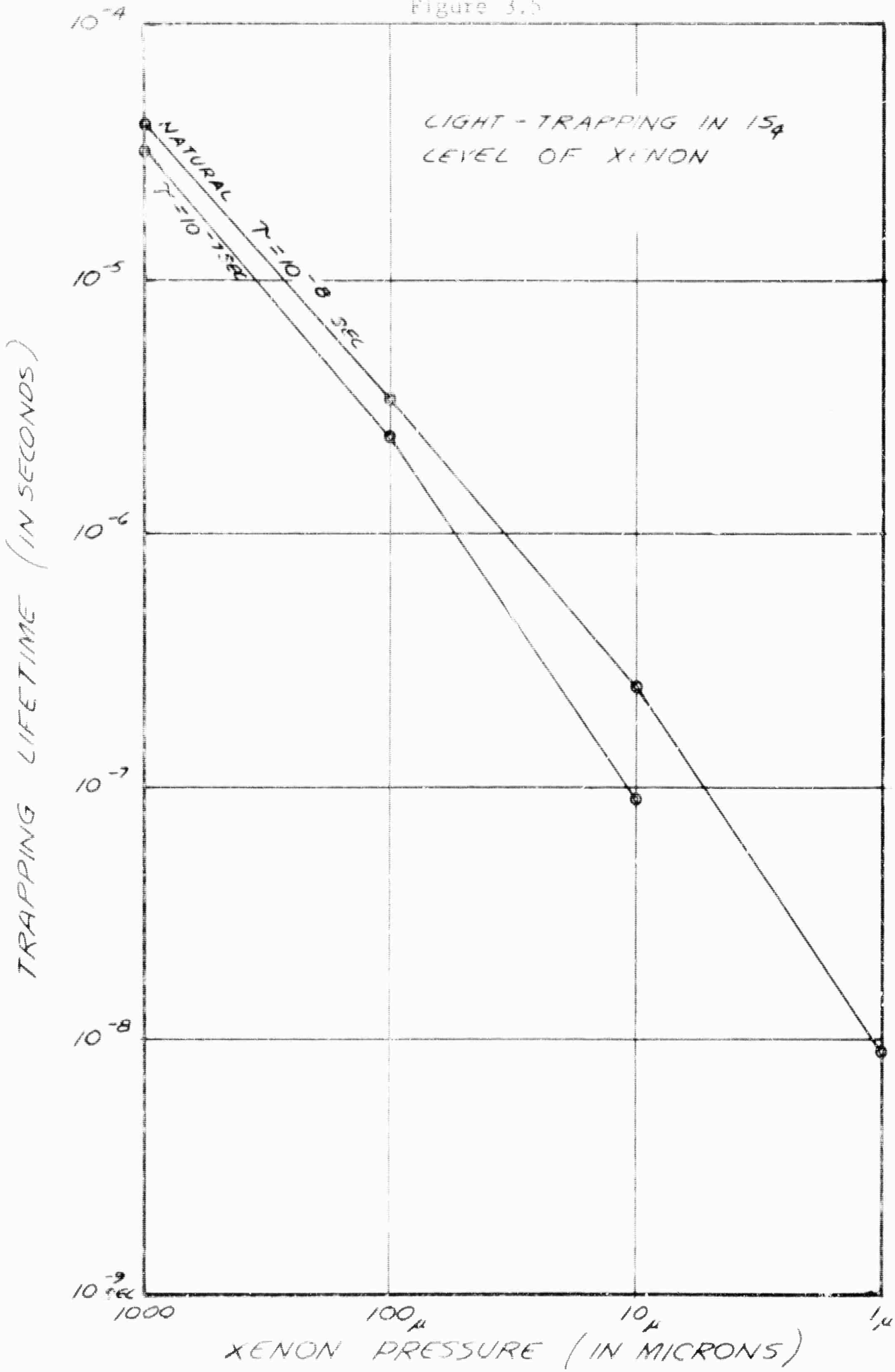

TECHNICAL RESEARCH GROUP

2.2.1 Double Beam Apparatus

In this experiment we wished to measure the relative populations of the xenon $1s_4$ (light trapped) and the $1s_5$ metastable states. To do this we needed a system that would allow measurements to 1% absorption.

If light of a wavelength corresponding to a transition out of the metastable state up to some higher state, is directed through a volume of excited gas, a certain percentage of atoms in the lower state can be excited to the upper state with the associated absorption of the photon that did the exciting.

Thus to measure the populations, we need a source of light at the appropriate wavelength, a volume of excited gas to direct it through and a means for measuring the change in the light transmitted.

Light from a 20 cm long source lamp 8 mm i.d. is alternately sent through the 1 meter absorber tube 14 mm i.d. and through a parallel air path. This is accomplished by means of a rotating sectored mirror set at 45° to the source lamp - absorber tube common axis. The intensities at the detector from the air path and absorber path are made equal by means of an iris diaphragm in the air path. The phase sensitive detector is locked to the source lamp chopping frequency and does not respond to the dc signal generated by the spontaneous

emission from the absorber tube. See block diagram of double-beam apparatus, Figure 3.6.

The lines of interest were all in the 8000Å to 10,000Å region and were detected with an S1 response phototube.

The source tube and absorber tube are attached to the same vacuum system so that they can be filled with the same Xe-Kr gas mixture.

In the experiments showing the depopulation of the Kr $1s_5$ by collision with the Xe 2p states, the Xe pressure was controlled with a liquid nitrogen cold trap connected to the absorber tube. In the Xe-Kr mixture the partial pressure of Xe can be conveniently changed from 10μ to 1μ and back to 10μ by the addition and removal of liquid N_2 in the trap.

2.3 Zinc-Zinc System

2.3.1 Theoretical

Collisions of the second kind in a 3-component gas mixture can effectively populate the upper of two LASER levels in the atoms of one component. Helium [illegible] selectively excite a sufficient population in an upper level of admixed neon (see Figure 3.1) to give an observed coherent gain coefficient, $\alpha_c \approx 5\%$/meter.[29] In such media a severe inherent limitation exists on achievable excess upper state

(29) A. Javan, W. R. Bennett and D. R. Herriott, Phys. Rev. Letters 6, 106, (1961)

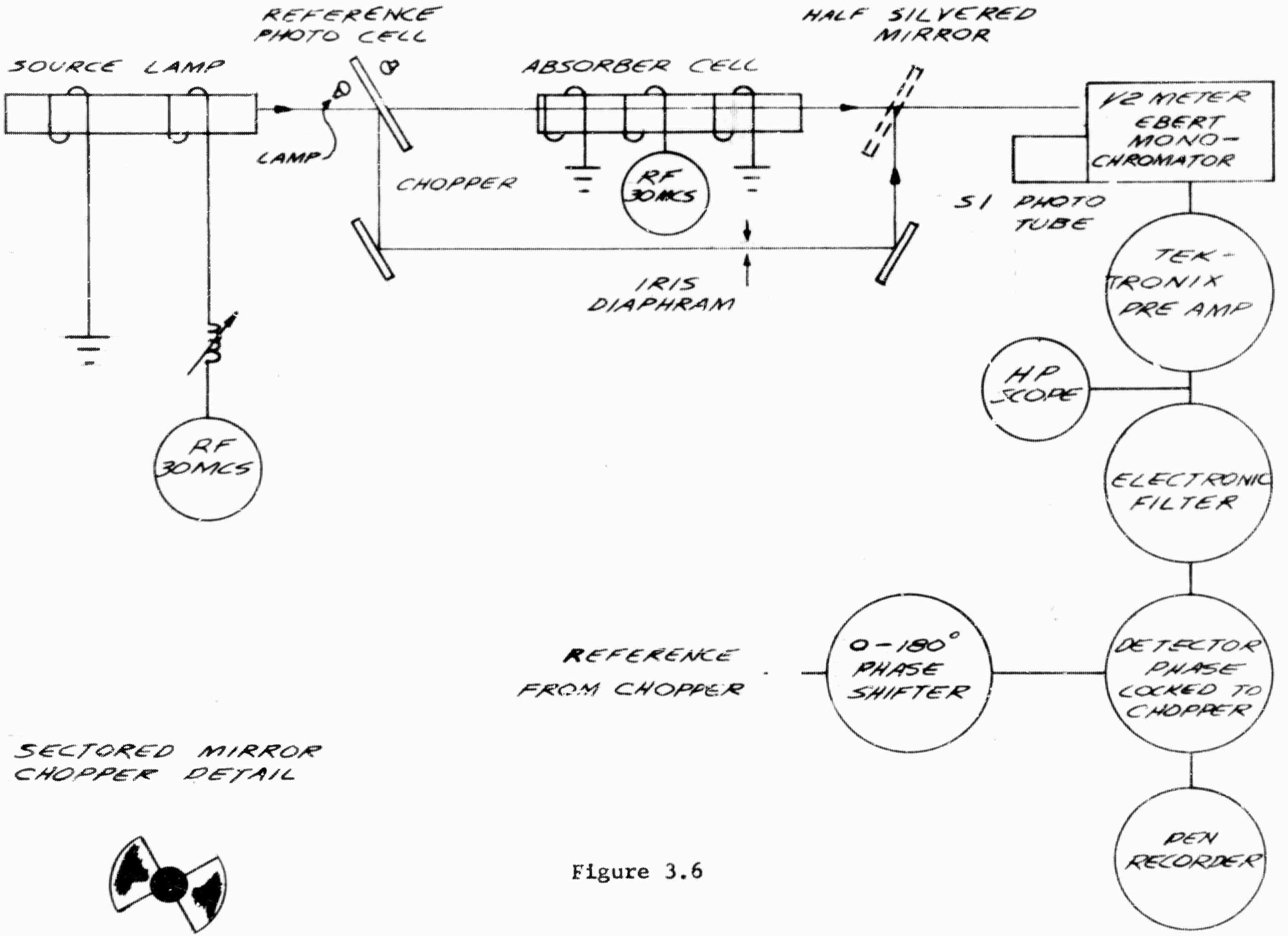

Figure 3.6

DOUBLE BEAM APPARATUS

population density and therefore gain, efficiency ($\lesssim 0.03\%$), and power output ($\sim$ 10 mw) because,

1. inevitably the lower level atoms (neon) decrease the electron temperature, and therefore the maximum population, of the impinging metastables (helium).

2. since the lower LASER level is below the metastable level, direct electron excitation of this lower level tends to reduce or preclude an excess upper state population.

These drawbacks of the two component gaseous medium are side-stepped in a single component gaseous discharge medium, using a different collisional process: Let two atoms of the same kind be in metastable or light-trapped resonance levels. If a higher level exists with energy equal to the sum of metastable energies, there is a high probability that a collision will leave one atom doubly excited while the other returns to the ground level[30].

The zinc atom has an energy level structure particularly favorable for LASER excitation by self-collisions of the second kind. An energy level diagram of zinc (Figure 3.7) shows that the collision processes $4^3P_n - 4^3P_m \longrightarrow 6^3S_1 + 4^1S_o$ n, m = 0, 1 and 2 are energetically probable; the energy defect in the worst case is less than kT. Since

(30) Such a two-step excitation process was suggested for mercury in TRG Proposal No. P-329 to ARPA December, 1958.

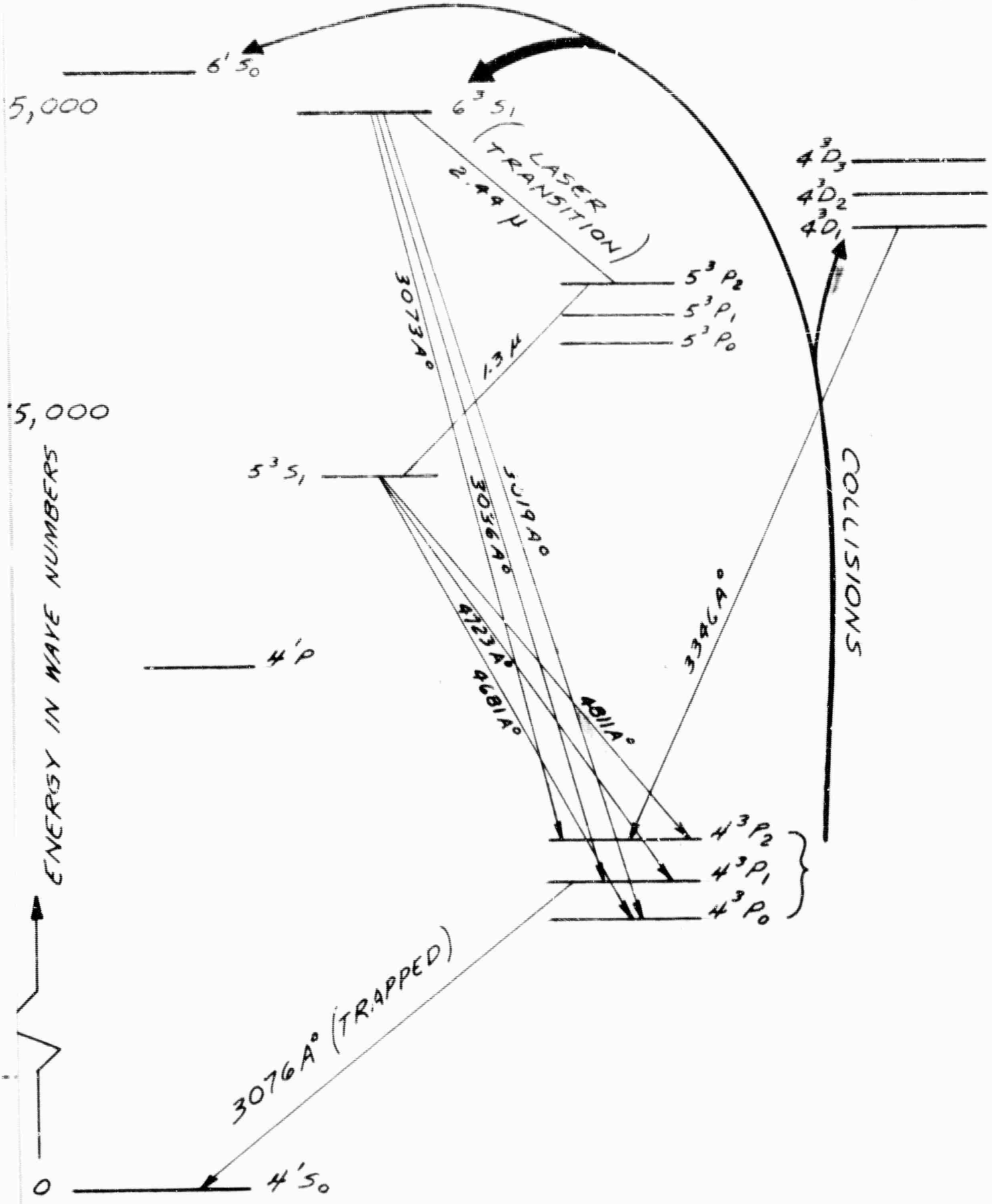

ZINC ENERGY LEVELS

Figure 3.7

the 4^3P_n is metastable, or light-trapped at pressures of 1 mm, the number of atoms in these states is considerable. (At pressures of 1 mm one can expect $n \approx 9 \times 10^{12}$ atoms/cc where n is the total population density in all of the metastable and trapped states). If one assumes populations approximately proportional to statistical weight for the 3 levels and an average cross-section $\sigma = 10^{-16}$ cm^2, then the number of effective collisions per second is $\gamma = n^2 \sigma \bar{v}_{rel} \approx 3 \times 10^{14}$/sec, where $\bar{v}_{rel}$ is the relative velocity of the colliding particles. Thus the rate of photons leaving the 6^3S_1 state would be 3×10^{14}/sec if we neglect the back collision rate, which is a small fraction of the total spontaneous emission rate.

There are six transitions from the 6^3S_1 state, three of which are trapped, because they terminate on the metastables. The other three transitions are in the infra-red at about 2.4 microns wavelength and are suitable LASER transitions. It is reasonable to assume that if three of the transitions are sufficiently trapped, then among the untrapped ones there must be one transition with a rate of about 10^{15} photons/sec. With this figure one calculates a gain in excess of 20%/meter, assuming an unpopulated lower state. The lower LASER state (5^3P) will be rapidly "dumped" since the spontaneous emission rate, A(5P→5S), is estimated to be ~ 25 x A($6^3S \rightarrow 5^3P$). Thus a population inversion is likely.

While the discharge is on, the collision process is difficult to detect since complete knowledge of the discharge parameters and Einstein A coefficients is not yet available, and since direct electron excitation is simultaneously present. However, intensity measurements of the several visible lines $5^3S_1 \longrightarrow 4^3P_n$ $n = 0,1,2$, made in the afterglow, will give an accurate measure of the number of photons passing through the LASER transitions, and hence a calculable gain.

2.3.2 Experimental

An experiment was devised to measure the number of photons passing through the LASER transition. A continuously pumped vacuum system similar to that used in the cesium gain experiment was employed. The cell containing the zinc was cylindrical, 1-1/2" in diameter and 4" long; the light output was viewed from the ends of the cylinder. The geometry was chosen to maximize the diffusion time of metastables to the wall and to maximize the trapped lifetime of the 4^3P_1 state. The cell was contained in an oven capable of continous temperature various up to 700°C.

The discharge was powered by an rf transmitter operating at 28 megacycles and square-wave modulated at about 20 cycles/sec. The relaxation time of the transmitter was about 5×10^{-6} secs.

The detection apparatus consisted of a monochromator with S-5 response phototube and an oscilloscope with a delayed sweep. The electrical bandwidth was adjusted to allow observation of decay times as short as 10^{-5} sec.

It was expected that, with metastable lifetimes of the order of milliseconds, the decay from the upper LASER level would be about 500μ secs, always having 1/2 the decay of the resonance lifetime, and that this would easily be observable when contrasted with other spectral lines. A survey of spectral lines between 3000-6000A, however, yielded results that were inconclusive. The difficulty that occurred was two-fold: Firstly the electron thermalization time was found to be about 100μ secs, so that all lines had a decay time in excess of this amount. Secondly, the presence of impurities limited the lifetime of the trapped (4^3P) states to about 500μ secs. With these effects, no significant lengthening of the lifetime of the upper LASER level with respect to other states was observed.

An improved apparatus was built in which the lifetime of the trapped line was increased to 1 millisecond and the thermalization time reduced to 10μ secs. This was achieved by using a larger closed system to which 1 mm of helium buffer gas was admixed. The new cell was a 3"

diameter quartz sphere (Figure 3.8) which has minimum surface to volume for maximum trapping of the resonance line and maximum diffusion time to the walls for the metastables. The helium buffer gas, which plays no active role in the discharge, maintains the diffusion time at low zinc vapor pressure and also reduces the electron thermalization time to 10μ secs.

With this new apparatus the collision process has been observed. By varying the vapor pressure, and hence the trapping time of the resonance line, the lifetime of the upper LASER level was observed to follow in linear fashion; its lifetime always being approximately one half of the resonance lifetime. This is to be expected, since the number of atoms in the 6^3S_1 state depends on the square of the number of metastables. It was also observed that the decay of light from the 5^3S_1 had a characteristically rapid decay followed by a longer decay. Since the chief source of the 5^3S_1 atoms is from electron excitation of the metastables, one would expect a rapid fall in the intensity, consistent with the electron thermalization time, plus a longer decay due to cascading from the 6^3S_1 state. Figure 3.9 shows the time resolution of several of these lines. It is interesting to note that the intensity due to the cascade phenomenon is a sizeable fraction of the total intensity (as much as 50%).

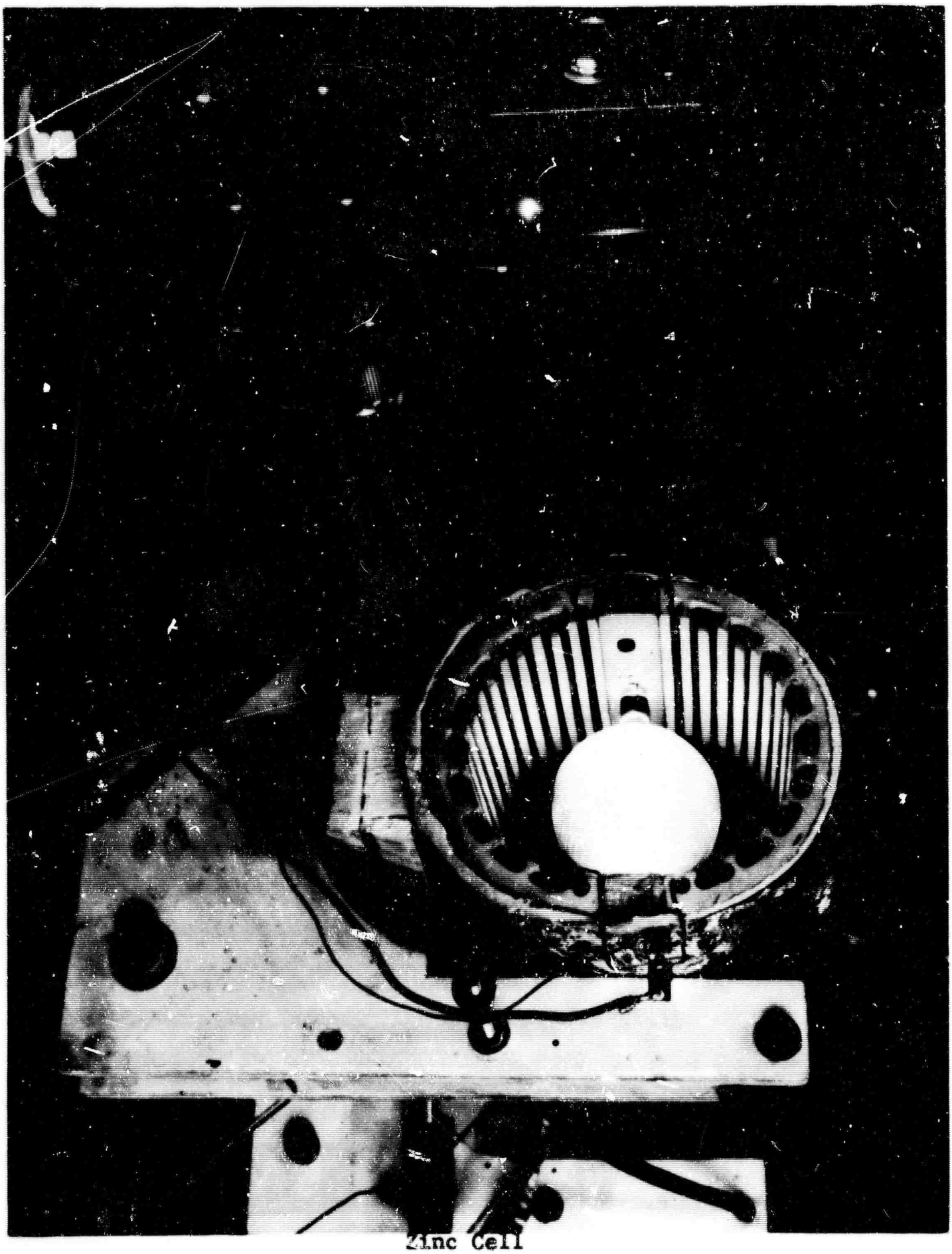

Zinc Cell
Figure 3.8

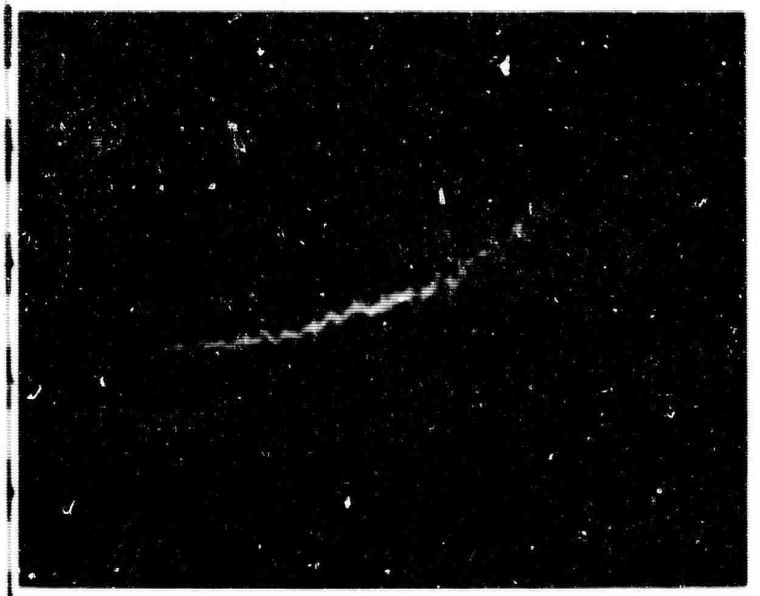

a) 3036A 6^3S_1-4^3P_1 (Showing decay of upper LASER state)

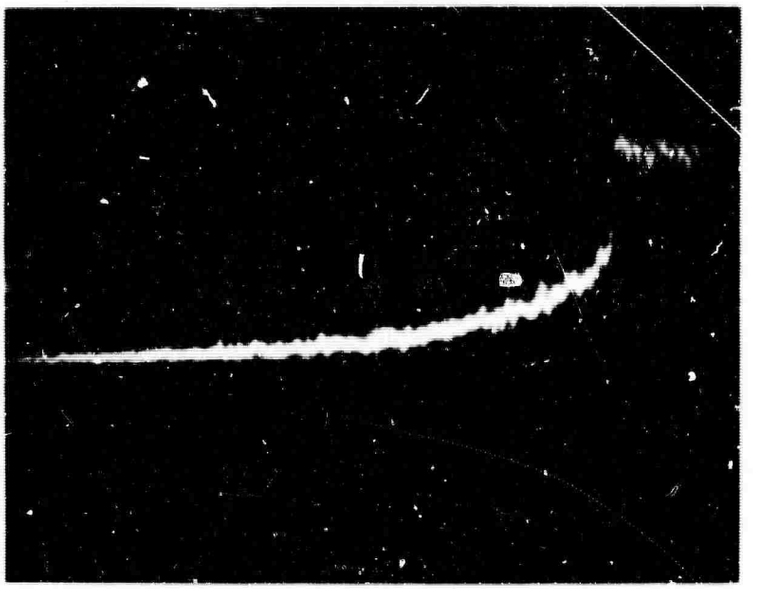

b) 4812A 5^3S-4^3P_2 (Showing electron decay and cascade decay from 6^3S_1)

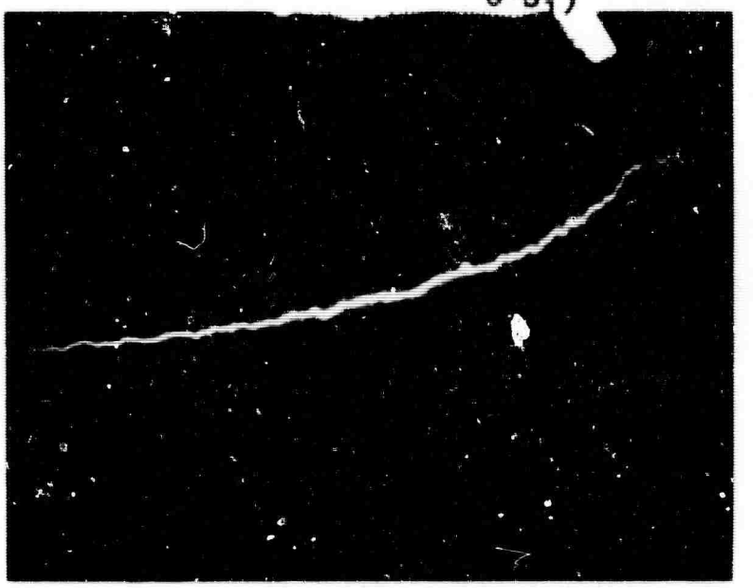

c) 3076A 4^3P_1 - 4^1S_0 (Trapped resonance line)

Decay of Several States in Zinc
(Time Scale - 100μ sec/div)

Figure 3.9

3.0 Work Planned for Next Period

3.1 Helium-Neon System

A study of the amplification as a function of the tube diameter, partial pressures and excitation conditions will be continued in an effort to raise the gain higher than the currently attained value of 9% per meter. The properties of the currently operative LASER will receive some study, preparatory to building a prism cavity LASER.

3.2 Xenon-Krypton System

Because an inversion of the 2p - 1s configuration, if at all possible, may occur only for xenon partial pressures in the neighborhood of a half micron or so, it is necessary to ascertain whether there are enough atoms in a 2p level to provide useful amplification and reach threshold for oscillation. A measurement of the absolute emission of photons from the individual 2p levels yields the quantity nf, the product of 2p population times oscillator strength for the transition. This same quantity gives the measure of the maximum amplification possible for the transition, i.e. the gain for zero lower state population. After this measurement is made, the decision as to whether further experimentation is desirable shall be made. It should not be forgotten that the 3d - 2p configuration is much more favorable as a potential LASER

3.3 Zinc-Zinc System

During the next period it is planned to make absolute intensity measurements of selected zinc transitions in order to calculate the expected gain and efficiency. Calculation of spontaneous emission rates of selected transitions will be made by the Bates-Damgaard method. It is planned to determine the cross-section for the self-collision double-excitation process in zinc vapor. A measurement of gain will be attempted and, if feasible, an oscillator will be constructed.

3.4 Mercury-Krypton System

It is hoped that gain which was previously predicted for the Hg-Kr of 1.0% per meter at 1.8 microns, will be measured in the near future.

IV. Optical Pumping of Ruby - Amplifier

1.0 Summary of Work Performed

Direct amplification of the output of a ruby oscillator in a second ruby rod was demonstrated. The measured single pass gain was 2 at room temperature in a ruby cylinder 5.56 cm long. The inferred single pass gain of 12.5 in a ruby 8" long was obtained by exciting it to oscillation at room temperature with no coating at either end.

2.0 Analysis of Work Performed

Direct amplification of light of 6934A wavelength in a ruby rod has been demonstrated. A schematic diagram of the experimental setup is shown in Figure (4.1). The oscillator used was a pink ruby rod (.04% Cr) with one end coated with an opaque silver film and the output end with a silver film of ~10% transmission. It was excited with the GE 524 helical lamp in our standard light pot. The output beam was collimated by passing through two 1 mm holes 8" apart. This insures a beam of sufficiently small size and angular divergence that it will pass through the amplifying ruby without hitting the walls of the ruby. The output beam from the amplifying ruby is focussed with a lens to enter a small aperture (~ 10 mils) ahead of a 7102 photomultiplier used as the detector. A diaphragm ahead of the lens served to cut down the stray light from the amplifier flashtube and spontaneous emission from the ruby without intercepting any of the transmitted beam. The input beam to the amplifier was monitored by another 7102 photomultiplier detecting the reflection from an unsilvered glass plate in the beam. It was found necessary to shield this detector from the

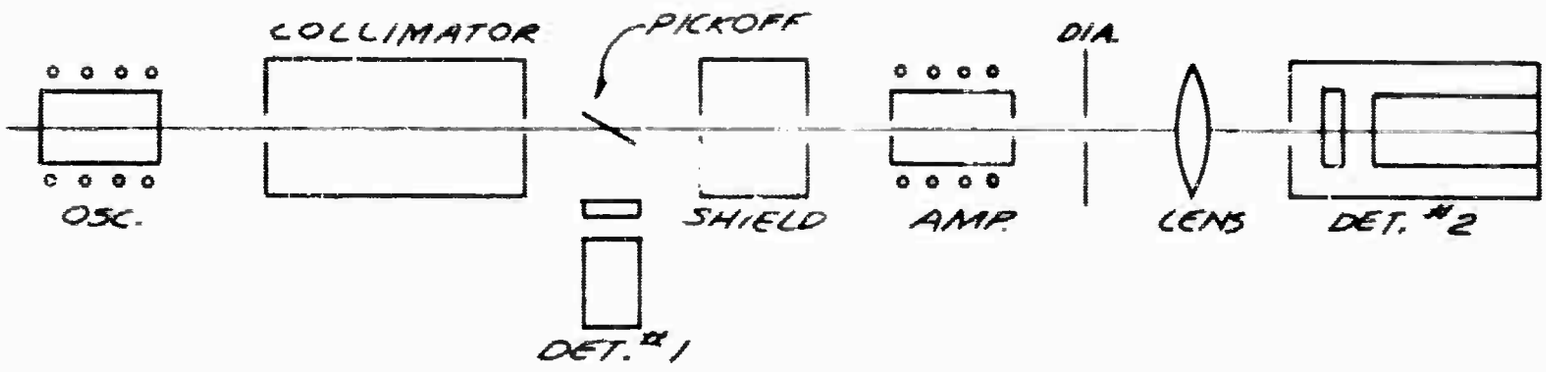

AMPLIFICATION SETUP

Figure 4.1

amplifier flashtube by a second collimator with larger openings as shown. Both detectors contained 100 A interference filters at 6940A (2nd order), red filters to cut out the third order transmission of the interference filters in the blue, and neutral density and ground glass filters. Some amount of stray light and spontaneous emission was still observed from each detector but this was small compared to the LASER beam, which was easily detected by its different time of occurrence. The outputs of each detector were observed simultaneously on the dual trace of the Hughes Memoscope. The detection rise time was purposely made ~10 μsec to smooth the oscillation spikes and make the pulse heights easier to measure. Saturation of the individual spikes was not observed and was not expected in this experiment.

The amplifier ruby was 1 cm diameter, 5.56 cm long, standard orientation ($\sim 60^{\circ}$), and the ends were uncoated. It was excited with a helical GE 524 lamp. The amplification measurement consisted of measuring the ratio of the output of detector 2 to that of detector 1 with and without the amplifier ruby in place for various excitation levels in the amplifier. This is necessary because the unexcited ruby is a strong absorber of the LASER light. The two lamps were triggered simultaneously. This would be very nearly the correct timing to observe the peak inversion density of the amplifier rod if the two lamps were identical. The precise timing to observe maximum gain could be different for a number of reasons, however, and this factor will be investigated in future experiments.

Some difficulties were encountered with heating in the rubies, particularly in the amplifier rod. This made consistency and reproducibility somewhat difficult since the variation of the center of the R_1 line, $\delta\lambda$, is about 0.065A/^{o}C. Thus a 30^{o}C difference in temperature of the oscillator and amplifier rods would be a 2A difference in the peak wavelengths and this would be serious. An attempt to overcome this effect by waiting 5 minutes between flashes seems to have been successful and each point was repeated several times. Water cooling of the rubies is planned for future experiments.

The output beam of the LASER oscillator was observed to be completely plane polarized with the electric vector perpendicular to the projection of the c axis on the plane of the end of the rod. The absorption and gain in the amplifier ruby varied with the relative orientation of the two rubies (contrary to reports from other laboratories). Gain measurements were made for the two orthogonal situations: with the E vector of the incident beam perpendicular and parallel to the projection of the c axis on the end of the amplifier rod. The results of the measurements are shown in Figure (4.2) Each point is the average of several measurements and has been corrected for the reflection losses at the ends of the rod. Except for some spurious points not included in Figure (4.2) the highest gain was observed with maximum excitation power was $\alpha = 0.132$ cm^{-1}. This is a single pass gain of 2.08 in the 5.56 cm rod at room temperature. No saturation of the type reported by Bell Telephone Laboratories was observed although their measurements were made at -40^{o}C where higher gains should be observed.

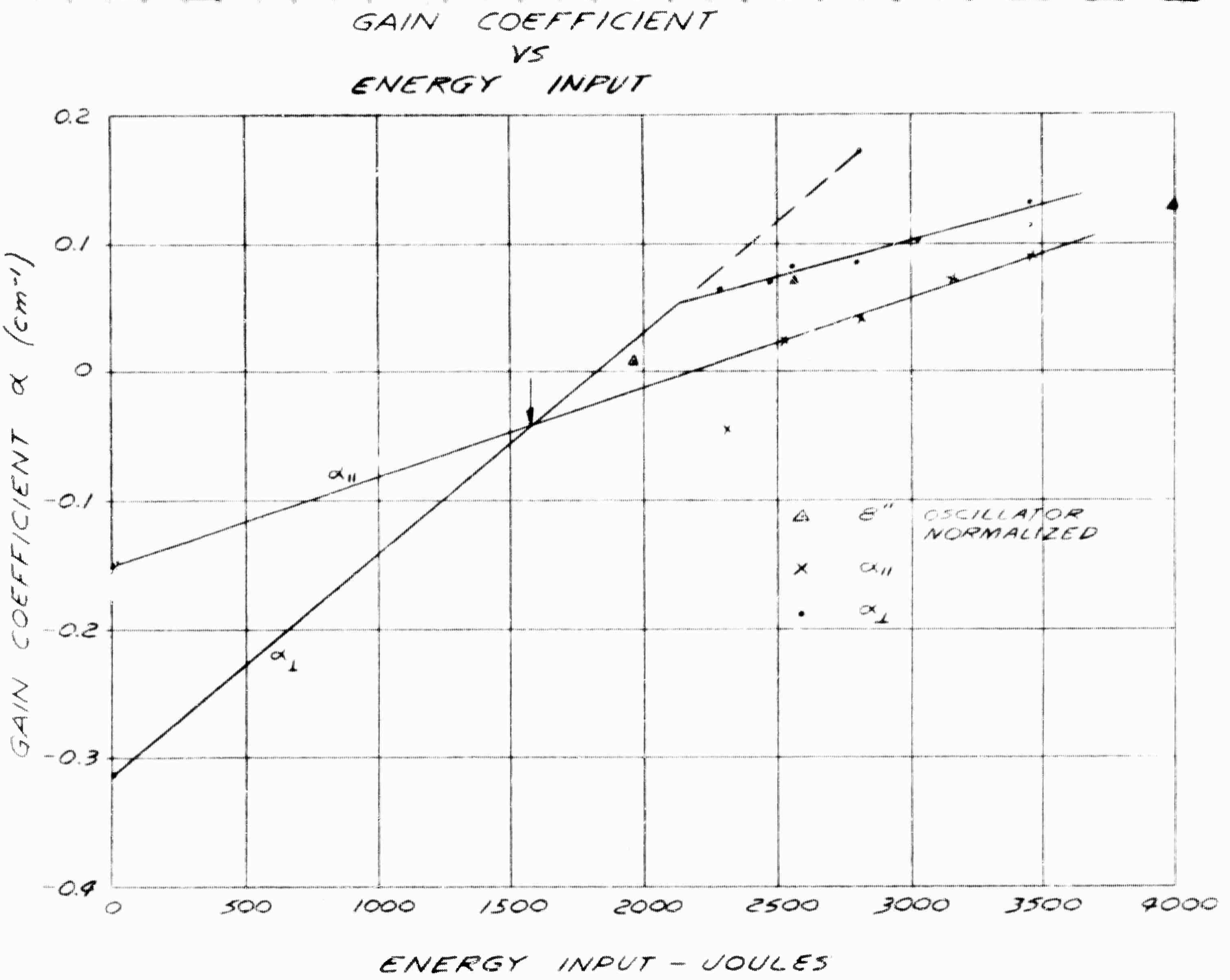
GAIN COEFFICIENT
VS
ENERGY INPUT
GAIN COEFFICIENT α (cm⁻¹)
0.2
0.1
0
-0.1
-0.2
-0.3
-0.4
0
500
1000
1500
2000
2500
3000
3500
4000
ENERGY INPUT - JOULES
α||
α⊥
θ'' OSCILLATOR NORMALIZED
α||
α⊥

Figure 4.2

The main emphasis of the amplifier program will be on the 8" ruby rod because of the higher gains obtainable (wi. the same gain coefficients). Thus if saturation of gain is to be observed it will occur most readily in this rod. For this end a helical 8" xenon lamp has been constructed and tested at TRG. It will require more input electrical energy than the GE 524 because of its longer length. The brightness in the green band of this lamp compared to the GE 524 was measured. Equal brightness of the two lamps were observed with 6700 joules input to the 8" lamp and 2500 joules into the 524 lamp. Since the ratio of surface areas of the lamps is 2.5 this indicates that the efficiency of the 8" lamp is comparable to that from the shorter one. Furthermore, in the presence of strong lamp self absorption, the energy density in a cavity should be proportional to lamp brightness. Then the threshold for oscillation might be expected to be increased for the 8" rod with this lamp by about this same factor, 2.5, over that of a short rod in the GE 524 cavity. The measured thresholds were as follows:

8" ruby - 8" lamp - 5150 joules

2-3/16" ruby - GE 524 lamp - 1960 joules

This is surprisingly good agreement considering the accuracy with which thresholds are measured. Lower thresholds have been measured in the GE 524 with shorter pulses (less capacity and higher voltage). However the figure quoted above is the usual threshold with 400 μf, and the brightness comparison was made with this capacity.

Figure 4.2

A preliminary measurement of the gain of the 8" ruby was made by observing the threshold for 3 different conditions of end reflection. The results are summarized in Table 4.1

TABLE 4.1

End Reflection	Threshold Energy	Gain($e^{\alpha l}$)
Opaque - 10% Trans.	5150 joules	1.2
Opaque - No Film	6720 joules	4.0
No film either end	10500 joules	12.5

The value of the gain coefficient computed from these data and the threshold condition $e^{\alpha l} = 1/R_1R_2$ is plotted on Figure (4.2). The input energies were normalized by the ratio $\frac{1960}{5150}$ to make the ratio of $E_{in}/E_{threshold}$ comparable.

While this is a very preliminary part of the amplifier program several interesting points have already appeared.

1. The gain depends on polarization. This is to be expected from the theoretical work of Sugano and Tanabe[31] on the transition probabilities of ruby and the absorption measurements by Schawlow.[32] However, Kisliuk[33] reports that the gain was independent of the orientation of the amplifier rod. One explanation for this difference might be that the input beam was not plane polarized in his experiments. That this is possible can be seen from Figure (4.2) Imagine that for a given length rod and end losses

(31) S. Sugano and Y. Tanabe, J. Phys. Soc. (Japan) 13, 880 (1958).

(32) F. Varsanyi, D. L. Wood, and A. L. Schawlow Phys. Rev. Letters 3, 544 (1959).

(33) P. P. Kisliuk, private communication.

the oscillation condition requires $\alpha = .05\ cm^{-1}$. Then the perpendicular polarization would reach threshold at about 1950 joules input while the parallel polarization would require 2900 joules for threshold. Between these two energies the output beam must be plane polarized with the E vector perpendicular to the projection of the c axis on the end of the rod. At higher energies, however, either or both polarizations may oscillate because of relaxation oscillations and the situation is not clear. The gain coefficient, α, is inversely proportional to $\Delta\nu$ so that at lower temperatures all values of Figure (4.2) (both positive and negative) will be increased by a linewidth factor. This will considerably reduce the difference in threshold energies for the two polarizations and make the above explanations more plausible. Kisliuk measurements were at $-40^{o}C$ for which $\alpha = 1.7\ \alpha_{RT}$. This question may be cleared up when we observe the polarization of the output beam under conditions such that both linear polarizations are above threshold, as at liquid nitrogen temperature.

2. The fact that the gain is different for the two polarizations makes the amplification measurement as a function of excitation power an excellent means of observing extraneous losses which are independent of polarization. Scattering losses would be an example. At the excitation power such that the α of the material is zero ($\Delta N = 0$) any residual absorption is attributed to other than R_1 line absorption. This point occurs when the gain curves for the two polarizations intersect (see Figure4.2)and can be measured accurately if points are taken below

inversion. The extrapolated curves of Figure (42) give this value of scattering loss as 0.04 cm^{-1}, although insufficient points were taken to put much faith in this value. However, it is not very different than the figure for scattering loss measured by Nelson[34], et al, of 2% in a 2" ruby rod. Another possibility must be considered. The residual loss could be dependent on polarization, as it would be if it were green band absorption on the wings of the absorption line. It is somewhat disturbing that if the green band were Lorentzian with a full width of 700A centered at 5350A and a peak absorption coefficient of 1 cm^{-1} (for .05% Cr) then the green band absorption at 6940A would be .045 cm^{-1}. This question can be cleared up by observing this loss as a function of temperature and concentration but better data is needed. Measurements by Jacobs[35] indicate that the residual green band absorption at 7000A (in more concentrated ruby) is 1% of the peak absorption. This data would give the residual absorption coefficient as 0.01 cm^{-1} for .05% ruby.

3. The gain coefficient indicates the following population ratios of $N_2:N_1:_{ground}$ = 36:36:28 at maximum excitation. Kisliuk reports population ratios of 39:39:22 at $E_{in} = 1.25\ E_{threshold}$. However, our analysis of his data gives population ratios of 30:30:40.

4. It is obvious that a great deal of information of a fundamental nature about ruby can be learned from this type of experiment. These questions will be looked into in the course of the amplifier program, whose main objectives are as follows:

---

(34) R. J. Collins and D. F. Nelson, Opt. Soc. Am., Pittsburgh, Pa., March 2, 1961.

(35) S. Jacobs, Doctoral Thesis, Johns Hopkins University, (1956), unpublished.

A. Obtain High Peak Power

1. whether greater than the same ruby as an oscillator or

2. better angular divergence and frequency characteristics

B. Investigate Saturation and Pulse Sharpening

C. Obtain a Better Understanding of Ruby.

3.0 Work Planned for Next Period

During the next report period it is planned to continue the ruby amplifier experiments in order to observe saturation effects.

V. Optical Pumping of Ruby - Oscillator

1.0 Summary of Work Performed

Two long ruby crystals were excited to oscillation to obtain high output energy. The measured output at room temperature was 2 joules from a rod .362" in diameter and 7.56" long and ~12 joules from a rod .625" in diameter and 5.5" long.

Single pulse output was obtained from ruby by two methods. In the first a Kerr cell was used to modulate the Q of the oscillation cavity (consisting of a ruby rod with an external mirror). Single pulses of 0.2 μsec duration were obtained with a peak power of about 2 megawatts The second method employed the optical thyratron action of an unexcited ruby absorber within the oscillation cavity. Single pulses were achieved but are not yet always reproducible.

A prior attempt to achieve intense single pulses is reported. This technique consisted of exciting the ruby with a second intense flash of short duration superimposed on a normal excitation flash. A series of strong relaxation oscillations of about 15 μsec duration was achieved.

A broad band emission was discovered in normally pink ruby (.04% Cr_2O_3 by weight). It accounts for 30% of the total emission from the ruby rod, making the quantum efficiency unity.

The output energy from a ruby LASER as a function of the end coating (reflectivity and transmission) of the ruby crystal was measured. The results confirm the existence of an optimum reflectivity of a relatively low value for maximum output energy.

2.0 Analysis of Work Performed

2.1 High Energy Output

Two ruby rods of larger volume than the normal LASER crystal have been tested. These are intended for the amplifier program to obtain sufficient amplification and output power to observe saturation effects. Each requires a special lamp for excitation since no lamps of the proper size exists commercially. Helical zenon flash lamps were constructed at TRG for this purpose.

The first of these rods is 0.364" in diameter and 7-9/16" long. It has a Cr^{3+} ion concentration of .04% and is standard orientation (c axis $\sim 60^{\circ}$ from rod axis.) Some of the measurements on this rod and the lamp used to excite it are reported in the section on the ruby amplifier. In addition to these threshold measurements the output energy at room temperature was measured with an opaque film on one end and a clear ruby-air interface on the transmitting end. The output energy was measured by the energy absorption in a thermopile described in a later part of this section. An output of 2 joules was obtained with 10,500 joules electrical input to the lamp. The usual "relaxation oscillation" type of output was observed with a total time duration of 600 μsec.

The second of the large ruby rods was 0.625" in diameter and 5.5" long. It also contained .04 wt% Cr_2O_3 and was standard orientation. It was coated with an opaque silver film on one end and a silver film of 30% transmission on the other. It was watercooled at a few degrees below room temperature. The exciting lamp was a helical

xenon flash lamp constructed at TRG for relatively low voltage, high capacity operation. With an input of 4300 volts at 1500 μf (13,800 joules) an output of 4.1 joules was measured on the thermopile. The lamp was capable of withstanding larger input energies and was tested at 24,000 joules. At this excitation energy the ruby output was estimated to be about 12 joules by the volume of Ti foil vaporized. Some uncertainty exists in this measurement, however, because of the possibility that chunks of the foil were blown off without vaporizing. The duration of the output beam in the latter experiment was about 2 msec.

2.2 Single Pulse Output *

Two types of "Q Spoiling" experiments have been conducted with the ruby LASER for the purpose of generating a single, short, energetic optical radiation pulse. The technique of "Q Spoiling", consists of reducing the optical resonator feedback in such a way that oscillation is prevented until the LASER medium gain has been raised far above normal. When the feedback connection is made, the radiation field builds rapidly to a high value, carrying with it substantially all the energy stored as population excess in the medium.

In the first experiment, an electro-optic shutter consisting of a half wave Kerr-effect nitrobenzene cell and calcite Nicol prism was used to frustrate the reflection from one of the Fabry-Perot mirrors placed some distance from the ruby rod. (See Figure 5.1). Delay circuits applied the high voltage pulse opening the Kerr cell approximately 600 μsec after ignition of the LASER pump lamp. Peak powers of 100 kw

---

* Work in this section was partially supported under Contract DA-30-069-ORD-3368.

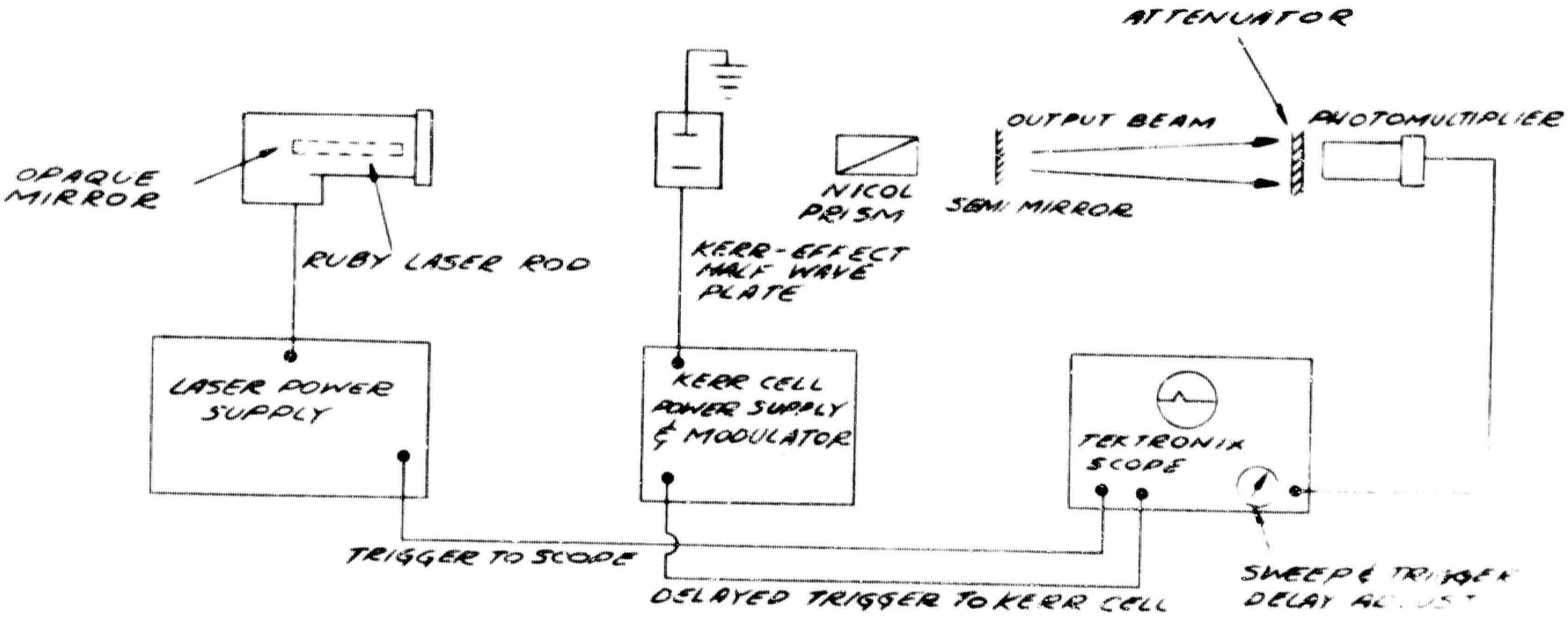

Q SPOILING WITH KERR CELL SHUTTER

Figure 5.1

and 2 megawatts were obtained, as inferred from a measurement of the total pulse energy and the time development of the radiation output. The two measurements refer to two different ruby LASERs of correspondingly different power inputs.

The second method of "Q Spoiling", termed "optical avalanche", is shown schematically in Figure (5.2). In this case oscillation is discouraged by the presence, in the optical feedback path, of a section of non-pumped ruby having a high optical density for ruby R light. When sufficiently high gain in the active ruby has been achieved to approach oscillation (in spite of the low feedback) the attenuating section saturates, becomes nominally transparent and restores a high value of feedback coupling.

The experimental results to date with the avalanche method have not been as clear cut as in the Kerr cell method. The single large pulses obtained have been difficult to reproduce. No intensity or energy measurements have been made. Because the avalanche method depends critically on the behavior of the ruby material, i.e. the poorly understood filamentary oscillation paths, erratic results initially are to be expected.

In the following, the experiments and their results will be described in more detail.

2.2.1 Q-Spoiling with an Electro-Optical Shutter

From the simple theory of the LASER oscillator, the population difference density between two quantum levels which is just sufficient to sustain oscillation is given by $D = N_u - N_\ell = (B\tau)^{-1}$.

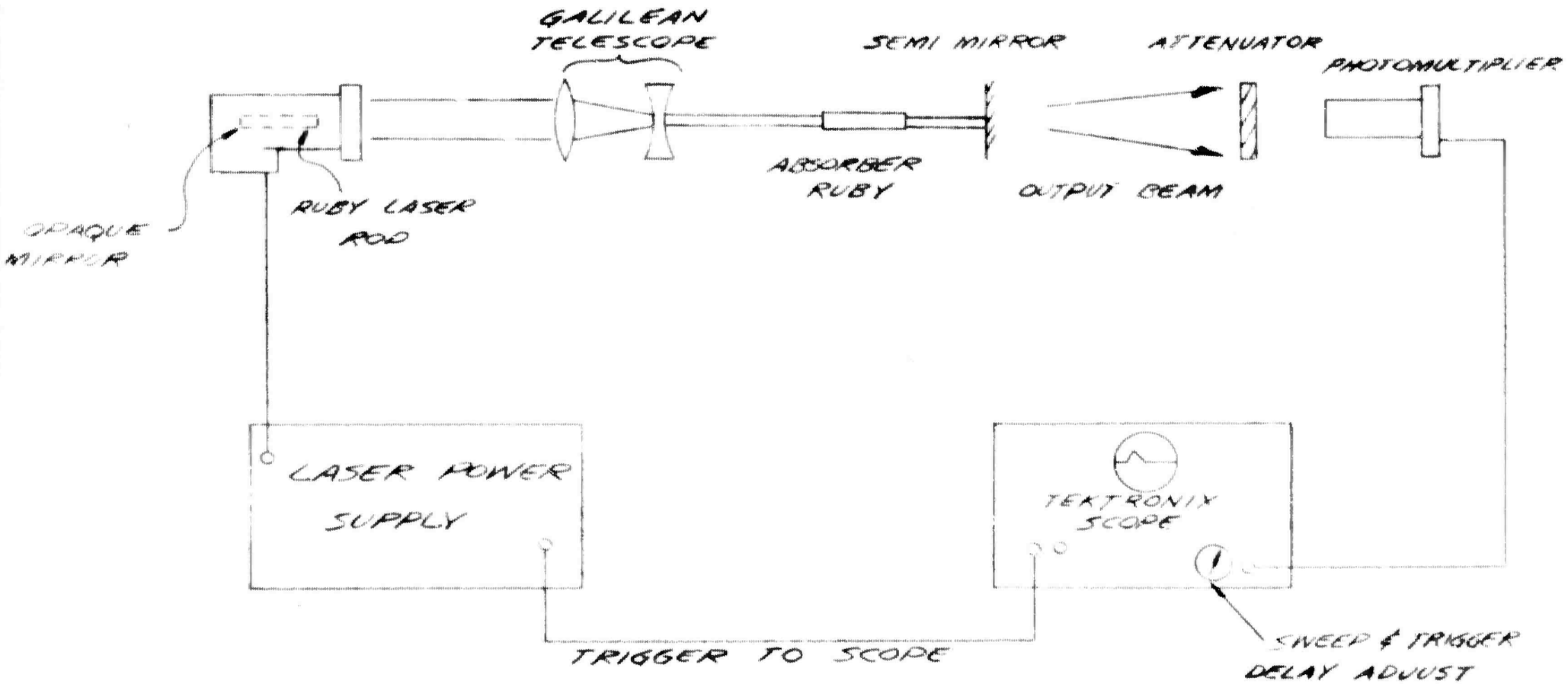

Q SPOILING WITH OPTICAL AVALANCHE

Figure 5.2

In this relation D is the population difference density, $N_{u,\ell}$ the upper (lower) state population density, B is the rate of induced emission per ion, between the quantum levels, at frequency ν into the given oscillator mode when the energy stored in that mode corresponds to one photon/cm^3, and τ is the mean life of one photon in the absence of any stimulated emission.

Referring to Figure (5.3) which illustrates the time development of a Q-Spoiling experiment, we show the origin of time coinciding with the pump lamp ignition. Initially D is large and negative, corresponding to $N_u = 0$. For $t > 0$ it builds towards a steady state value determined by the relaxation rate of the upper state and the pump lamp brightness and coupling to the ruby rod. Because the finite duration of the pump lamp pulse is comparable with the inverse of the ion relaxation rate, a lower maximum difference D_{max} is attained. With the Kerr cell inactive, the feedback path from the external mirror is blocked for polarized light crossed with the Nicol prism. In the case of a ruby rod with optic axis 90° to the rod axis, the induced emission coefficient for light polarized in a plane normal to the optic axis ($B_\perp$) is 5 times that of the orthogonal component. Thus if the value $1/\tau$, corresponding to the inactive Kerr-cell and Nicol, just exceeds the value $B_\perp D_{max}$, no oscillation can occur in either polarization.

Approximately at the time D_{max} is achieved, the Kerr cell is activated by the triggered discharge of a pulse forming network. The peak electric field applied to the cell is such as to produce the effect

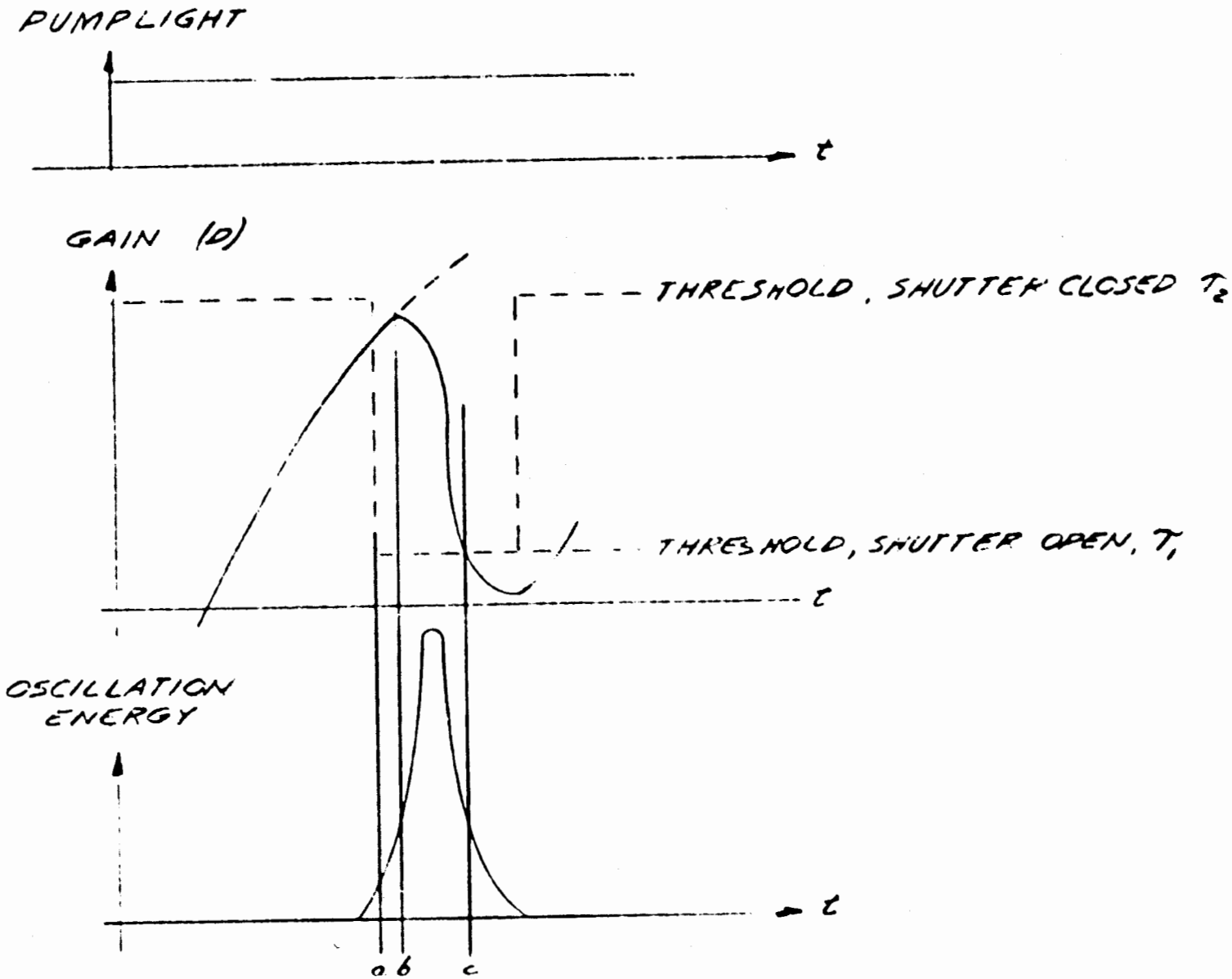

Q SPOILING WITH SHUTTER

Figure 5.

of a birefringent $\lambda/2$ plate, allowing light in the perpendicular (strong) polarization to "see" the external mirror through the normally crossed Nicol. Under these conditions, $\tau \rightarrow \tau_2 \gg \tau_1$ (point "a" on the time axis of Figure 5.3 and the resonator finds itself with a considerable excess gain over that required to sustain oscillation with resonator time constant τ_1. The oscillation energy builds exponentially, quickly exceeding that value which could be sustained by the pump lamp in the steady state ("b" in Figure 5.3). Compared with the rate at which the growing oscillation field drives the excess population density down, the pump lamp contribution now is negligible. At point "c" the decreasing population difference density passes through the value $(B_1\tau_2)^{-1}$, or the value at which the medium gain just balances the residual resonator losses. At this time, the oscillation energy is decreasing, meanwhile driving D toward zero (equal upper and lower quantum state population).

Figure (5.4) is a photograph of the experimental apparatus showing the LASER head, Kerr-cell, Nicol and external semi-mirror. The output from the semi-mirror was arranged to fall either on a special photo-multiplier tube capable of following a 5×10^{-8} sec. rise time, or on a ballistic thermopile. The former provided an oscilloscopic record of the pulse time development (Figure 5.5c and the latter gave an absolute measure of the pulse energy. The pulse, very nearly triangular in shape, is easily calculated to have peak power $\frac{2W}{\Delta}$ where W is the energy and Δ the time duration (at the base).

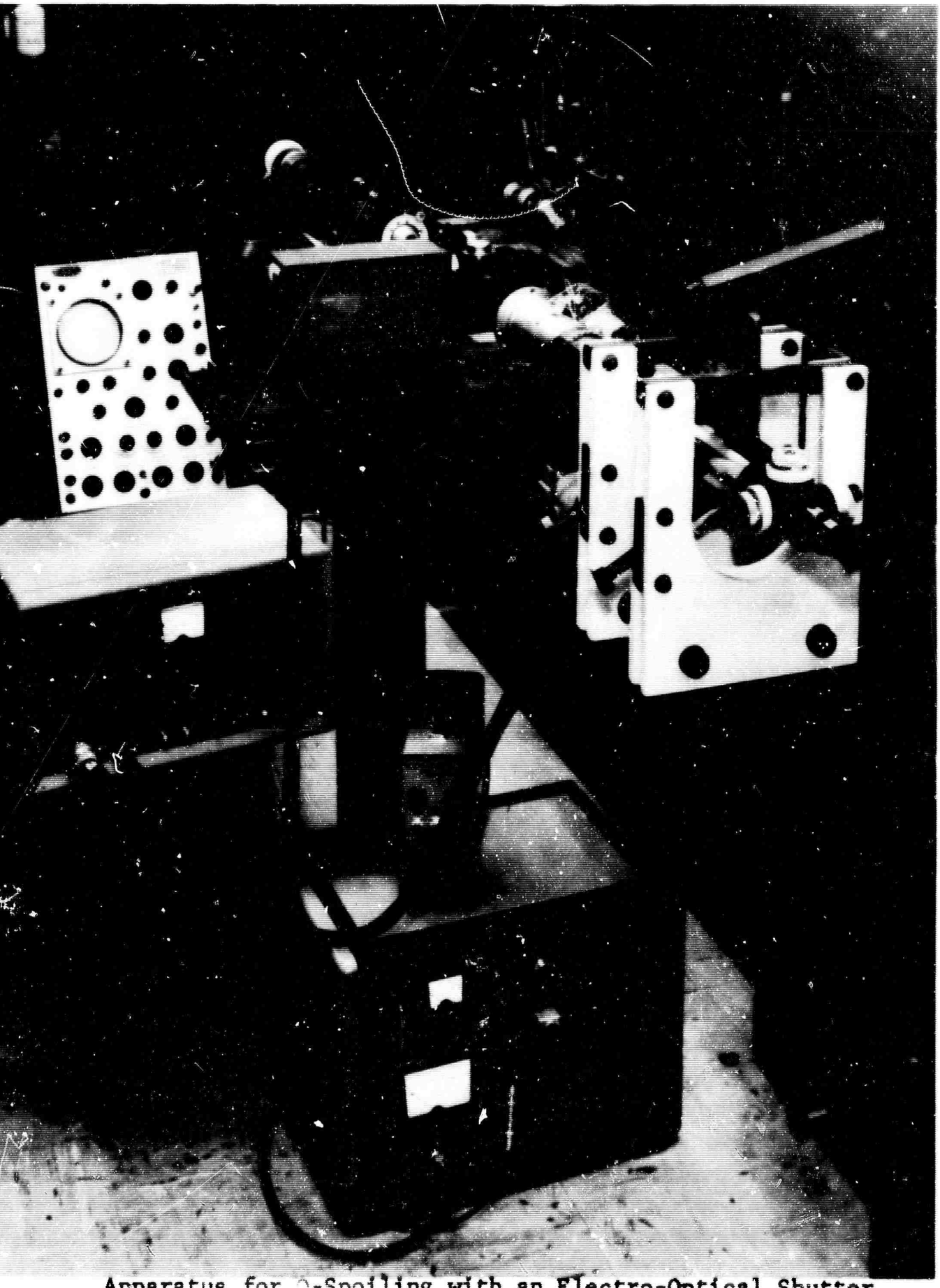

Apparatus for Q-Spoiling with an Electro-Optical Shutter

Figure 5.4

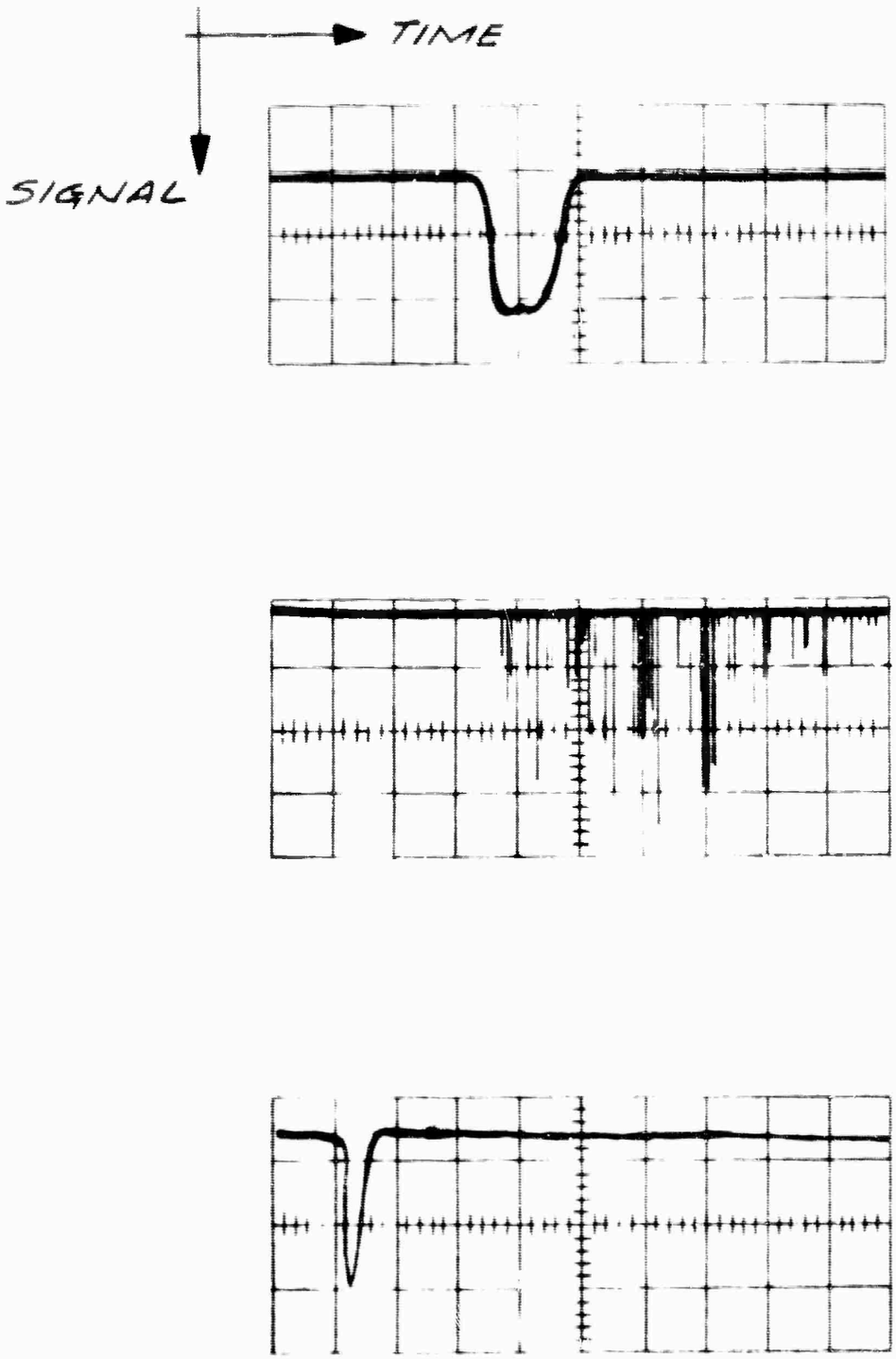

Figure 5.5

(a) Transmission of Kerr cell/Nicol for red component of xenon light. Time scale 1μsec/major div.

(b) Ruby LASER output, shutter fixed open. Time scale 100μsec/major div.

(c) Single ruby LASER spike induced by opening Kerr cell shutter 600 μsec after pump lamp ignition. Time scale 1μsec/major div.

2.2.2 "Q-Spoiling with the Optical Avalanche Technique

Figure (5.2) shows, schematically, the experimental arrangement for the optical avalanche method. The active (pumped) ruby rod is reflection coated on one end. The opposite end is uncoated.*

Although not corresponding exactly to the arrangement used, Figure (5.2) shows the light from the active rod magnified by a Galilean telescope and projected through a smaller, passive, ruby rod onto the semi-mirror. Neglecting lens losses, the effective intensity reflectivity of this assembly, viewed from the uncoated end of the active ruby, is $Re^{-2\alpha L_2}$ where R is the reflectivity of the mirror, L_2 the length of the passive rod and α its spectral absorption coefficient at the LASER wavelength. α depends upon the distribution of ions between the two states responsible for the characteristic ruby fluorescence. Normally, when the ruby is unexcited, α is large and positive. The quantity α will approach 0 as the ion distribution, initially in the ground state, approaches equilibrium in the presence of an intense radiation field. Under these conditions we may expect the intensity reflectivity of the rod-mirror combination to switch from $Re^{-2\alpha L_2}$ to R.

2.2.2.1 Kinetic Equations of the Avalanche Process

The analysis which follows is strictly true only for weak absorption by the passive crystal. Machine computation is required for a complete solution, even in this approximation. Also, it has been assumed, without loss of generality, that the beam passing through the passive rod

* MgF_2 anti-reflection coatings on the ruby rod were found to deteriorate rapidly. We believe photoelectric emission charges the film, and attracts dust particles which subsequently burn, producing a "measled" appearance.

is of uniform cross-section as if a Galilean telescope had been used.

Let the energy density in the first crystal be ρ_1 and that in the second, ρ_2.

By conservation of total flux, we have for every cross-section A(x)

$$\rho(x)\ A(x) = \frac{\rho_1 A_1}{\eta} = \frac{\rho_2 A_2}{\eta} \quad \text{thus, the total energy E in the} \qquad (2.1)$$

cavity is given by:

$$E = \rho_1 A_1 L_1 + \rho_2 A_2 L_2 + \frac{(\rho_1 A_1)}{\eta}\left[L - L_1 - L_2\right] \qquad (2.2)$$

where A_i and L_i are the area and length of the i^{th} crystal,

L is the total cavity length, and

η is the index of refraction of ruby.

The time rate of change of the energy in the resonator, $\frac{dE}{dt}$, is the sum of three terms:

a) The rate of decay due to the finite time constant, τ, of the cavity: $-E/\tau$. If ruby i has the scattering coefficient α_i, then $1/\tau = 1/\tau_o + (\alpha_1 L_1 + \alpha_2 L_2)\, c/\eta L'$ and $\tau_o = \eta L'/c(1-R)$ where $L' = L_1 + L_2 + (L - L_1 - L_2)/\eta$.

b) The rate of increase due to induced emission in the first crystal:

$$\left(\frac{n_2^{(1)}}{g_2} - \frac{n_1^{(1)}}{g_1} \right) h\nu\ B_1 \rho_1\ A_1 L_1 ,$$

c) The rate of decay due to absorption in the second crystal:

$$\left(\frac{n_1^{(2)}}{g_1} - \frac{n_2^{(2)}}{g_2} \right) h\nu\ B_2 \rho_2\ A_2 L_2 ,$$

where $n_j^{(i)}$ is the population density in the $j^{\underline{th}}$ level in the $i^{\underline{th}}$ crystal.

$n_1 + n_2 = N$ = constant

$h\nu$ is the energy of a LASER photon, and

B_i is proportional to the Einstein B coefficient for the i^{th} ruby.

Upon adding these rates of change, we obtain:

$$\frac{dE}{dt} = -\frac{E}{\tau} + \frac{h\nu E}{L'} \left(\left(\frac{n_2^{(1)}}{g_2} - \frac{n_1^{(1)}}{g_1} \right) L_1 B_1 - \left(\frac{n_1^{(2)}}{g_1} - \frac{n_2^{(2)}}{g_2} \right) L_2 B_2 \right). \qquad (2.3)$$

The time rate of change of the population density in crystal (1) is determined by the competition between optical pumping and induced and spontaneous emission:

$$\frac{d}{dt}\left[\frac{n_2^{(1)}}{g_2}-\frac{n_1^{(1)}}{g_1}\right]=\left[P\left(\frac{g_1}{2g_2}+1\right)\frac{n_1^{(1)}}{g_1}-A\left(1+\frac{2g_2}{g_1}\right)\frac{n_2^{(1)}}{g_2}\right]-\left(\frac{1}{2g_2}+\frac{1}{g_1}\right)\left[\frac{n_2^{(1)}}{g_2}-\frac{n_1^{(1)}}{g_1}\right]B_1\rho_1 \quad (2.4)$$

where P is the pumping rate and A is the spontaneous emission rate. The time rate of change of the population density in crystal (2) is determined by the competition between absorption and spontaneous emission:

$$\frac{d}{dt}\left[\frac{n_2^{(2)}}{g_1}-\frac{n_1^{(2)}}{g_1}\right]=-\left(1+\frac{2g_2}{g_1}\right)A\frac{n_2^{(2)}}{g_2}-\left(\frac{1}{2g_2}+\frac{1}{g_1}\right)\left[\frac{n_2^{(2)}}{g_2}-\frac{n_1^{(1)}}{g_1}\right]B_2\rho_2. \quad (2.5)$$

2.2.2.2 Threshold Conditions

We will now inquire into the conditions after threshold, $(dE/dt) = 0$, when the energy and population densities are changing rapdily due to induced emission. Thus in equations (2.4) and (2.5) we may neglect the small effect of the pumping and spontaneous emission terms compared to the induced emission terms. These equations then become, using the relations (2.1) and (2.2):

$$\frac{d}{dt}\left[\frac{n_2^{(1)}}{g_2}-\frac{n_1^{(1)}}{g_1}\right]=\left(\frac{1}{2g_2}+\frac{1}{g_1}\right)\frac{B_1}{A_1}\frac{E}{L}\left[\frac{n_2^{(1)}}{g_2}-\frac{n_1^{(1)}}{g_1}\right] \quad (2.6)$$

$$\frac{d}{dt}\left[\frac{n_2^{(2)}}{g_2}-\frac{n_1^{(2)}}{g_1}\right]=\left(\frac{1}{2g_2}+\frac{1}{g_1}\right)\frac{B_2}{A_2}\frac{E}{L}\left[\frac{n_2^{(2)}}{g_2}-\frac{n_1^{(2)}}{g_1}\right] \quad (2.7)$$

* This expression takes into account that only one half of the atoms are pumped into level 2.

At threshold, when $dE/dt = 0$, we have

$$n_1^{(2)} = N^{(2)},\ n_2^{(2)} = 0,\ E = E_0, \tag{2.8}$$

and equation (2.3) may be written:

$$\frac{\left[\frac{n_2^{(1)}}{g_2} - \frac{n_1^{(1)}}{g_1}\right]_{TH}}{\left(\frac{L'}{h\nu B_1 \tau L_1}\right)} \quad 1 + \alpha = \frac{\left[\frac{n_2^{(1)}}{g_2} - \frac{n_1^{(1)}}{g_1}\right]_{TH}}{\left(\frac{N^{(2)} L_2 B_2}{\alpha g_1 L_1 B_1}\right)} \tag{2.9}$$

where

$$\alpha = \left(\frac{h\nu B_2 \tau L_2 N^{(2)}}{L' g_1}\right) . \tag{2.10}$$

We see from equation (2.9) that the quantity α has the following significance:

In the absence of the second crystal, $\alpha = 0$, the threshold value of $\left[\frac{n_2^{(1)}}{g_2} - \frac{n_1^{(1)}}{g_1}\right]$ is given by $\frac{L'}{h\nu B_1 \tau L_1}$. The effect of introducing the second crystal is to increase the threshold value by the factor $1 + \alpha$.

2.2.2.3 Condition for Avalanche

We now ask: What is the condition that when we have reached threshold, $(dE/dt) = 0$, the field will increase ($(d^2E/dt^2) > 0$) from its initial value E_o because the loss decreases faster than the gain?

Upon differentiating equation (2.3), substituting from (2.6) and (2.7) and evaluating at $dE/dt = 0$, we obtain the condition: the second derivative (d^2E/dt^2) is greater than zero when:

$$\frac{A_1}{A_2} \cdot \left(\frac{B_2}{B_1}\right) > 1 + \frac{1}{\alpha} \qquad (2.11)$$

Thus the amount of demagnification necessary in order to achieve automatic shutter action depends on the amount by which the threshold for oscillation has been increased by the addition of the second ruby crystal. For a small increase in threshold, a large demagnification is required, and visa-versa.

2.2.2.4 Time Development of Pulsation

The shape of the pulsation can be determined by integrating the three differnetial equations (2.3), (2.6) and (2.7) subject to the initial conditions:

$$\text{At threshold:} \begin{cases} E = E_o, \; dE/dt = 0 \\ n_1^{(2)} = N^{(2)}, \; n_2^{(2)} = 0 \\ \dfrac{n_2^{(1)}}{g_2} - \dfrac{n_1^{(1)}}{g_1} = (1+a) \dfrac{L'}{h\nu \, B_1 \, \tau L_1} \end{cases}$$

$$= \left(\frac{n_2^{(1)}}{g_2} - \frac{n_1^{(1)}}{g_1} \right)_{TH} .$$

From equations (2.6) and (2.7) one may obtain $\left(\frac{n_2^{(1)}}{g_2} - \frac{n_1^{(1)}}{g_1} \right)$ as a function of $\frac{d}{dt} \left(\frac{n_2^{(1)}}{g_2} - \frac{n_1^{(1)}}{g_1} \right)$. Upon substituting into equation (2.3) one obtains:

$$\frac{dE}{dt} = -\frac{E}{\tau_1 \left(\frac{1}{2g_2} + \frac{1}{g_1} \right)} \frac{d}{dt} \left[L_1 A_1 \left(\frac{n_2^{(1)}}{g_2} - \frac{n_1^{(1)}}{g_1} \right) + L_2 A_2 \left(\frac{n_2^{(2)}}{g_2} - \frac{n_1^{(2)}}{g_1} \right) \right], \tag{2.12}$$

From equation (2.6) we have:

$$E = -\frac{A_1 L}{B_1 \left(\frac{1}{2g_2} + \frac{1}{g_1} \right)} \frac{d}{dt} \ln \left(\frac{n_2^{(1)}}{g_2} - \frac{n_1^{(1)}}{g_1} \right) . \tag{2.13}$$

Upon substituting the expression for E from equation (2.13) into the right hand side of equation (2.12) we may integrate (2.12) directly to obtain

$$E(t) - E(0) = \frac{A_1 L'}{\tau B_1 \left(\frac{1}{2g_2} + \frac{1}{g_1}\right)} \left[\ln \left(\frac{n_2^{(1)}}{g_2} - \frac{n_1^{(1)}}{g_1} \right) \right]_0^t \qquad (2.14)$$

$$- \frac{h\nu}{\left(\frac{1}{2g_2} + \frac{1}{g_1}\right)} \left[L_1 A_1 \left(\frac{n_2^{(1)}}{g_2} - \frac{n_1^{(1)}}{g_1} \right) \right]_0^t + L_2 A_2 \left(\frac{n_2^{(2)}}{g_2} - \frac{n_1^{(2)}}{g_1} \right) \Bigg]_0^t .$$

By taking the ratio of equations (2.6) and (2.7) and integrating over the population densities, we obtain:

$$\frac{\left(\frac{n_2^{(2)}}{g_2} - \frac{n_1^{(2)}}{g_1} \right)}{\frac{N^{(2)}}{g_1}} = \left(\frac{\frac{n_2^{(1)}}{g_2} - \frac{n_1^{(1)}}{g_1}}{\frac{n_2}{g_2} - \frac{n_1}{g_1}} \right)_{TH}^{\frac{A_1/B_1}{A_2/B_2}} \qquad (2.15)$$

Upon substituting into equation (2.15) we may obtain the energy E(t) completely as a function of $\left(\frac{n_2^{(1)}}{g_2} - \frac{n_1^{(1)}}{g_1} \right)$. Thus, we may integrate equation (2.6) to obtain:

$$t = \tau \int_x^1 \frac{dx'}{x' - f(x')} \qquad (2.16)$$

where

$$\epsilon(x) = \frac{E_0}{\epsilon} + \ln x + \frac{h\nu\left(\frac{n_2^{(1)}}{g_2} - \frac{n_1^{(1)}}{g_1}\right) TH\, L_1\, A_1}{\epsilon\left(\frac{1}{2g_2} + \frac{1}{g_1}\right)}(1-x) \qquad (2.17)$$

$$= \frac{h\nu}{\epsilon}\,\frac{\left(\frac{N^{(2)}}{g_1}\right)(T_2 A_2}{\left(\frac{1}{2g_2} + \frac{1}{g_1}\right)}\left(1 - \right)^{(A_1 B_2/A_2 B_1)}$$

and

$$\tau = \frac{A_1 L'}{\left(\frac{1}{2g} + \frac{1}{g_1}\right) B_1 \tau} \qquad (2.18)$$

Equation (2.16) may be integrated numerically to obtain x as a function of t; then from equation (2.17) one may obtain E as a function of t.

2.7.1.5 Energy Output in a Pulsation

Power is radiated from one mirror at the rate

$$P(t) = \beta A c T = \frac{cT}{L'\eta} E(t), \qquad (2.19)$$

where T is the power transmission coefficient of the mirror. The third term in equation (2.19) is equal to the second because of equation (2.1). In the case T = 1-R we have:

$$P(t) = E(t)/\tau_c \,. \qquad (2.20)$$

The total energy, E(t), radiated during the time t is, from equation (2.19):

$$E(t) = \int_0^t P(t) = \frac{cT}{L'\eta} \int_0^t E(t),\ dt. \tag{2.21}$$

From equations (2.13) and (2.14) we have

$$\frac{1}{\tau}\int_0^t E(t)dt = E(o) - E(t) + h\nu L_1 A_1 \frac{\left(\frac{n_2^{(1)}}{g_2} - \frac{n_1^{(1)}}{g_1}\right)_{TH}}{\left(\frac{1}{2g_2} + \frac{1}{g_1}\right)} \left[1 - \frac{\left(\frac{n_2^{(1)}}{g_2} - \frac{n_1^{(1)}}{g_1}\right)}{\left(\frac{n_2^{(1)}}{g_2} - \frac{n_1^{(1)}}{g_1}\right)_{TH}}\right] \tag{2.22}$$

$$-h\nu L_2 A_2 \frac{\frac{N^{(2)}}{g_1}}{\left(\frac{1}{2g_2} + \frac{1}{g_1}\right)} \left[1 - \frac{\left(\frac{n_2^{(2)}}{g_2} - \frac{n_1^{(2)}}{g_1}\right)}{\frac{N^{(2)}}{g_1}}\right].$$

Using equations (2.9), (2.10) and (2.15), we may write:

$$\frac{1}{\tau}\int_0^t E(t)\ dt = E(o) - E(t) + h\nu L_1 A_1 \frac{\left(\frac{n_2^{(1)} n_1^{(1)}}{g_2} - \frac{}{g_1}\right)_{TH}}{\left(\frac{1}{2g_2} + \frac{1}{g_1}\right)} \left\{(1-x) - \frac{A_2/B_2}{A_1/B_1} \frac{a}{1+a}\left(1-x^{(A_1B_2/A_2B_1)}\right)\right\} \tag{2.23}$$

where

$$x = \frac{\left(\frac{n_2^{(1)}}{g_2} - \frac{g_1^{(1)}}{g_1}\right)}{\left(\frac{n_2^{(1)}}{g_2} - \frac{n_1^{(1)}}{g_1}\right)_{TH}} ,$$

If we consider the case that at the end of the pulse,

$E(t') = E(o)$ and $x \approx 1$, then we have:

$$\frac{1}{\tau}\int_0^{t'} E(t)\,dt = h\nu L_1 A_1 \frac{\left(\frac{n_2^{(1)}}{g_2} - \frac{n_1^{(1)}}{g_1}\right)_{TH}}{\frac{1}{2g_2} + \frac{1}{2g_1}} \left[1 - \left(\frac{A_2/B_2}{A_1/B_1}\right)\left(\frac{\alpha}{1+\alpha}\right)\right] \qquad (2.24)$$

and equation (21) for the total energy E radiated during a pulsation becomes:

$$E = \left[\frac{T}{1-R + \alpha_1 L_1 + \alpha_2 L_2}\right] h\nu\, L_1 A_1 \frac{\left(\frac{n_2^{(1)}}{g_2} - \frac{n_1^{(1)}}{g_1}\right)_{TH}}{\left(\frac{1}{2g_2} + \frac{1}{g_1}\right)} \left[1 - \left(\frac{A_2/B_2}{A_1/B_1}\right)\frac{\alpha}{1+\alpha}\right] , \qquad (2.25)$$

where we have used:

$$\frac{1}{\tau} = \frac{c\,(1-R + \alpha_1 L_1 + \alpha_2 L_2)}{nL'} .$$

A minimum condition for the applicability of equation (2.25) is that there should be a pulsation at all, i.e.

$$\frac{A_1/B_1}{A_2/B_2} > \frac{1+\alpha}{\alpha} \qquad (2.26)$$

2.2.2.6 Experimental Results of the Avalanche

Using several absorber crystals, the avalanche experiment was carried out. Under some conditions, the expected pattern of pulsations appeared, but was difficult to reproduce. Considerable difficulty was experienced with the telescope lenses especially in the case of cemented doublets where the cementing material inevitably burned. For this reason, the use of a Galilean telescope, where the magnified beam of small diameter passed through the lens, was soon abandoned. A unity power Keplerian telescope (two confocal, positive lenses, equal focal length) was substituted and the absorber ruby placed near the common foci. See Figure 5.6.

It was found that the onset of oscillations with respect to pump lamp ignition was delayed by a substantial amount when the telescope-absorber components were inserted into the space between the active ruby and the external mirror. Approximately half of the threshold increase, however, was due to losses other than resonance absorption, i.e. scattering.

A typical oscilloscope record of a successful avalanche is shown in Figure 5.7. The large first spike which appears is due to the avalanche effect, the succeeding small pulses are of the "normal" type, since the absorber cannot relax from transparency for a millisecond or so.

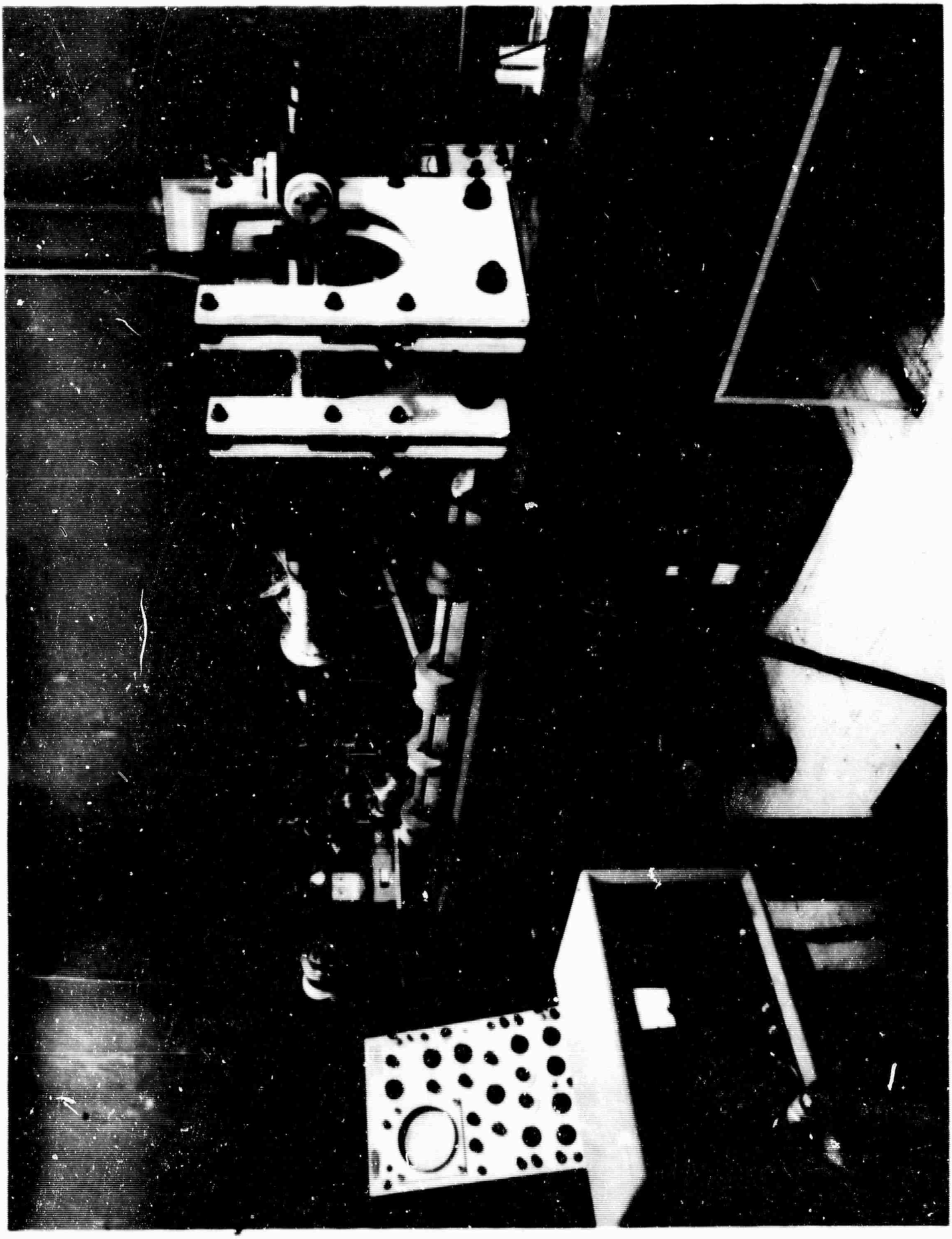

Figure 5.6
Apparatus for Avalanche Experiment

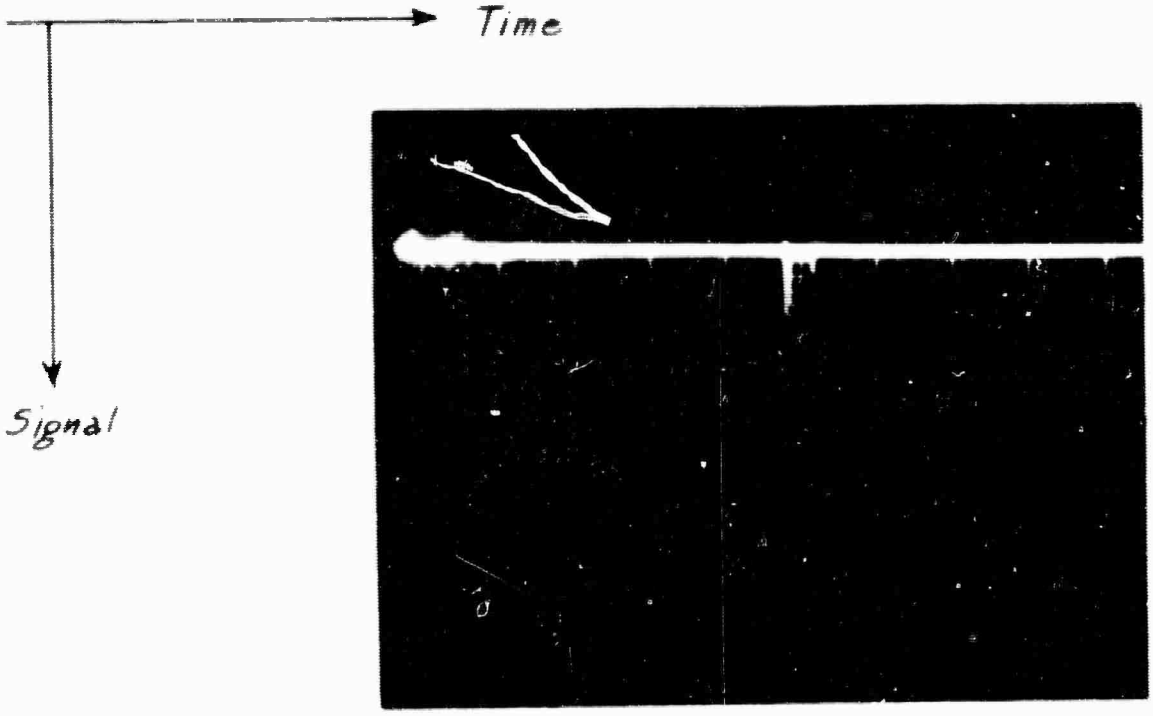

Oscilloscope Record of Successful Avalanche

Figure 5.7

2.3 The Double Excitation Pulse

A second voltage pulse of high intensity and short duration was superimposed on the normal capacitor discharge through a helical xenon lamp used to excite a ruby LASER. A series of relatively strong relaxation oscillations were observed for about 15 μsec following the second intense flash.

This experiment was performed in April 1961. It was not presented in the last report of June 1961.

During the time that the ruby is oscillating the popu' 'n density of the upper level would be clamped to its threshold value, at least in the ideal case of continuous oscillations during the excitation pulse. Of the energy absorbed a definite (and relatively small) percentage is emitted as spontaneous emission from the fixed level population density. This energy is lost to the oscillation. The remainder of the absorbed energy must appear in the oscillation. The instantaneous output power therefore should be nearly proportional to the instantaneous rate of energy absorption and hence to the power input to the flash lamp.

In the case of the GE FT 524 he ical xenon lamp a customary lamp input of 3,000 joules for a duration of about 1 msec is applied. This is an average input power of about 3 megawatts or 3 joules/μsec. Considerable higher input powers should be possible for a very short time, as for instance, the discharge of 1 μf at 10,000 volts. If this second pulse is applied during the time the gas is already ionized the resistive load due to the discharge is about one ohm, resulting in a time

duration of the second flash of 1 μsec. The instantaneous input power should be 50 joules/μsec, or an order of magnitude higher than the normal case.

The experimental arrangement is shown in Figure (5.8). The main power supply is adjusted to excite the ruby relatively slowly just to the threshold of oscillation. At this time the high voltage low capacity flash is triggered through an air gap. A choke between the lamp and the main discharge condensers prevents dissipation of the energy of the second flash in the latter condensers.

The timing of the second flash was varied to achieve maximum output. As expected because of the low total energy in the second flash no oscillation was observed if it was fired 20-30 μsec before the normal onset of oscillations. In addition the main flash must excite the ruby very close to oscillation. For this reason the first flash was adjusted just above threshold and a low level of normal oscillation allowed. The timing of the second flash to occur after the cessation of the low level of oscillations was not nearly so critical and oscillations due to the second flash were observed with delays of 200-300 μsec. This is also expected because of the long decay time of the R levels and the fact that some pumping from the first flash still exists.

A typical oscilloscope trace of the detected output beam is shown in Figure (5.9). While the second voltage pulse to the lamp had a duration of ~1μsec, relaxation oscillations are observed for about 15μsec. This duration appears to be due to the electron relaxation time in the lamp. The spiked oscillations appear to be higher in peak power than the

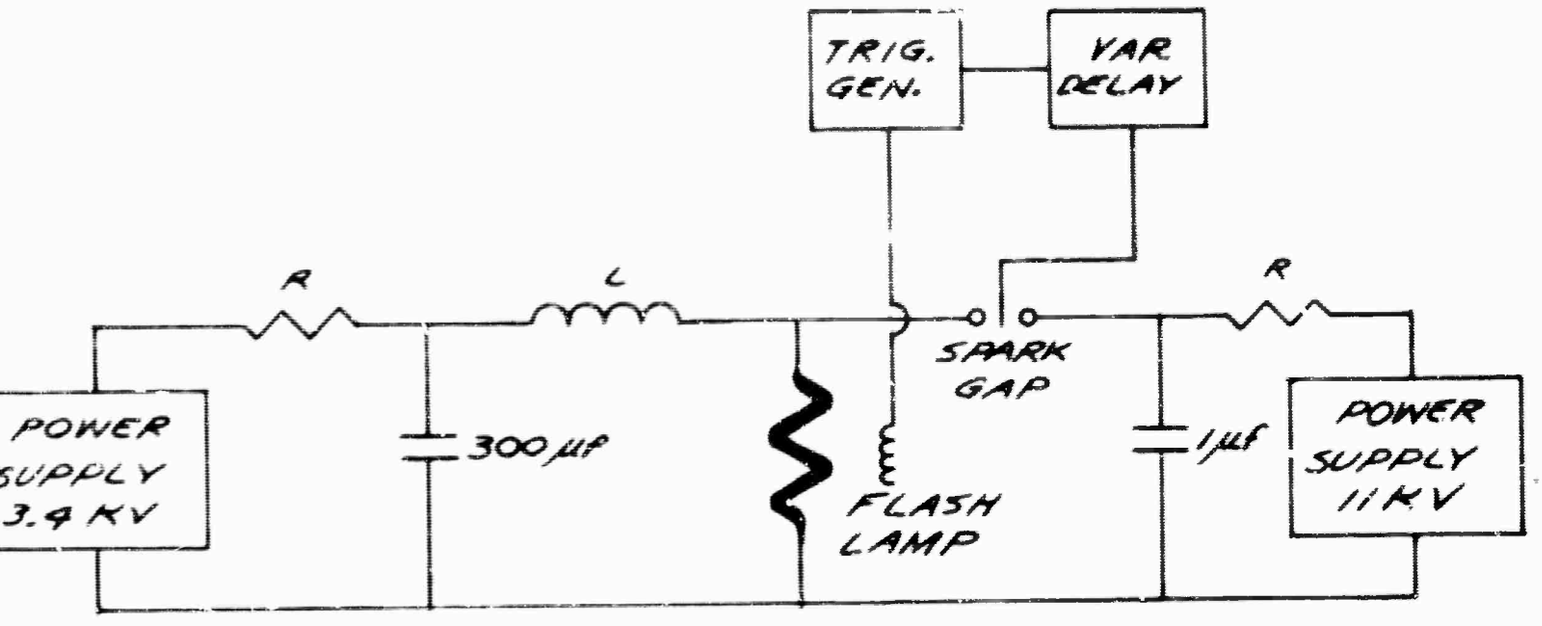

RUBY DOUBLE PULSE SCHEMATIC

Figure 5.8

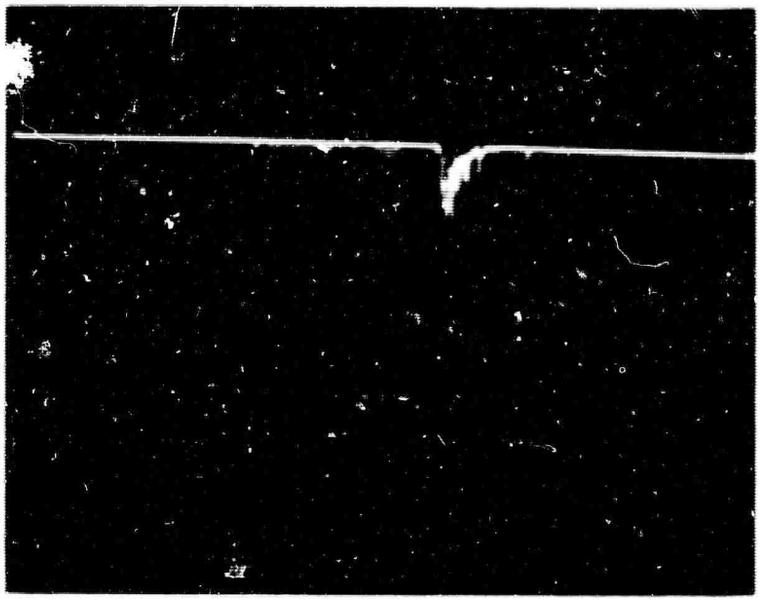

Ruby Output with Double Excitation Pulse. Time scale is 50μsec per division

Figure 5.9

normal oscillations with the ruby fully excited but not by the factor of 10 that was anticipated.

No further work has been done on this technique during this period and none is presently contemplated for the future.

2.4 Broadband Emission from Ruby

A weak but broad emission band has been observed at longer wavelengths than the R lines in nominally pink ruby (0.04 wt%). Excitation was by a CW xenon lamp and the emission detected monochromatically. In addition to the R lines at 6943A and 6927A two diffuse peaks were observed not well resolved, at 7080A and 7140A. Their peak brightness was less than that of the R lines by about a factor of 20 but the total integrated emission was $\sim$1/2 that of the R lines. Such bands were observed by S. Jacobs[36] on the long wavelength side of the R lines in emission and on the short wavelength side in absorption. These were in addition to the neighbor lines he observed in more concentrated ruby and suggest the possibility that they arise from the emission of a phonon in the normal absorption or emission process from the R lines. Although they have not been studied sufficiently to draw any concrete conclusions the emission into these bands is of about the right magnitude to account for the measurement by T. Maiman[37] of a quantum efficiency of the R lines of 70%.

---

(36) S. Jacobs, Dissertation, Johns Hopkins University (1956) unpublished.

(37) T. H. Maiman, R. H. Hoskins, I. J. D'Haenens, C. K. Asawa, and V. Evtuhov, Phys. Rev. 123, 1151, (1961)

2.5 Output Energy vs Reflectivity

The following characteristics of a Ruby LASER were measured:

1. Light output as function of coating (reflectivity/transmission)for a 1 cm diameter, 0^{o} orientation ruby.
2. Light output as a function of ruby angular orientation.
3. Light output as a function of flash rate.

The ruby was contained in an efficient excitation cavity consisting of the exterior sections of two intersecting cylindrical reflectors, each containing a straight xenon flashlamp.

The output of the ruby was focused into a ballistic thermopile (see Figure5.10).The thermopile consists of 2 copper cylinders, a detector and a reference, each with blackened 10^{o} conical holes. The two cylinders are thermally connected by 8 series iron-constantan thermocouples. The emf generated as a result of heating of the detector due to absorption of the LASER light is measured with a microvoltmeter. The thermopile generates 146 μ volts/joule of light absorbed.

2.5.1 Light Output vs Coating Reflectivity

The coating on the transmitting end of the ruby was varied from about 87-64% reflectivity and the output measured as a function of power input to the lamps. The data are shown in Figure (xx).

The reflectivity and transmission were not measured on the rut itself. A glass slide coated at the same time and in close proximity to the ruby was used instead. Measurements were made on a reflectometer in which the reflectivity of the sample is measured relative to the

FIG. 5.10

Apparatus to Measure Ruby Output Energy

FIG. 3.11

Light Output vs Laser Input for Various Reflectivities

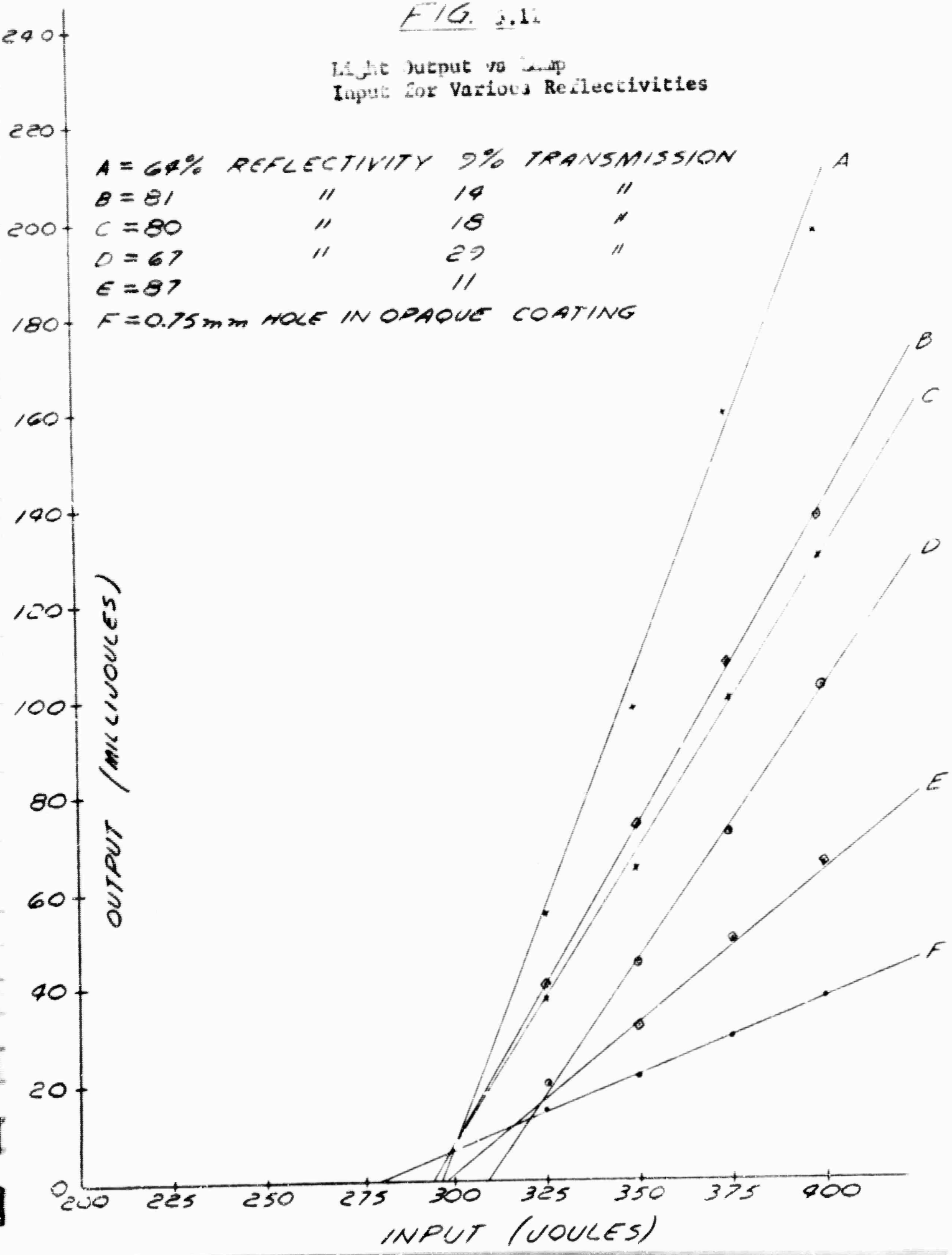

reflectivity of two standard mirrors, R_1 and R_2. (see Figure (5.12) The measurements are made as follows:

A. Reflectivity:

1. Light of intensity I_o is sent through a monochromator (tuned to the green to compare with previous data taken on a Jarrell-Ash densitometer), reflected off mirror R_1 and the intensity of the reflected beam measured with a photometer (path ABC).

2. Then the sample (with reflection coefficient R_s) is placed between the light source and R_1. In this position the light is reflected from the sample (path A'DF) reflects off R_2 (path DFE) and then again reflects off the sample and onto the photometer (FEC'). In this measurement black opaque paper is placed between the sample and R_1.

3. The two mirrors R_1 and R_2 are interchanged and steps 1 and 2 repeated for R_2.

4. The reflectivity is calculated as follows.

Path ABC $\rightarrow R_1 I_o$ or $R_2 I_o$

Path ADFEC $\rightarrow I_o R_2 R_s^2$ or $I_o R_1 R_s^2$

$$R_s = \left(\frac{I_o R_1 R_s^2}{I_o R_1}\right)^{1/2} = \left(\frac{I_o R_2 R_s^2}{I_o R_2}\right)^{1/2}$$

B. Transmittance:

1. R_1 measured as in 1 above.
2. Sample placed between R_1 and the source and R_2 is covered with opaque paper. The path of the beam is A'B'C'.

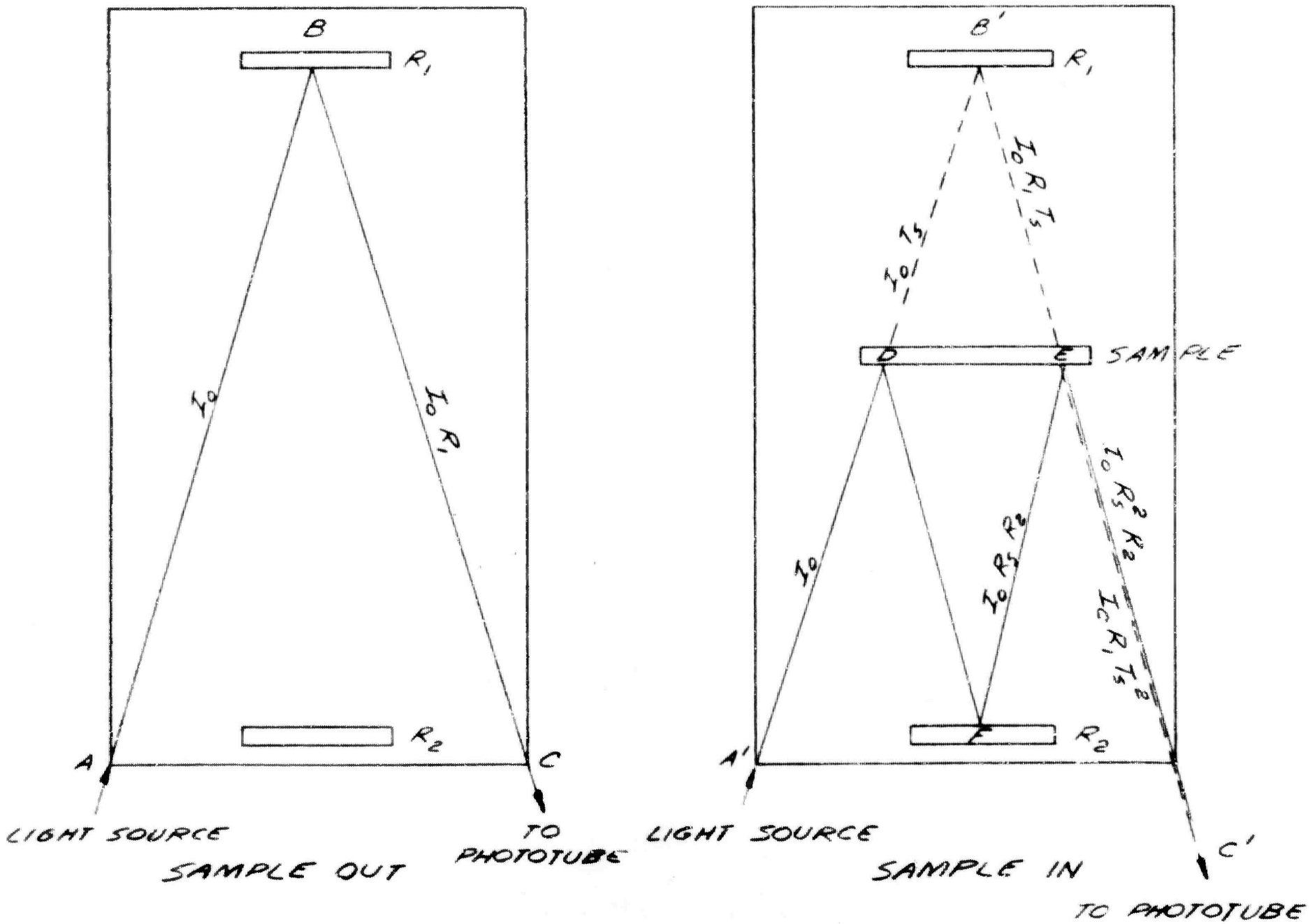

FIG. 5.12

Reflectometer

3. Calculation:

$$ABC \rightarrow R_1 I_o$$

$$A'B'C' \rightarrow R_1 I_o T_s^2$$

$$T_s = \left(\frac{R_1 I_o T_s^2}{R_1 I_o} \right)^{1/2}.$$

The values for reflectivity and transmission are an average of two separate sets of measurements. Values for ruby light output at each value of power input are an average of three measurements.

2.5.2 Output vs Rotational Orientation

The optical output of a 1 cm 0° ruby with a 66% reflective coating, was measured at 325 and 400 joules input, as the ruby was rotated in 90° steps about its longitudinal axis. The variation in output with orientation is small enough to be within experimental error.

In a zero degree ruby, the angular position of the ruby with respect to the lamps is irrelevant since the light absorption is the same in all directions. However, in a 90° ruby, the absorption of light varies considerably with direction. In order to determine whether this would be an important consideration, a 1/4" diameter, 90° ruby was checked in 2 positions. In the first position the light side of the ruby was facing the lamps and in the second, the dark side was facing the lamps. The data show no significant difference between the 2 positions.

2.5.3 Light Output as a Function of Flash Rate:

The light output was measured as a function of flash rate (from 1 up to 20 flashes per minute) for a 0° 1 cm diameter ruby with

a) lattice structures with which rare earth dopants are compatible,

b) stability toward thermal and other environments,

c) enhancing the photoactivation of rare earth ions and/or not quenching their luminescence, and of course,

d) growability as single crystals.

A ready compilation of crystal structures(4) furnishes many selections of candidates to choose from. The particular case of yttrium vanadate (YVO_4), with which most of the rare earth vanadates are isomorphous,

(3) C.G.B. Garrett, W. Kaiser, and D. L. Wood, "Fluorescence and Optical MASER Effects in $CaF_2:Sm^{++}$". Preprint.
(4) Landolt-Bornstein, Zahlenwerte und Funktionen, 1. Bd., 4. Tl. Berlin: Springer-Verlag (1955).

was prepared and its melting point established at about 1800°C. A furnace was set up to heat a melt of Li_3VO_4 and YVO_4 in a platinum crucible and to cool the melt slowly in order to obtain well-formed microcrystals of YVO_4 for evaluation.

The possibility of thulium ion (Tm^{++}) in the divalent state for effective light absorption seems worth investigating. Toward this end, a small quantity of anhydrous thulium trichloride ($TmCl_3$) was prepared by the usual dehydration method. The reduction of this compound will require an unusually vigorous method.

(5) E. Broch, Zeit. Physik. Chem. B20, 345 (1933)
(6) N. V. Sidgwick, The Chemical Elements and Their Compounds. Oxford: The Clarendon Press (1950); page 809

or fluxes. A very possible decomposition product (P_2O_5) is very volatile.

3.0 Work Planned for Next Period

3.1 Future Plans in Growing the Tungstate Type of Crystal

The perfection of calcium tungstate crystals is considered worth further investigation. Generally, the crystals have been grown at a linear rate of 3/8" per hour, which is about as slow as is practical. Perfection probably will entail more exact preparations of seed crystals, various atmospheres about the crystal-growing crucible, systematic material balances and chemical analyses throughout a given series of rare-earth doped crystals, and improved temperature controls during

previously. Besides venting of the apparatus, care is necessary to check the composition of $PbMoO_4$ (MoO_3 volatilization) and correct it by addition of MoO_3. The relative stability of unusual valence states of rare earth elements in $PbMoO_4$ may be compared with that in $CaWO_4$ and $CaMoO_4$. Calcium molybdate undoubtedly melts at a higher temperature than lead molybdate. Hence a vented induction furnace is recommended for $CaMoO_4$, which probably has hardness and photo-excitation properties superior to those of $PbMoO_4$.

Planning the work with new crystal candidates is subject to frequent revisions as experience with their preparation may dictate.

The yttrium vanadate should be obtainable in micro-crystalline form for evaluation at an early date. The design and construction of a very high temperature furnace (for 1800°C operation) is under way in anticipation of growing crystals of YVO_4 or other material from the melt.

Several other kinds of oxy-salts will be considered for preliminary examination: titanosilicate ($CaTiSiO_5$), yttrium gallium garnet ($Y_3Ga_5O_{12}$), and cerates (Na_2CeO_3), to mention only three types.

Oxide crystals (other than TiO_2, Al_2O_3 or MgO) will require

(8) N. Chatterjee, Zeit. f. Physik 113, 96 (1939)

2.1 Efficient O

A common te
the crystal in a heli
for oscillation in su
into the discharge la

If the shap
as it is in the case
more efficient scheme
An ideal configuratio

a ...tograph, the relative diameters of the two fringe systems. The measured value was 16- $\pm$ 10°, compared with $\Delta\sigma$ = 152.7° calculated by Peck. The deviation from Peck's value may be due to two causes: distortion of the fringe contours by overlapping of neighboring fringes, and the fact that the system optic axis is slightly skew from the normal to the entrance face, an orientation built into the prism and differing slightly from the case Peck analyzed.

These observations, although made with an etalon, demonstrate the feasibility of using cube-corner elements in a Fabry-Perot interferometer with the flat and cube as separate elements. (See Figure 5) With such an interferometer the free spectral range and resolution are

the cube corner is set by the requirement for total internal reflection in the cube-corner prism. (If a triple mirror with metallic coatings is used, rather than a prism, the limit of rotation is set by reduction of aperture). The limit of tilt of the flat is set by the gross requirement that the beam be returned to the cube corner.

The property of angular insensitivity makes the Fabry-Perot interferometer, composed of separate cube and flat, especially suited for applications where stability of alignment is a major consideration. In particular, the motivation for this work was to develop a more stable resonator than the plane Fabry-Perot interferometer for LASER applications.

outside the visible region of the spectrum involving the use of materials which are opaque in the visible. With cube-corner Fabry-Perot interferometer, good alignment will be assured, provided there is adequate optical homogeneity in the optical material.

LIST OF FIGURES

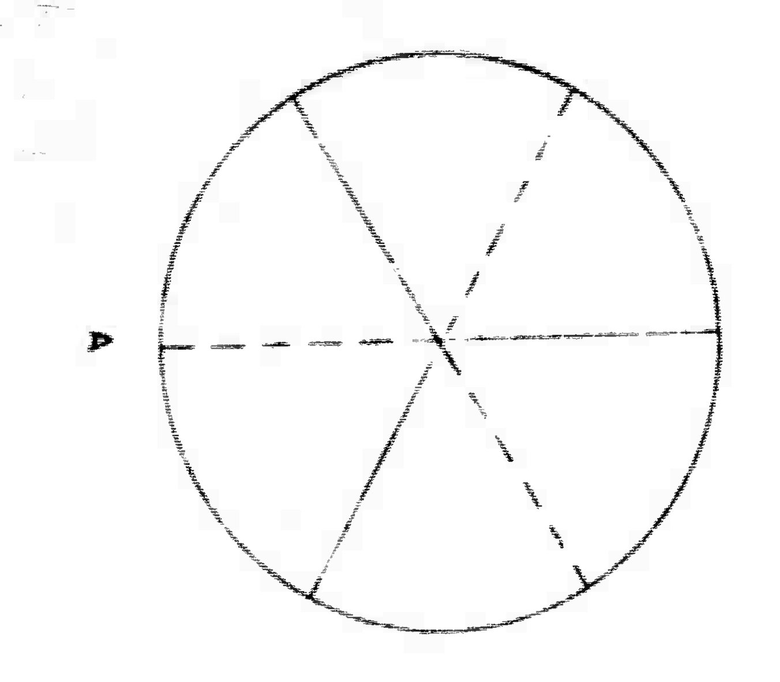

Figure 1

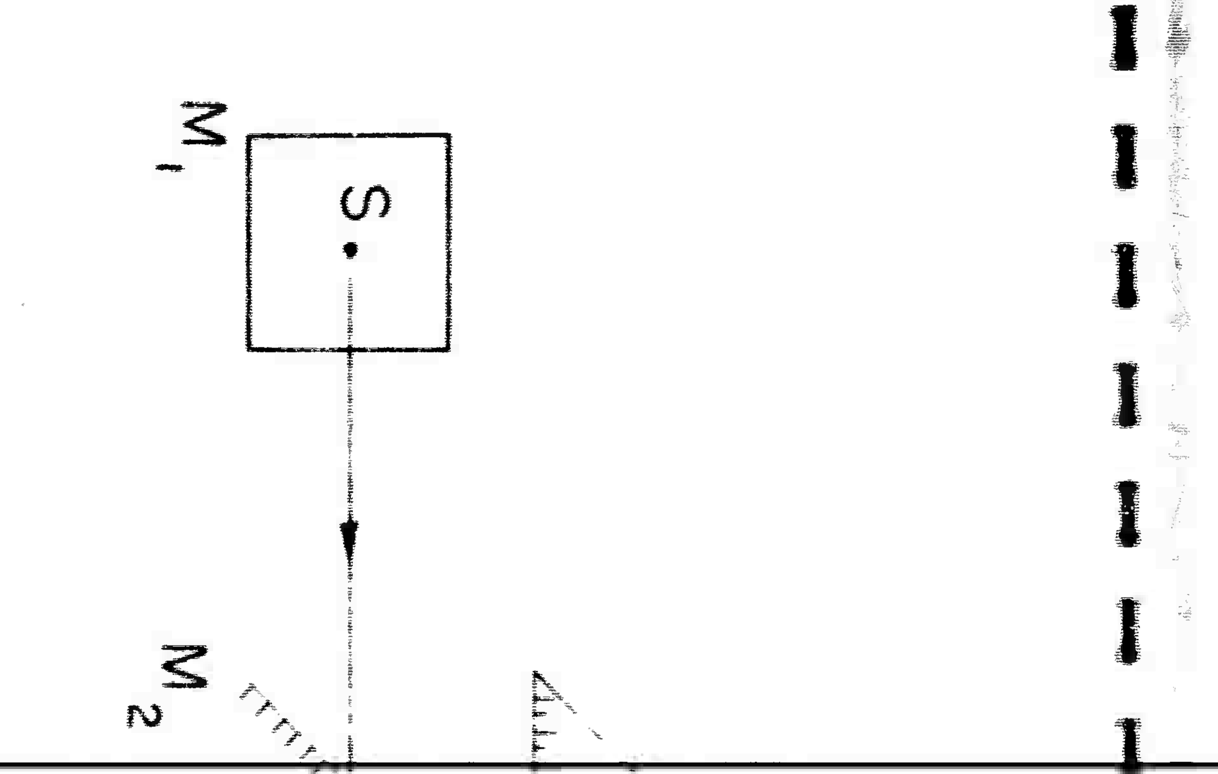

a 93% reflective coating. At each flash rate the output was measured on the 11th shot after 10 consecutive firings. The data are shown in Figure (5.13).

2.3.4. Comparison with a 4 lamp light pot

A 0° - 1 cm diameter ruby with an 80% reflective, dielectric film was tested in the two lamp light pot and its energy output measured from 300-600 joule input. Then the ruby was transferred to the four lamp light pot and the energy output measured from 650 to 800 joule input. The data are shown in Figure (5.14) The slope of the curve remains about the same for both light pots but the output at 650 and 700 joules is somewhat low. This is to be expected since the lamps are not operating at maximum efficiency at these low power levels. This effect also occurs at 325 and 350 joules but since the ruby is so close to threshold at that output, the difference is much smaller.

3.0 Work Planned for Next Period

For the next period we plan a continued investigation of high peak power pulses by the Kerr cell, rotating mirror, and avalanche methods, and the effect of these pulses on materials.

Output vs Flash Rate

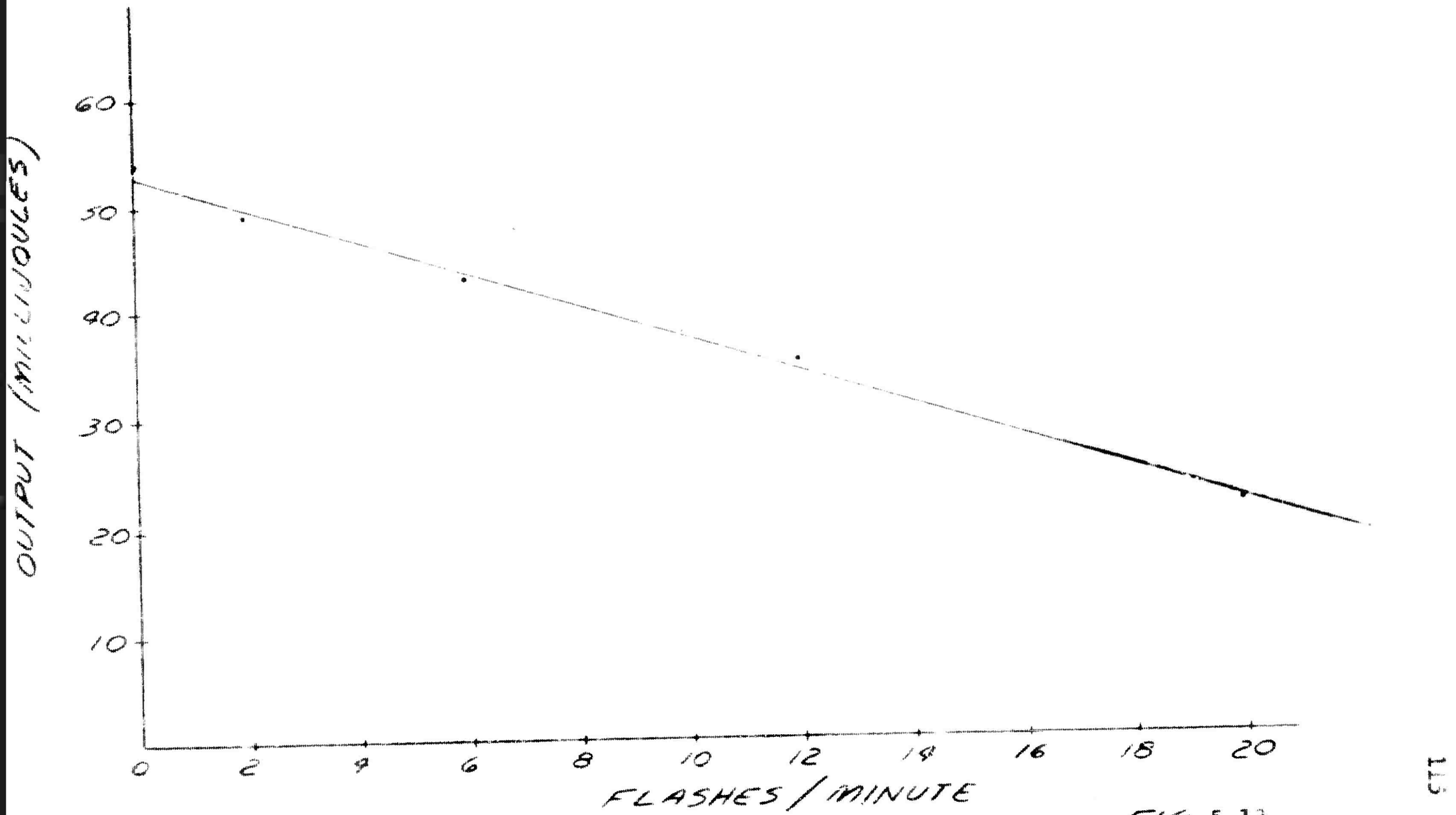

FIG. 5.13

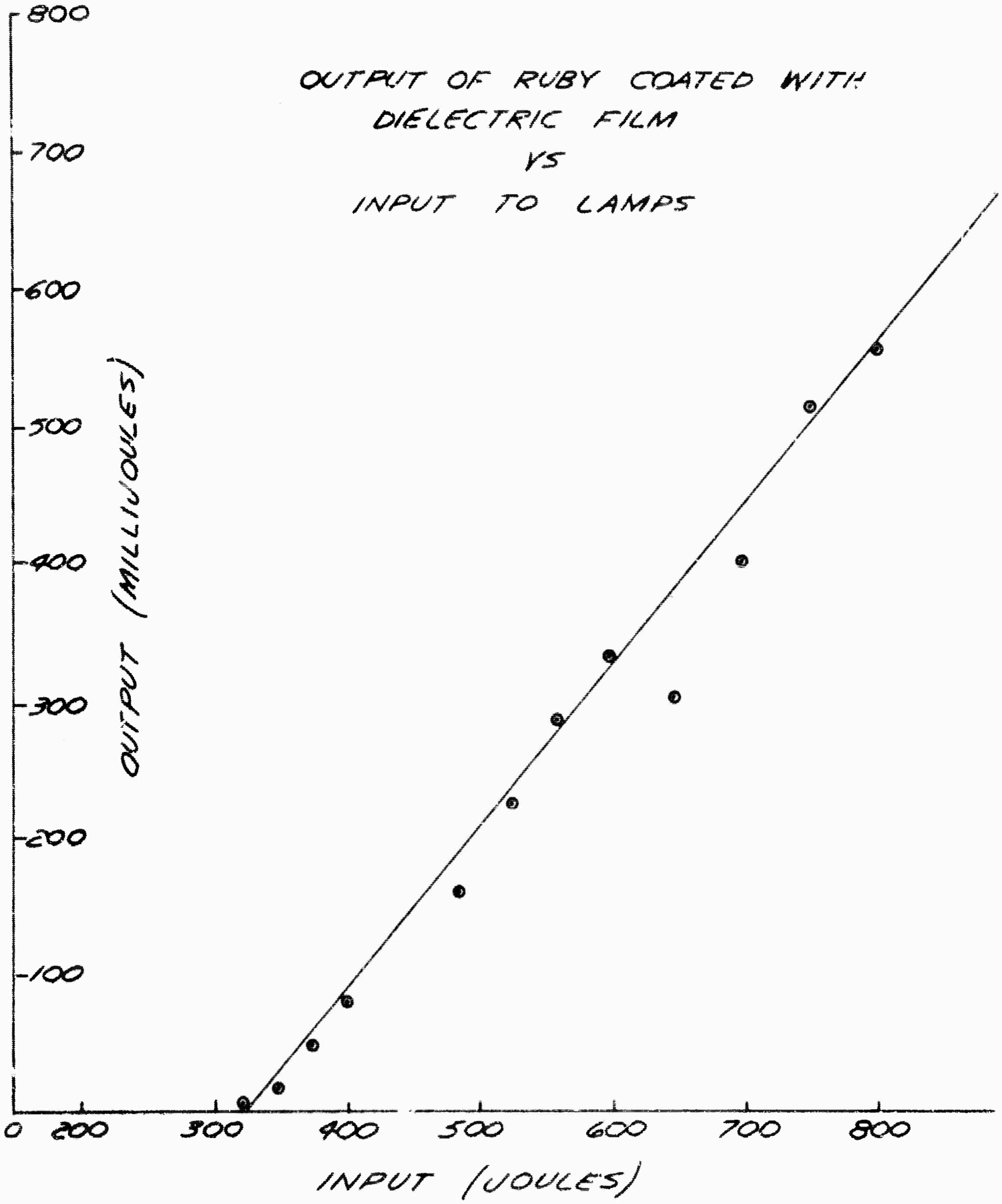
OUTPUT OF RUBY COATED WITH
DIELECTRIC FILM
VS
INPUT TO LAMPS
OUTPUT (MILLIJOULES)
800
700
600
500
400
300
200
100
0
200
300
400
500
600
700
800
INPUT (JOULES)

Figure 5.14

VI. Optical Pumping of Rare Earth Crystals

1.0 Summary of Work Performed

The study of the optical pumping of rare earth ions during this period has mainly centered on the investigation of calcium tungstate crystals containing either Dy^{3+} or Nd^{3+}. Two crystals of $CaWO_4$:Nd have been polished to optical tolerances. LASER oscillation has been observed in both at 1.065μ. No oscillation has yet been observed (at 5740A) in the several crystals of $CaWO_4$:Dy tried.

2.0 Analysis of Work Performed

2.1 The Neodymium LASER

Emission from the Nd^{3+} ion occurs from the $^4F_{3/2}$ level primarily to the $^4I_{9/2}$, $^4I_{11/2}$, and $^4I_{13/2}$ levels at wavelengths centered around 8800A, 1.06μ, and 1.34μ, respectively. Each group consists of a series of sharp lines. The lifetime of the $^4F_{3/2}$ level for 0.1% molar concentration of Nd in $CaWO_4$ was observed to be 150 μsec. The strongest of the emission lines are those around 1.06μ. Oscillation of these lines have previously been reported by Johnson and Nassau[38] (Nd in $CaWO_4$) and by Snitzer[39] (Nd in glass).

At TRG three boules of $CaWO_4$ containing 0.1 molar percent of Nd have been ground into cylindrical rods and two of these have been polished with the ends flat and parallel to optical tolerances. The third is presently in the process of being polished. All of these crystals

(38) L. F. Johnson and K. Nassau, Proc. IRE 49 1704 (1961)

(39) E. Snitzer, Phys. Rev. Let. 7, 444 (1961)

were annealed for five days at 1250°C and cooled slowly. Fabrication of a cylindrical rod from a fourth boule was attempted without annealing. This boule however shattered in the grinding process.

Each of the two polished crystals was coated with an opaque silver film on one end and a film of ~5% transmission on the other. They were inserted in a quartz dewar mounted inside the helical GE FT 524 flash lamp surrounded by an Al reflecting foil. Cold nitrogen gas was passed through the dewar to cool the crystal. Output gas temperatures were normally about 100°K and the crystal temperatures were probably close to this value.

LASER oscillation was observed from each of the crystals with an input to the xenon lamp of 300 joules. Initial detection was accomplished with an RCA 7102 photomultiplier, suitable neutral density filters, and an infra-red filter to eliminate all wavelengths below 8500A. Figure (6.1)shows a typical oscilloscope trace with excitation above threshold. The spiked oscillation is observed superimposed on a background of scattered light from the flash lamp, accepted over a very wide range of wavelengths. The wavelength of oscillation was determined by passing the light through a Jarrell-Ash monochromator. In one of the crystals oscillation occurred at 10,649A with a width certainly less than 1A, and probably very much less. These results have been achieved very recently and the characteristics of the LASER are being investigated.

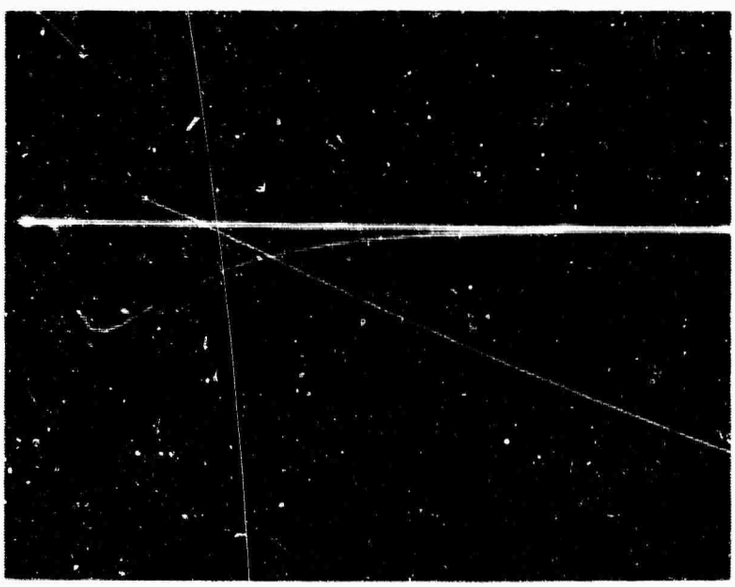

LASER Oscillation from $CaWO_4:Nd$

Figure 6.1

2.2 Investigation of Dy in $CaWO_4$

Since the last report several attempts have been made to excite Dy to oscillation at 5740Å. No oscillations have been observed.

Six different crystals have been investigated. These included two concentrations of Dy ion and three different orientations of the c-axis to the axis of the rod. The finished crystals varied in diameter from .25" to .4" and in length from 1" to 1-5/8". All were polished with ends flat and parallel. Silver films were generally used for the reflecting coatings, although one of the crystals had a multilayer coating of 5% transmission on the output end. One of the crystals, 0.5% Dy with the c axis along the axis of the cylinder (0° crystal), appeared to be of exceptional optical quality.

Several excitation geometries were tried. These included the normal helical GE-FT-524 flash lamp, a similar lamp modified to obtain a faster flash (by filling with Xe to higher pressure), a helical flash lamp filled with He at relatively high pressures, and a more efficient cylindrical geometry with straight Xe flash lamps.

The crystal was cooled in a quartz dewar to about $100^\circ K$ by cold N_2 gas in each case. While the inclusion of the dewar reduces the excitation efficiency, there remains a net gain for low temperature operation. Measurements at low power indicate that the brightness of emission at $100^\circ K$ is about 4 times greater than at room temperature (see Figure 6.2).

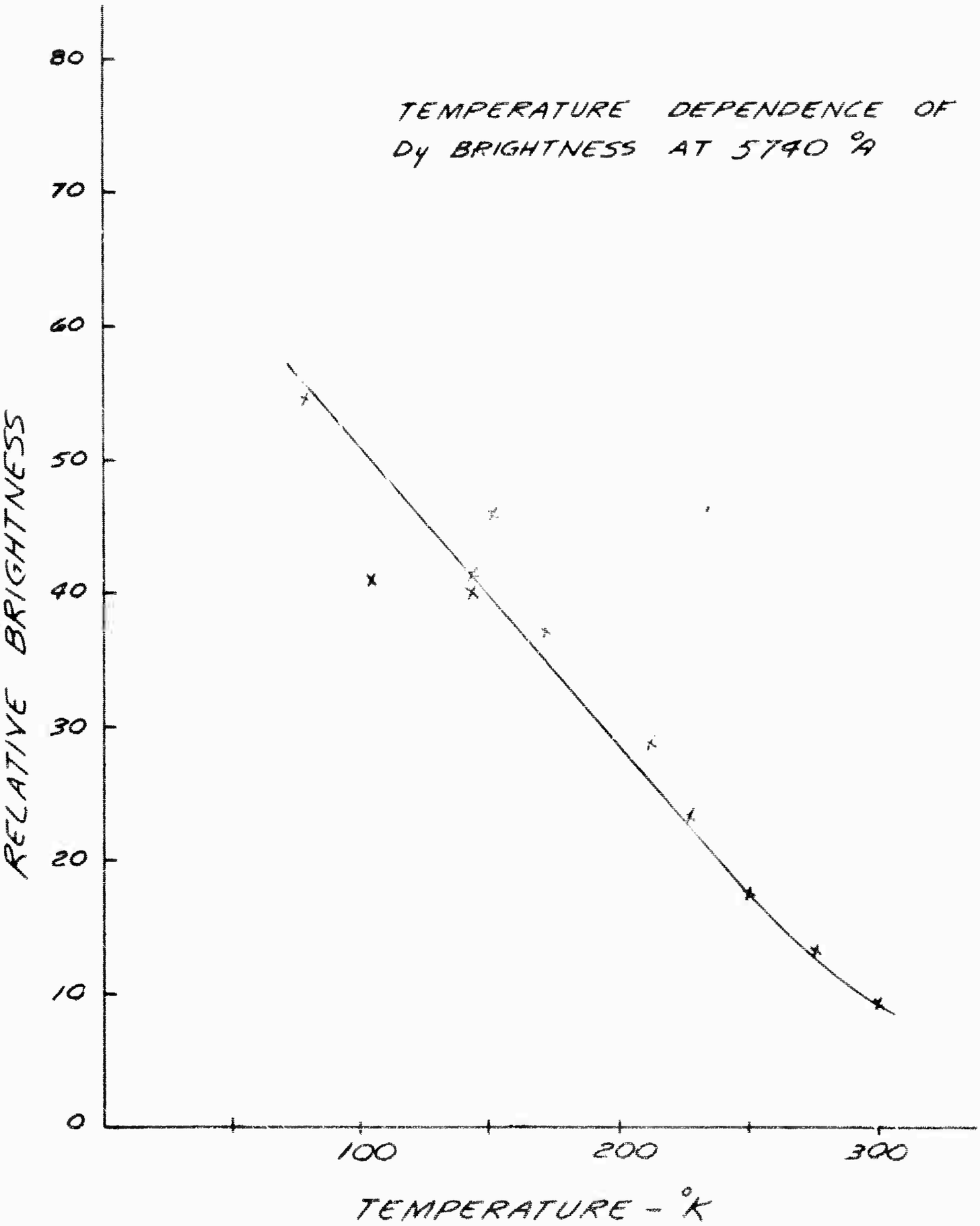

Figure 6.2

TECHNICAL RESEARCH GROUP

The presence of the dewar also makes the problem of shielding against stray light from the flash lamp more difficult. This background light does not prevent the observation of an oscillation, since the output beam of an oscillating crystal is normally (through a monochromator) orders of magnitude brighter than the background. However, the observation of the intensity of spontaneous emission in the presence of this stray light is more difficult. It has not yet been measured adequately at high power on any of the crystals investigated.

This intensity measurement is a crucial test to indicate the direction in which the investigation must proceed to be successful. An emission brightness in excess of the critical brightness for oscillation can only mean either

a) the lower level of the transition has also been populated (either by the lamp directly at infra-red wavelengths, or by decay from upper levels) or

b) the crystal quality is not adequate.

Since the latter is not believed to be the case filtering to exclude infra-red pumping to the lower levels would be called for. On the other hand, if the emission brightness at high power is below the critical brightness for oscillation, then it would not have been linear with excitation power. Measurements at low power indicate that the crystals will oscillate at 5740A at lower excitation power than ruby. Such saturation effects might come about for several reasons, namely,

a) pumping out of the excited state

b) a bottle neck in the non-radiative transitions from the absorbing level to the excited state and

c) line broadening at high population densities in the excited state.

Investigation of these crystals and others at lower power has yielded the following information.

A high pressure Hg flash lamp excites Dy more efficiently than Xe. However, much of this excitation is in the UV below 3200A and in the absorption band of the $CaWO_4$ lattice itself. This may not prove to be desirable because of the large heat loss involved in excitation at this wavelength and subsequent decay to the lowest excited state of Dy at 21,000 cm^{-1}. High power Hg flash lamps must be operated hot because of the low vapor pressure of Hg at room temperature. While this involves difficulties it remains a possibility for higher excitation of Dy.

With the xenon flash lamp, which has very little energy below 3,000A blue phosphorescence has been observed from the crystal after an intense flash. The connection between this and an observed decrease in emission intensity directly after the flash has not been established. This decrease in emission intensity is observed with excitation by a CW xenon lamp between coils of the helical flash lamp. The 5740A line is detected through a monochromator and recorded continuously on a Sanborn recorder. When a shutter is inserted momentarily between the crystal and the monochromator the detected signal goes to zero and returns

to its original value. If, however, the flash lamp was fired during the time that the shutter was in place the signal returns to only about half of its original value. It increases slowly to nearly its original value with about a 90 sec time constant. The long time constant suggests the connection between this decrease in intensity and the observed phosphorescence of the crystal. The excitation of Dy by xenon is mainly in a series of lines in the blue between 4200 and 4500A. Filtering to eliminate the UV may reduce this phosphorescence and give better results on emission intensity. At the present time, however, the loss of efficiency due to filtering could not be tolerated.

Investigation of the infra-red spectrum of Dy has not revealed any lines sufficiently strong to oscillate before the yellow 5740A line. However, the investigation has not been very complete and this possibility is not entirely eliminated. The critical population density for oscillation in an infra-red transition from the same upper level could be less than for the 5740A transition. If an oscillation did occur in the infra-red without being observed it would clamp the population density of the upper level, $^6F_{11/2}$, and the yellow line would never reach oscillation. The use of a multilayer reflector on one of the crystals should eliminate this possibility since it only reflected well in a wavelength band centered at 5740A and is transparent in the infra-red.

Differences are observed in the structure of the emission spectrum for different orientations of the crystal axis to the axis of the rod. This indicates the existence of both σ and π radiation in

different transitions. Some polarization of the emission must then exist. These investigations will be reported more fully when the polarization has been studied.

Excitation of Dy by a high pressure He flash lamp proved less efficient than Xe although Dy has a series of sharp absorption lines in the neighborhood of a pressure broadened 3888A He line.

2.3 Other LASER Materials

An improved low temperature apparatus for investigating the LASER possibilities of other materials has been constructed, tested, and is ready for operation. It is shown in Figure (63). The preparation of various other materials for investigation is reported in another section.

3.0 Work Planned for the Next Period

The program on rare earths for the next period will include the following:

a) Continued investigation of the output characteristics of the $CaWO_4$:Nd LASER, including its operation at CW,

b) Continued investigation of Dy in $CaWO_4$ to achieve an operating LASER at 5740A, and

c) Investigation of the LASER possibilities of the rare earth ions in other host lattices. These will mainly include the molybdates and the vanadates.

Apparatus for Low Temperature Investigation of Possible LASER Materials

Figure 6.3

TECHNICAL RESEARCH GROUP

VII. Growth of Rare Earth Doped Crystals

1.0 Summary of Work Performed

The foremost type of single crystals grown in this period was the tungstate (scheelite) type. The great majority of specimens consisted of calcium tungstate ($CaWO_4$) doped with various concentrations of $Na_{0.5}Dy_{0.5}WO_4$ in one series and of $Na_{0.5}Nd_{0.5}WO_4$ in another series. Six Dy-doped crystals were grown (all at predetermined orientation by seeding), and five of these were annealed. Six Nd-doped crystals were similarly grown, three of which were annealed. One crystal was grown from a melt of $Na_{0.5}La_{0.5}WO_4$, which proved to be inhomogeneous by observation and by chemical analysis of the crystal. In place of the induction furnace used for the above crystal growths, a resistance furnace was designed and built for the lower-melting host material: lead molybdate ($PbMoO_4$).

The earlier study of anhydrous lanthanum chloride as a host crystal was supplemented in this period by a study of anhydrous strontium chloride ($SrCl_2$). The resistance furnace used for lead molybdate was modified by maintaining an inert gas-hydrogen chloride atmosphere about the crucible of molten $SrCl_2$ to prevent its hydrolysis and oxidation. Pulling a crystal from this melt (to be doped with divalent samarium chloride) will be attempted.

A new material for incorporating rare earth ions was prepared: yttrium vanadate (YVO_4). It melts at about 1800°C and seems to promote line fluorescence of rare earths.

2.0 Analysis of Work Performed

2.1 Tungstate Type of Crystal

2.1.1 Introduction

Since the beginning of 1961, TRG has conducted studies on the growth of calcium tungstate ($CaWO_4$) as single crystals. The technique used is to initiate crystal growth centrally at the surface of the melt and to withdraw the growing crystal slowly by means of a pulling (and rotating) mechanism. The melt is contained in a large rhodium crucible which is heated inductively by a 45 kw source of rf power. Suitable insulation surrounding the crucible is provided and the insulation above the melt is adjusted by trial until temperature gradients are right for growth of a rod-like boule by pulling and rotation.

Various furnace configurations (for example, the number and size of turns in the rf coil) were tried, together with increasing amounts of calcium tungstate melt. Best results are obtained when the rhodium crucible is filled nearly to capacity and adequate rf power is used to maintain the melt.

At first, crystal growths were initiated by dipping a slender platinum rod into the melt. Later, when a supply of single crystal specimens had accumulated, seed crystals were prepared by cutting out pieces of crystals and drilling holes in them for attachment to the platinum rod.

In both initiation methods (bare platinum and seed crystal), some unusually hot streaks in the emerging crystal occurred all too frequently, until resort was made to insulation of the platinum rod from the metal chuck holding it. The electrical insulation at this point consists of a

Teflon sleeve over the end of the platinum rod and this effectively insulates the entire supporting rig from the melt-to-rod junction. The hot streak at this junction was thereby eliminated.

2.1.2 Experimental Results

In the period covered by this report, several series of tungstate type crystals were grown reliably, once the technique described above was established. The host compounds for rare-earth dopants were:

calcium tungstate	$CaWO_4$ (foremosc)
sodium lanthanum tungstate	$Na_{0.5}La_{0.5}WO_4$
lead molybdate	$PbMoO_4$

All of these compounds crystallize in the tetragonal system (scheelite - $CaWO_4$ - structure). The approximate ionic diameters (in A) are listed below:[40]

Ca^{++}	1.0	Pb^{++}	1.2	
Na^{+}	1.0	W^{6+}	0.6	$O^{=}$ 1.4
La^{+++}	1.2	Mo^{6+}	0.6	

The tripositive ions of the rare earth elements Ce(At.No. 58) through Lu (At.No.71) have diameters diminishing gradually from 1.1 to 0.9A. Substitution of these ions in place of Ca^{++} or Pb^{++} requires addition also of Na^{+} in equal number for charge compensation. Otherwise, there would be vacancies in the scheelite lattice.

Therefore, the rare earth dopants were $Na_{0.5}R_{0.5}WO_4$ or $Na_{0.5}R_{0.5}MoO_4$ (R denoting the tripositive rare earth ion). These dopants were synthesized at TRG by combining stoichiometric quantities of Na_2WO_4 and WO_3(or Na_2MoO_4 and MoO_3), and R_2O_3 and firing the well-blended powders at 700°C.

40 J. Green, Bull. Geol. Soc. Am. 70, Table 2 (1959)

Alternatively, the double salt $Na_{0.5}R_{0.5}SO_4 \cdot 1/2\ H_2O$ is readily obtained in pure form and, when fired (above 700°C) with the stoichiometric amount of WO_3, displacement of SO_3 and 1/2 H_2O ensues with formation of $Na_{0.5}R_{0.5}WO_4$.

Nearly all the single crystal specimens of the tungstate type which were produced during this period are listed in Table II. The only additional specimens of any significance are Nos. Dy-17, 18 and 19 ($CaWO_4$ host) grown most recently with 0.01 Dy concentration and standard orientation. Fig. (7.1) shows two of these boules in addition to three finished crystals containing Nd and Dy.

A few explanatory remarks should be made now on the crystals produced. Standard orientation denotes the angle with respect to the tetragonal c-axis at which the crystal grows spontaneously (from bare platinum rod initiation or sintered pellet initiation). The standard orientation is not a matter of chance but is quite characteristic as demonstrated by directions of cleavage and by polarimetric examination. Seed crystals prepared on the basis of this information lead to the more definite orientations of new crystal growths (0° and 90°).

The experiment with $Na_{0.5}La_{0.5}WO_4$ was performed with the same apparatus used for $CaWO_4$ crystals. The experiment with $PbMoO_4$, however, was performed with another arrangement (specially built resistance heater furnace) located adjacent to a ventilating hood because of toxic fumes from $PbMoO_4$.

TABLE 7.1

List of Single Crystals Produced
(chronological order)

Host Material	Melting Point (°C)	Dopant Concentration*	Crystal Orientation	Weight (grams)	Annealed	Code Number
$CaWO_4$	1550	None	Standard	17.8	No	Ca-1
$CaWO_4$	1550	None	Standard	17.6	No	Ca-2
$CaWO_4$	1550	None	90° to Std.	46	No	Ca-3
$CaWO_4$	1550	0.005 Dy	90° to Std.	35	No	Dy-11
$CaWO_4$	1550	0.005 Dy	0° to c-axis	45	Yes	Dy-12
$CaWO_4$	1550	0.01 Dy	0° to c-axis	36	Yes	Dy-13
$CaWO_4$	1550	0.01 Dy	90° to c-axis	22	Yes	Dy-14
$CaWO_4$	1550	0.01 Dy	90° to c-axis	18.5	Yes	Dy-15
$CaWO_4$	1550	0.005 Dy	90° to c-axis	26	Yes	Dy-16
$Na_{0.5}La_{0.5}WO_4$	1220	None	Standard	13	No	____
$PbMoO_4$	1068	0.005 Eu	Standard	___	Yes	Pb-1
$PbMoO_4$	1068	0.005 Eu	Standard	___	No	Pb-2
$PbMoO_4$	1068	0.005 Eu	Standard	___	No	Pb-3
$CaWO_4$	1550	0.001 Nd	Standard	15	No	Nd-1
$CaWO_4$	1550	0.001 Nd	90° to c-axis	48	No	Nd-2
$CaWO_4$	1550	0.001 Nd	90° to c-axis	65	Yes	Nd-3
$CaWO_4$	1550	0.001 Nd	0° to c-axis	68	No	Nd-4
$CaWO_4$	1550	0.001 Nd	0° to c-axis	82	Yes	Nd-5
$CaWO_4$	1550	0.001 Nd	0° to c-axis	54	Yes	Nd-6
$PbMoO_4$	1068	0.005 Eu	Standard	15	No	Pb-4

*Numerical value is for x in the formula $Ca_{1-2x}\ Na_xR_xWO_4$ where R is the rare earth element noted.

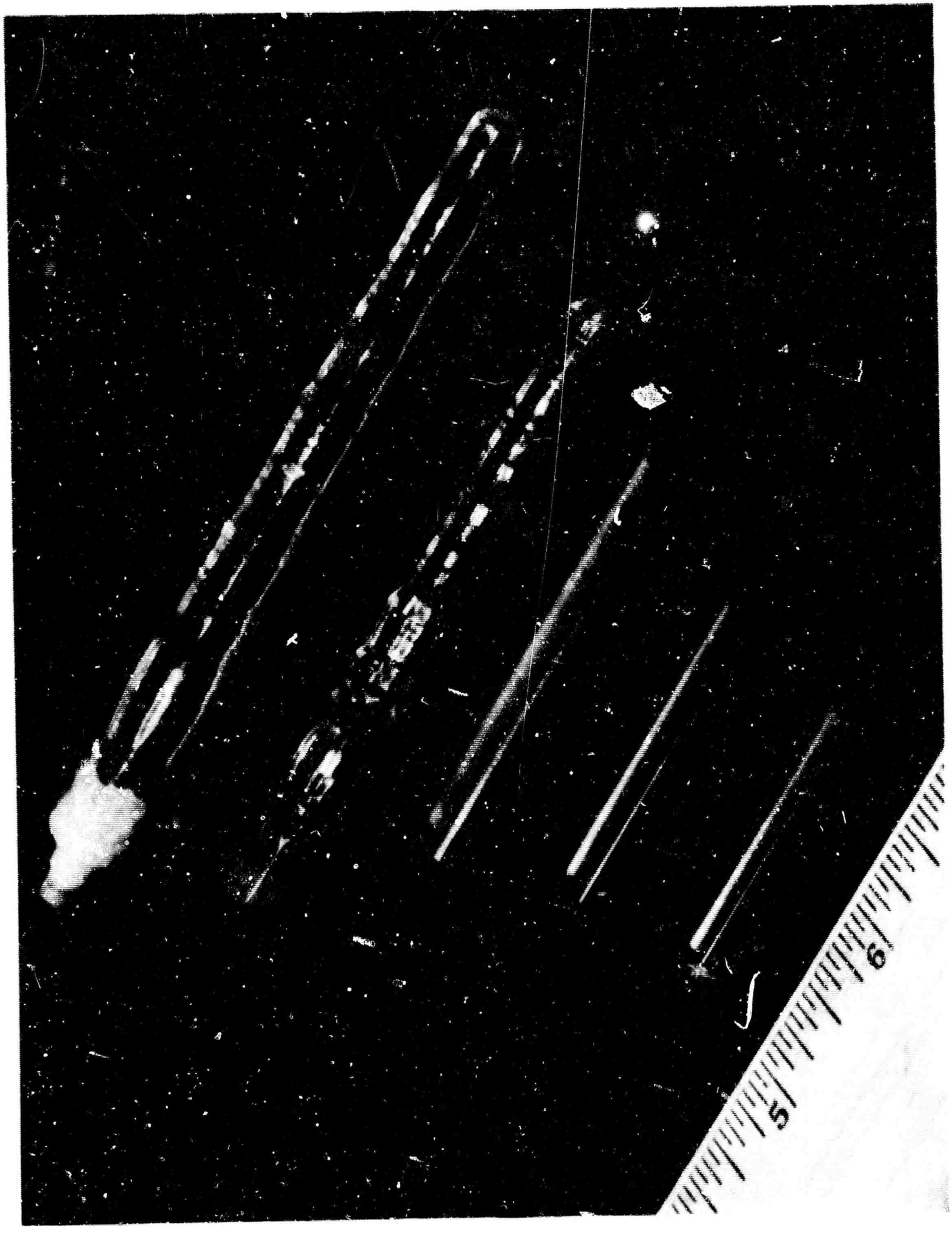

Boules and Finished Crystals of Nd and Dy in $CaWO_4$

Figure 7.1

TECHNICAL RESEARCH GROUP

The annealing of crystals was done by propping the crystals upright (as they had been grown) inside alumina crucibles packed loosely with alumina pebbles and heating the objects inside a silicon carbide resistance furnace. The annealing cycle was manually programmed to a temperature rise over a 2-day period from ambient to 1450°C maximum temperature (in the case of Dy-12---16) or 1225°C (in the case Nd-3,5,6), held there for five to seven days and lowered to ambient temperature (in two days for Dy-crystals, in seven days for Nd-crystals). Not a single crystal was cracked by these annealings.

2.1.3 Discussion of Results in Growing the Tungstate Type of Crystal

Calcium tungstate (melting point approximately 1550°C) is readily grown as large single crystalline boules by the technique described above. As the boules are fragile, annealing is essential before they can be finished into cylindrical rod forms. Optical clarity varies but some rod specimens have been found to be of good quality.

Examination of $CaWO_4$ crystal fracture surfaces shows that often these are multi-faceted and not merely conchoidal. Whether these represent various faces of a truly single crystal or a mosaic pattern of an imperfect crystal is not certain. Occasionally there is found sharp cleavage of the crystals.

The composition of rare-earth ion dope ($Na_{0.5}R_{0.5}WO_4$ for example) establishes the dopant concentration in the $CaWO_4$ melt, because the weights of the two are always known. It is assumed that the dopant con-

centration in the crystal is the same as that of the melt. This assumption is reasonably valid, because of the isomorphous character of the two compounds (the partition constant of the dope between melt and crystal is close to unity). The variation in dope concentration along the axis of a single boule should be very slight, because at most only 10 to 20 per cent of the melt is withdrawn to form a single boule.

Just how the Na^{+} and R^{+++} ions occupy the Ca^{++} sites in $CaWO_4$ is not certain. Partly to secure information on this, and partly to find a more suitable host than $CaWO_4$ for europium ion (which has a tendency to change from +3 to +2), an experiment was undertaken with $Na_{0.5}La_{0.5}WO_4$ as a host crystal. A preliminary value for the melting point of this was taken to be 1220°C. In the rhodium melting pot, however, there was evidence of a melt existing above a heterogeneous layer at this temperature. Although a crystal was pulled from the melt, chemical analysis showed that its composition was not $Na_{0.5}La_{0.5}WO_4$.

The best available lead molybdate ($PbMoO_4$) was purchased and used to test its growth as a single crystal doped with $Na_{0.5}Eu_{0.5}MoO_4$. In the course of densifying the commercial $PbMoO_4$ by preheating, evolution of NO_2 fumes at 500°C clearly indicated impurity consisting of lead nitrate, $Pb(NO_3)_2$. The crystal boule from the doped melt subsequently was too dark-colored for acceptance as a candidate crystal.

2.2 The Anhydrous Chlorides

2.2.1 Experimental Results

The very first crystal growth system investigated at TRG was anhydrous lanthanum chloride ($LaCl_3$). Our experience of finding this

system difficult to master agrees with that of other laboratories. It is felt, however, that the $LaCl_3$ host deserves further consideration because it is a favorable medium for sharp line fluorescence of rare earth trichlorides incorporated therein.

As the Bridgman technique used earlier did not yield good results, preparations have been made to try the pulling-from-melt technique. The large quantity of anhydrous chloride material required for this purpose has been made by a new procedure. A resistance furnace of the type used for lead molybdate has been constructed with the modification of maintaining an inert gas-hydrogen chloride atmosphere about the crucible of melt to prevent hydrolysis and oxidation of the molten chloride.

The procedure adopted has been applied to both anhydrous $LaCl_3$ and $SrCl_2$. The strontium chloride melt preparation and initial crystal growth test was better than that of lanthanum chloride, probably because of improved technique.

By means of procedures previously used for small quantities of chlorides, supplemented by reduction with hydrogen, anhydrous $EuCl_2$ and $SmCl_2$ have been prepared.

2.2.2 Discussion of Results in Growing the Chloride Type of Crystal

The difficulty of growing anhydrous chloride crystals can be overcome. However, special precautions in handling the crystal will have to be taken, because of its hygroscopic nature. This may not be an acute problem for a large single crystal, as it is for a loose powder of the anhydrous chloride.

The interest in strontium chloride ($SrCl_2$) as a host, especially for dichlorides such as $SmCl_2$, may be greater than that in $LaCl_3$ for trichlorides, because of broadband light absorption by Sm^{++}. The sample of reduced $SmCl_3$ which is available now for doping of strontium chloride is probably not 100% $SmCl_2$. However, as reported elsewhere[41] for the case of fluorides, even the partial existence of the Sm ion in the +2 state is effective in media such as CaF_2.

2.3 Miscellaneous Crystals

2.3.1 Experimental Results

The properties of numerous crystalline compounds have been surveyed in searching for other host compounds for rare earths. Hard, thermally conductive crystals are most desirable for high LASER power applications. This generally means that crystals with melting points above 1600°C are the best candidates. They should also fulfill the requirements of

a) lattice structures with which rare earth dopants are compatible,

b) stability toward thermal and other environments,

c) enhancing the photoactivation of rare earth ions and/or not quenching their luminescence, and of course,

d) growability as single crystals.

A ready compilation of crystal structures[42] furnishes many selections of candidates to choose from. The particular case of yttrium vanadate (YVO_4), with which most of the rare earth vanadates are isomorphous,

---

(41) C.G.B. Garrett, W. Kaiser, and D. L. Wood, "Fluorescence and Optical MASER Effects in $CaF_2:Sm^{++}$". Preprint.

(42) Landolt-Bornstein, Zahlenwerte and Funktionen, I. Bd., 4. Tl. Berlin: Springer-Verlag (1955).

was then investigated. Yttrium vanadate has the zircon structure. The method published[43] for the preparation of YVO_4 (from Y_2O_3 and NH_4VO_3) was followed. Sintering finally at 1000°C, as directed, did not yield the "gray" product. Repowdered, the orange product was fired at 1600°C (without melting) to give a white product with a whitish fluorescence. Repetition of this procedure resulted in a white product but with a bright red fluorescence. Visual spectroscopic examination showed the red fluorescence to be a line (not band) fluorescence, probably because of a minute impurity of europium ions.

The melting point of this yttrium vanadate was estimated by a flame fusion test (using pure alumina powder for comparison) to be in the neighborhood of 1800°C. It should be noted that the melting point of yttrium oxide (Y_2O_3) is 2410°C and that of vanadium pentoxide (V_2O_5) is 660°C. The latter cannot be sublimed or chemically decomposed up to 1800°C[44]

As a means of fluxing YVO_4, the salt lithium vanadate (Li_3VO_4) was prepared and its melting point established at about 1200°C. A furnace was set up to heat a melt of Li_3VO_4 and YVO_4 in a platinum crucible and to cool the melt slowly in order to obtain well-formed microcrystals of YVO_4 for evaluation.

The possibility of thulium ion (Tm^{++}) in the divalent state for effective light absorption seems worth investigating. Toward this end, a small quantity of anhydrous thulium trichloride ($TmCl_3$) was prepared by the usual dehydration method. The reduction of this compound will require an unusually vigorous method.

---

(43) E. Broch, Zeit. Physik. Chem. B20, 345 (1933)

(44) N. V. Sidgwick, The Chemical Elements and Their Compounds. Oxford: The Clarendon Press (1950), page 809

2.3.2 Discussion of Results

The discovery of sharp line fluorescence in yttrium vanadate due to a rate earth impurity (probably europium) suggests strongly that yttrium vanadate merits further consideration as a host crystal for rare earth ions. The compound YVO_4 offers the advantage also of directly incorporating tripositive rare earth ions in place of Y^{3+} without the necessity of additional ions such as Na^+ for charge compensation, which is necessary with $CaWO_4$ as a host.

Since the elements niobium (columbium) and tantalum are in the same family as vanadium, yttrium niobate ($YNbO_4$) and tantalate ($YTaO_4$) also offer promise, especially since minerals of this type are known. They should have melting points at least as high as that of YVO_4. The crystal structure of $YNbO_4$ or $YTaO_4$ is not clearly that of zircon.

The phosphates, also of analogous chemical composition but not the same structure as vanadate, do not appear feasible to grow from melts or fluxes. A very possible decomposition product (P_2O_5) is very volatile.

3.0 Work Planned for Next Period

3.1 Future Plans in Growing the Tungstate Type of Crystal

The perfection of calcium tungstate crystals is considered worth further investigation. Generally, the crystals have been grown at a linear rate of 3/8" per hour,which is about as slow as is practical. Perfection probably will entail more exact preparations of seed crystals, various atmospheres about the crystal-growing crucible, systematic material balances and chemical analyses throughout a given series of rare-earth doped crystals, and improved temperature controls during

growth of such crystals.

The rare earth ions (3+) of chief interest in $CaWO_4$ or any other crystal are Pr, Nd, Sm, Eu, Tb and Dy. The tendency for Pr to become +4 is more pronounced than that of Tb. On the other hand, Eu has a more pronounced tendency than Sm to become +2. These peculiarities must be considered in the interpretation of optical and electrical phenomena in crystals containing these ions. Specific atmospheres during growth and annealing of the crystals may be required.

The sodium lanthanum tungstate ($Na_{0.5}La_{0.5}WO_4$) host crystal should be tested for growth once again, but at a temperature higher than 1220°C. The melt from which the crystal is pulled should then be homogeneous. If this test is successful, the replacement of a small fraction of La by a rare earth ion would be attempted.

The lead molybdate crystal (melting point 1068°C) can be grown in the specially designed and constructed resistance furnace mentioned previously. Besides venting of the apparatus, care is necessary to check the composition of $PbMoO_4$ (MoO_3 volatilization) and correct it by addition of MoO_3. The relative stability of unusual valence states of rare earth elements in $PbMoO_4$ may be compared with that in $CaWO_4$ and $CaMoO_4$. Calcium molybdate undoubtedly melts at a higher temperature than lead molybdate. Hence a vented induction furnace is recommended for $CaMoO_4$, which probably has hardness and photo-excitation properties superior to those of $PbMoO_4$.

3.2 Future Plans in Growing the Chloride Type of Crystal

A limited effort should be devoted to obtain clear single crystals of $SrCl_2$ and/or $LaCl_3$ doped with $SmCl_2$ and/or RCl_3 (R-several rare earth elements). The case of yttrium chloride (YCl_3) may be advantageous for the heavier rare earths.

Plans have been formulated for study of a few fluoride systems: CaF_2 (which forms anomalous solid solutions with YF_3) and SrF_2 (which forms anomalous solid solutions with LaF_3). Heavier rare earth fluorides substitute readily with YF_3, the lighter ones with LaF_3. The measured fluorescence spectra of rare earths in CaF_2[65] suggest that the mixed fluoride LaF_3 . YF_3 be studied as host material. In general, fluorides are preferable to chlorides because they are not as hygroscopic as the chlorides.

3.3 Future Plans for Miscellaneous Crystals

Planning the work with new crystal candidates is subject to frequent revisions as experience with their preparation may dictate.

The yttrium vanadate should be obtainable in micro-crystalline form for evaluation at an early date. The design and construction of a very high temperature furnace (for 1800°C operation) is under way in anticipation of growing crystals of YVO_4 or other material from the melt.

Several other kinds of oxy-salts will be considered for preliminary examination: titanosilicate ($CaTiSiO_5$), yttrium gallium garnet ($Y_3Ga_5O_{12}$), and cerates (Na_2CeO_3), to mention only three types.

Oxide crystals (other than TiO_2, Al_2O_3 or MgO) will require

---

(65) N. Chatterjee, Zeit. f. Physik 113, 96 (1939)

extremely high temperatures in those relatively few cases which are stable in the melt. Moderate melting oxides such as B_2O_3 or SiO_2 tend to form glasses. Mixed oxides offer more possibilities, as do the oxy-salts. Many oxygen compounds cannot be classified definitely as an oxy-salt or mixed oxide.

VIII. Optical Devices

1.0 Summary of Work Performed

Experimental and analytical work has shown that efficient coupling in optical pumping can be achieved using a reflective circular cylinder. Efficiencies are higher than in diffuse cavities or reflective ellipses under conditions where the lamp and sample diameters are not negligible compared to the cavity diameter.

A theoretical analysis of the properties of cube corner interferometers has been experimentally verified. An attempt was made to build an oscillator using such an interferometer as a resonant cavity.

2.0 Analysis of Work Performed

2.1 Efficient Optical Pumping

A common technique for optically pumping ruby is to place the crystal in a helically shaped discharge tube. Typical thresholds for oscillation in such a configuration range from 1000 to 3000 joules into the discharge lamp.

If the shape of the object to be pumped is a slender cylinder, as it is in the case of ruby or some optically pumped gas systems, a more efficient scheme may be to image a line source onto the medium. An ideal configuration is that of an elliptical cylinder with the source

at one line focus and the ruby at the other.

Several such cavities were made for the helium pumped cesium system. Some were machined out of aluminum and one was fabricated from glass. It becomes apparent that while a line at one focus is imaged into a line at the other, a source of finite diameter will be imaged with varying magnification depending on the zone of the elliptical cross-section chosen. That is, rays focussed by that part of the cylinder nearest the focus will form an image reduced in size while those rays focussed by the part nearest the source will form an enlarged image. This comatic image formation results in a lack of pumping efficiency.

An effort was made to reduce this loss by constructing a diffuse reflecting cavity as discussed in the previous report. Similar small cavities were constructed for a ruby LASER and evaluated. Typical thresholds were 350 to 400 joules.

An alternative procedure to reduce the loss due to image magnification is to work with a specular elliptical cavity whose eccentricity is as small as possible. As a matter of fact, for a source of finite extent to be imaged on an absorber of like size, an efficient cavity is a circular cylinder with the source and absorber placed diametrically equidistant from the center. This structure was used with a ruby LASER and typical thresholds were 170 to 200 joules.

A LASER was constructed with a ruby whose dimensions were 1/4" x 1-1/2" in such a reflecting cavity and had a threshold of 70 joules.

This configuration has been applied to the helium-cesium experiment and a gain of two is expected in the pumping efficiency.

2.2 Cube-Corner Fabry-Perot Interferometer

The analysis of cube-corner reflectors has been submitted to the Journal of the Optical Society of America by Peck. His predictions as to the polarized nature of the fringe systems were experimentally verified at TRG and a paper submitted to JOSA. This paper is reproduced on the following pages.

Scheduled for publication in the JOSA, April 1962

ABSTRACT

CUBE-CORNER FABRY-PEROT INTERFEROMETER

by P. Rabinowitz, S. F. Jacobs
T. Shultz and G. Gould

TRG, Incorporated
Syosset, New York

Polarized Haidinger fringes have been observed in a Fabry-Perot interferometer with one flat replaced by a cube corner prism. Orientation of the polarization planes of the fringes and their relative phase shifts have been measured. Some applications are suggested.

The polarization properties of cube-corner reflectors have been analyzed theoretically by Peck in the preceding article. He has shown that when one flat of a Fabry-Perot cavity is replaced by a cube corner, 6 eigenpolarizations (invariant polarization states) exist; that is, 2 orthogonal, plane-polarized standing waves with different effective optical path lengths may be excited through each pair of opposite sextants (Figure 1a). Peck's results indicate that when this cavity is used as an interferometer, orthogonal plane-polarized Haidinger fringe systems will be observed, corresponding to two plane-polarized standing waves within the cavity.

The predicted fringes were observed with an etalon constructed in this laboratory (Figure 2). A solid etalon was used, rather than a separate cube corner and flat, to obviate the need to anti-reflection coat the entrance face of the cube prism. This etalon consisted of a cube-corner prism of BK7 crown glass whose entrance face was coated with a partially transmitting silver film (approximately 5% transmittance). The prism faces were flat to $\lambda/20$. The prism measured approximately 1/2" from apex to entrance face. No effort was made to construct the entrance face of the prism exactly normal to the cube symmetry axis. The right angles of the cube were accurate to within 2 seconds of arc.

Unpolarized light from a water-cooled Hg^{198} lamp was introduced by means of 2 front surface aluminized mirrors, each set at 45° to the beam (Figure 2). Since a mirror introduces elliptical polarization when used at non-normal incidence, the planes of incidence of the mirrors were made orthogonal so that the elliptical polarization of the first reflection was compensated by the second. A mask was placed over the face of the prism so that light entered and emerged from opposite sextants (Figure 1b), thus making possible measurements of the polarization direction with respect to individual sextants. The output light was analyzed with a Nicol prism whose angular position was measured to within 1°.

The two sets of fringes, observed from each sextant (Figure 3), could be independently extinguished by rotation of the Nicol prism. The orientations of the planes of polarization for light emerging from each sextant were separately measured to be $16 \pm 0.5°$ and $106 \pm 0.5°$, in good agreement with Peck's calculated values, $\theta = 16.32°, 106.32°$. Figure 4 shows the convention used for measuring these angles with respect to each cube edge.

Differential phase shifts upon reflection through the prism cause different effective optical path lengths for each of the pairs of standing waves. The phase difference was determined by measuring, on

a ›tograph, the relative diameters of the two fringe systems. The measured value was 16- $\pm$ 10°, compared with $\Delta\sigma$ = 152.7° calculated by Peck. The deviation from Peck's value may be due to two causes: distortion of the fringe contours by overlapping of neighboring fringes, and the fact that the system optic axis is slightly skew from the normal to the entrance face, an orientation built into the prism and differing slightly from the case Peck analyzed.

These observations, although made with an etalon, demonstrate the feasibility of using cube-corner elements in a Fabry-Perot interferometer with the flat and cube as separate elements. (See Figure 5) With such an interferometer the free spectral range and resolution are identical with those of a plane Fabry-Perot of comparable reflectance and twice the separation. This is true because a ray must make two reflections from the flat before interference takes place. The optical separation, to be compared with the t of the plane Fabry-Perot, is twice the optical path length measured along a ray constructed normal to the flat and extending to the apex of the prism, taking into account the refraction of the ray at the prism interface (see Figure 6).

Alignment of this interferometer (separate flat and cube corner reflectors) is insensitive to rotation of its elements because of the retrodirective property of the cube. The limit of rotation of

the cube corner is set by the requirement for total internal reflection in the cube-corner prism. (If a triple mirror with metallic coatings is used, rather than a prism, the limit of rotation is set by reduction of aperture). The limit of tilt of the flat is set by the gross requirement that the beam be returned to the cube corner.

The property of angular insensitivity makes the Fabry-Perot interferometer, composed of separate cube and flat, especially suited for applications where stability of alignment is a major consideration. In particular, the motivation for this work was to develop a more stable resonator than the plane Fabry-Perot interferometer for LASER applications. The present work demonstrates the feasibility of a cube-corner optical resonator and work is in progress in this laboratory to construct a He-Ne LASER utilizing a cube-corner resonator.

An additional application for this interferometer lies in the mechanical scanning of fringes by longitudinal motion of the prism, in much the same way as is done with the Michelson interferometer[1,2]. It should be possible to scan over large distances (several meters) without loss of alignment. Another application is in interferometry

---

(1) E. R. Peck, J. Opt. Soc. Am. 38, 66 1948
(2) E. R. Peck, J. Opt. Soc. Am. 38, 1015, 1948

outside the visible region of the spectrum involving the use of materials which are opaque in the visible. With cube-corner Fabry-Perot interferometer, good alignment will be assured, provided there is adequate optical homogeneity in the optical material.

LIST OF FIGURES

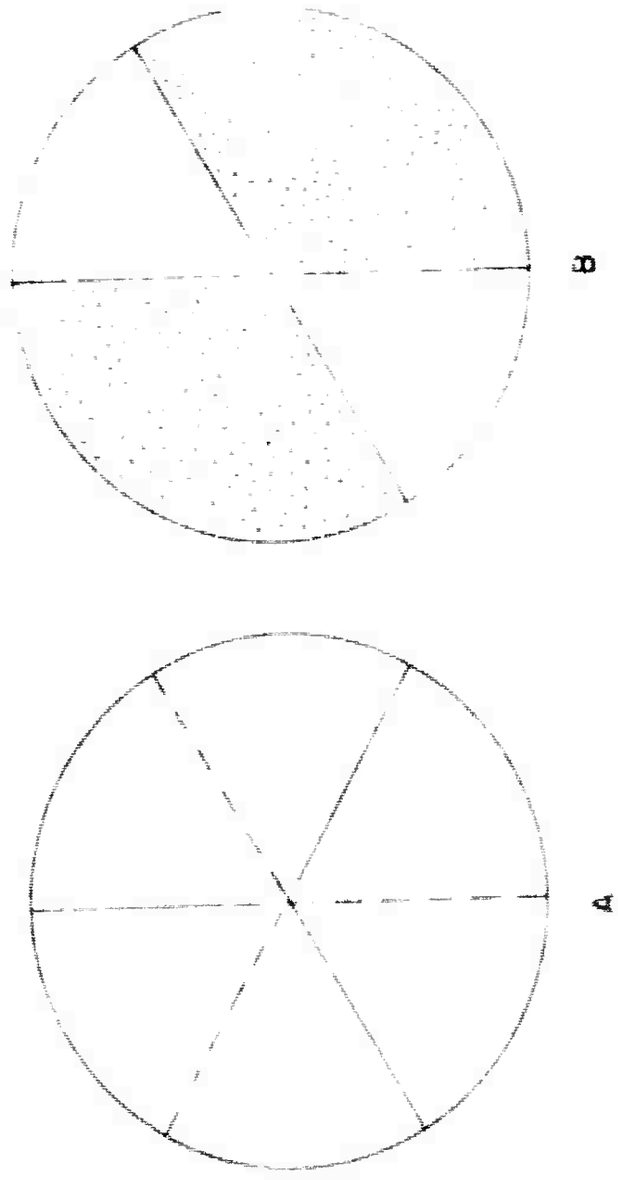

Figure 1

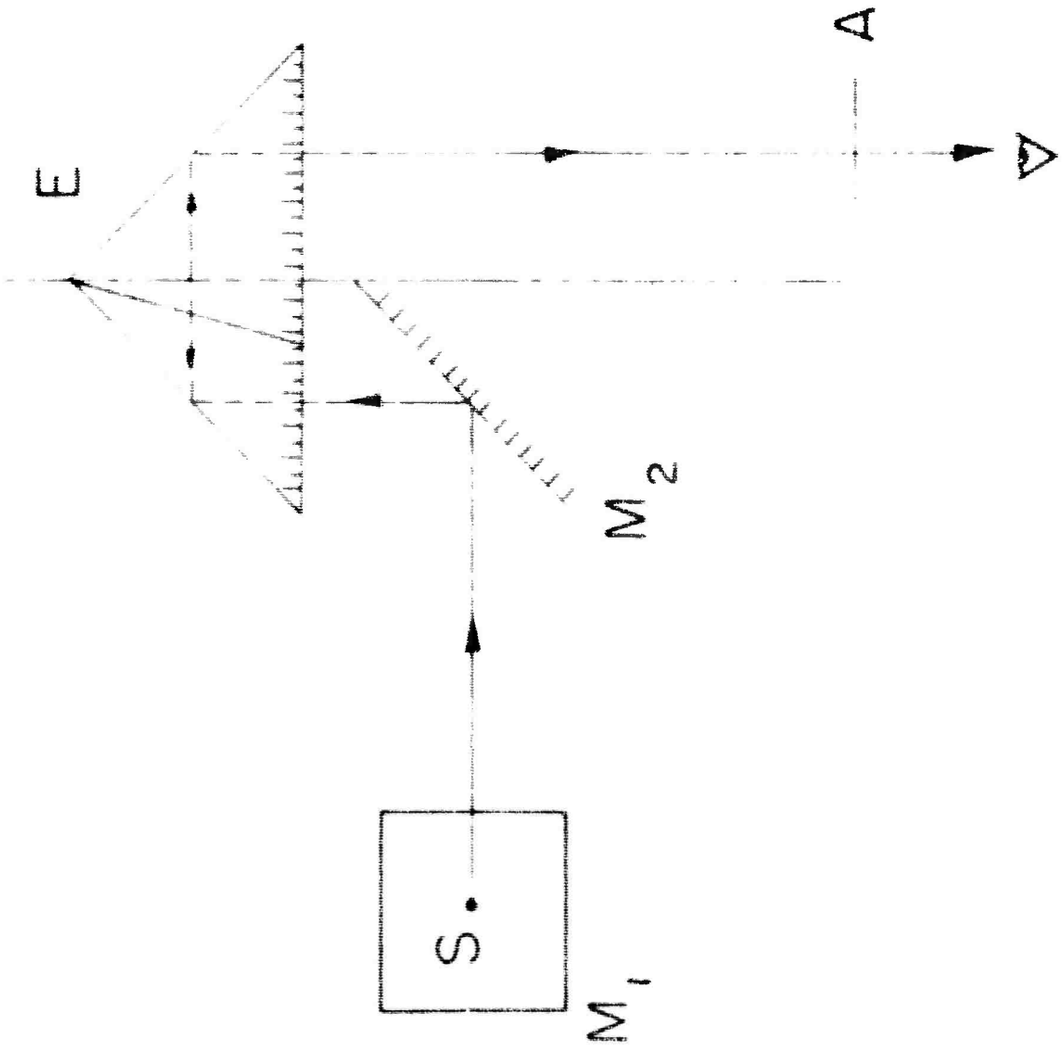
A
E
M2
S
M1

POLARIZED FRINGES OF CUBE CORNER FABRY-PEROT

∥ UNPOLARIZED ⊥

Figure 3

TECHNICAL RESEARCH GROUP

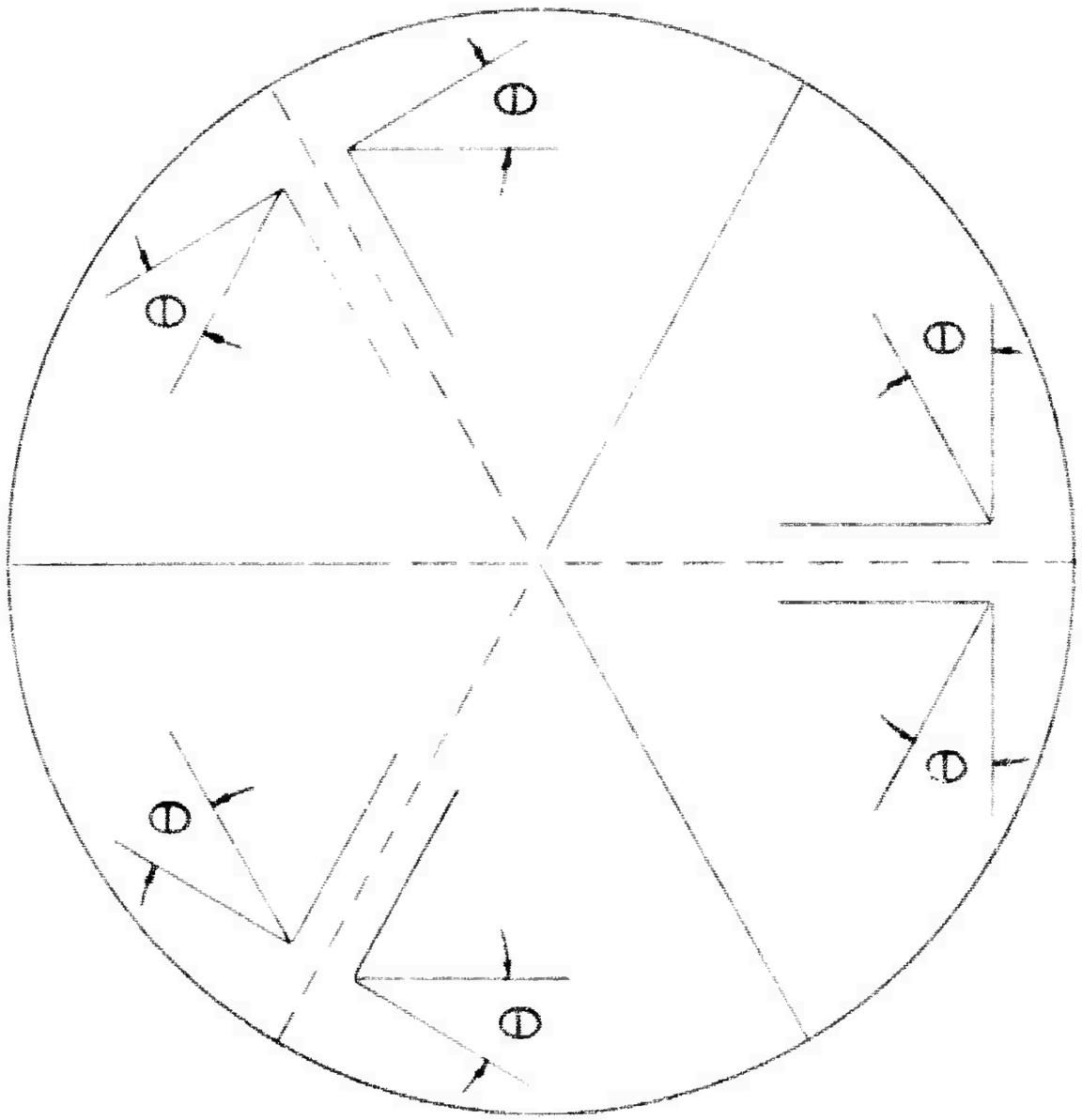

Fig. 1.

Inasmuch as the cube-corner used in this experimental work appeared to be of high quality, an effort was made to use it in a cavity with helium-neon. The simplicity of such a device is very appealing. With an optical flat at one end and the cube-corner on the other end, the only adjustment necessary is to align the normal to the flat parallel to the axis of the tube. This is done to avoid losses by vignetting and the angular tolerance, θ, is approximately given by:

$$\theta = \frac{D}{10L} ,$$

where D is the diameter of the amplifying medium and L is its length. This is based on a criterion of no more than 10% vignetting. The presence of vignetting means only that the beam diameter is reduced and does not other wise effect the threshold condition. In the case of helium-neon, D is approximately 1 centimeter and L = 100 centimeters. Thus the accuracy required is about 3 minutes of arc.

The apparatus was built and no oscillations were observed. A post mortem led to a more careful consideration of both diffraction losses and losses from lack of planarity of the cube surfaces, and it was concluded that this type of resonator is useful only for high gain systems. It is assumed that it is the cavity at fault rather than the remainder of the apparatus, and a type of confocal cavity is being substituted for the cube-corner. A confocal cavity is one in which two

spherical surfaces are used such that their focal points are coincident. Resonant modes with low diffraction loss can still exist if spheres are used with a smaller separation than their radius. The same is true if a flat is used against a sphere provided that the sphere has a radius of at least twice the separation of sphere and flat. Such a cavity has been constructed and does sustain oscillation.

3.0 Work Planned for Next Period

Several resonant cavities will be constructed for the helium-neon system. A sphere-flat combination with the radius of the sphere being more than twice the sphere-flat separation sustains oscillation and its mode patterns and other properties will be studied. A confocal type with two spheres separated by their radius is being designed. This will have external mirrors and have windows enclosing the helium and neon at Brewster's angle. A plane Fabry-Perot helium-neon cavity is also being built.

The crossed roof prism interferometer (see Figure 8.1) will be used with ruby. The ends of the ruby themselves will be polished at Brewster's angle, although for a first attempt anti-reflection coatings will be used.

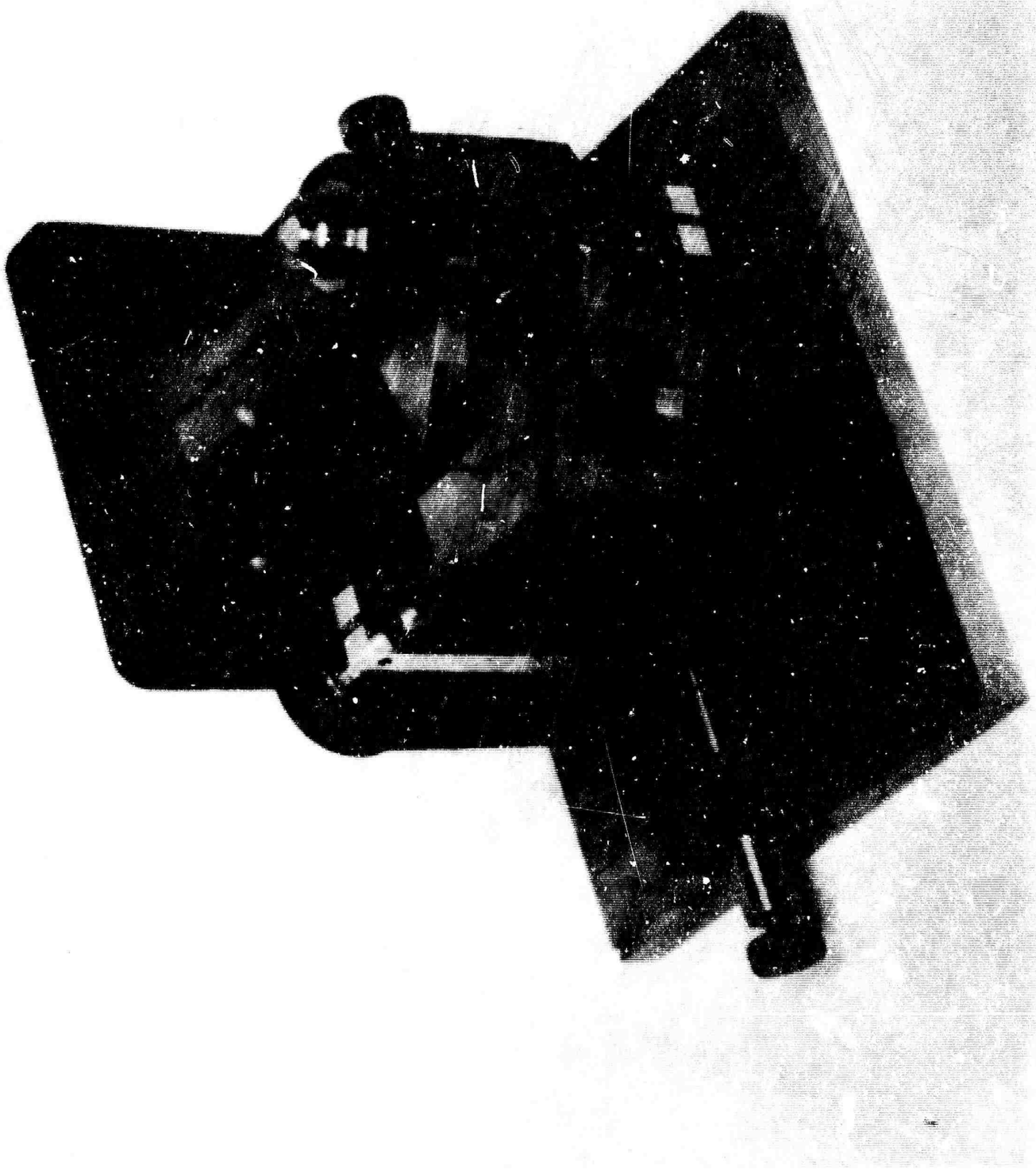

Crossed Roof Prism Interferometer
Figure 8.1

A long, (one meter), helium-cesium cavity is being built using a sphere-flat combination as in the helium-neon system. Should the gain reach the calculated values, a crossed roof reflector cavity will be substituted for the sphere-flat interferometer.